Max-Planck-Institut für Polymerforschung
Max Planck Institute for Polymer Research

Aus dem Max-Planck-Institut für Polymerforschung in Mainz

Carbohydrate nanocarriers in biomedical application: construction and surface modification

Dissertation

zur Erlangung des Grades

„Doktor der Naturwissenschaften“

Im Promotionsfach Physikalische Chemie

eingereicht am

Fachbereich Chemie, Pharmazie und Geowissenschaften

der Johannes Gutenberg-Universität in Mainz

Biao Kang

geboren in Shanxi, China

Mainz, 2015

Die vorliegende Arbeit wurde im Zeitraum von Dezember 2011 bis November 2015 am Max-Planck-Institut für Polymerforschung in Mainz im Arbeitskreis von Prof. Dr. Katharina Landfester angefertigt.

Dekan:

1. Gutachter:

2. Gutachter:

Tag der mündlichen Prüfung: 26.11.2015

"The things we love destroy us every time, but everything that kills me also makes me feel alive."

George R. R. Martin & Ryan Tedder

Acknowledgments

Table of Contents

Abstract

Nanomedicine is a key technology for the 21st century. The specific targeting of either tumor cells or immune cells *in vivo* by carefully designed and properly surface-functionalized nanocarriers may become effective therapeutics for the treatment of a variety of diseases. Carbohydrates, as prominent biomolecules, have shown their outstanding ability in balancing the biocompatibility, stability, biodegradability, and functionality of nanocarriers.

As a derivative of starch, hydroxyethyl starch (HES) possesses both high biocompatibility and improved stability against enzymatic degradation, but guarantees final body clearance due to its biodegradability. This thesis investigated the stealth properties of novel HES nanocontainers *in vitro* and *in vivo*. The HES nanocontainers were prepared via interfacial polyaddition in a water-in-oil miniemulsion. The synthesized hollow nanocapsules can be loaded with hydrophilic guests and tuned in size, chemically-functionalized in various pathways, and show high shelf life stability. The surface of the HES-NCs is further functionalized with poly(ethylene glycol) via different chemistries, which substantially enhanced blood half-life time (Chapter 3). Importantly, methods for precise and reliable quantification of the degree of functionalization are also introduced, which enable the precise control of the chemistry on the capsules' surface. The functionalized nanocapsules serve as a modular platform for specific cell targeting, as they show no unspecific up-taken by different cell types and show very long circulating time in blood (up to 72 h, chapter 3).

Subsequently, the PEGylated HES-NCs was further functionalized by mannose, and the targeting effect of them in both the absence and presence of protein corona was compared, while the influence of the additional mannose on the protein corona composition around the PEGylated HES-NCs was studied (Chapter 4). Whenever nanoparticles encounter biological fluids like blood, proteins adsorb on their surface, which consequently form a so called protein corona. As its importance is widely accepted, the information on the influence of surface functionalization of nanocarrier on the protein corona is still sparse, especially on the topic that how the functionalization of PEGylated nanocarrier with targeting agent will affect its protein corona formation, and how this protein corona may in turn influence the targeting

effect. In chapter 4, hydroxyethyl starch nanocarriers (HES NCs) were prepared, PEGylated, and modified “on top” with mannose to target dendritic cells (DCs). Their interaction with human plasma was studied: low overall protein adsorption with a distinct protein pattern and a high specific DCs binding affinity prove an efficient combination of “stealth” and targeting behavior.

Despite the long plasma halftime and specific targeting effect, encapsulation of complex molecules into the above described HES-NCs is difficult as nucleophiles like amines, thiols, or alcohols, and consequently will participate in the polycondensation reaction with the diisocyanate electrophile. New strategies have to be developed, which use bio-orthogonal reactions to generate the nanocarriers allowing the encapsulation of more complex pharmaceutical agents. In chapter 5, azide functionalized HES was prepared, so that capsules can be prepared by the bio-orthogonal copper free click reaction can be used to encapsulate any water-soluble drug or potential therapeutic agent.

1. Introduction

The work in this chapter and the following chapter has been accepted for publication in Chemical Society Reviews (Kang, B.; Opatz, T.; Landfester, K.; Wurm, F. R. Chem. Soc. Rev. 2015, 44, 8301.)[1] and has been altered for this thesis with permission.

Since Paul Ehrlich has coined the term of the "magic bullet" for modern medicine in the beginning of 20th century, the development of targeted drug delivery has received immense interdisciplinary attention, ranging from chemistry over biology to medicine.[2] In the last decades, the idea has gradually evolved to the application of nanometer-sized vehicles for the delivery of drugs, due to their advantages including i) to protect the payload from degradation *in vivo*, ii) to allow specific targeting to the diseased tissue and thus iii) to reduce the risk of systemic toxicity, and, finally, iv) to release the drug, while the carrier is eliminated from the body without trace. All these properties have been realized partly in today's nanomedicine, however, have still not been accomplished completely. The innovative design and chemical functionalization of suitable nanocarriers is thus still the challenge to finally generate "magic bullets", selective drug delivery systems, of the 21st century.

The early-stage nanocarriers were mostly prepared from artificial polymeric[3-6] or inorganic materials.[5,7-10] To increase their blood circulation times poly(ethylene glycol) (PEG) is often attached to their surface as the so called "stealth layer" decreasing protein adsorption.[5-7,11] These early nanocarriers suffered several intrinsic drawbacks, especially regarding their biocompatibility and biodegradability. More recently, the research focus shifts to use natural materials for the fabrication of nanocarriers, which are inherently compatible with the metabolic system and have great potential in their biological and biomimetic effects.

Together with lipids, proteins, and nucleic acids, carbohydrates (or saccharides) are one of the four major classes of biomolecules. The combination of several advantages of carbohydrates makes them unique candidates for application in nano-medicine:

i) chemically well-defined structure
ii) biocompatible/ biodegradable
iii) available on large scale
iv) protein-repellent
v) high water solubility
vi) no aggregation
vii) natural targeting agents

In contrast to proteins and nucleic acids, when oligo/poly-saccharides are formed through chain elongating and branching, the linkage points between sugar units are not restricted to constant positions. Regioisomers can be formed by elongating the sugar chain at different hydroxy groups, resulting in a significantly enhanced code capacity. While 20 amino acids yield $6.4*10^7$ hexapeptide isomers, the same amount of hexose repeating units in an oligosaccharide will result in $1.44*10^{15}$ different isomers.[12] In addition, most of the carbohydrates are located on the outer surface of the cell, in the extracellular fluid and blood,[13] which is the biological environment for the intravenously injected nano-medicines. The molecular understanding of the peculiarities of carbohydrates will help to pave the road for the translation of “sweet” nano-medicines to the clinic. Besides their role in biological signaling, carbohydrates also have other biological functions, including energy storage, protection of cell organelles[14], modification of the properties of peptides or proteins[15], etc., which might grant the nano-medicine additional advanced properties. In addition, carbohydrates are responsible for cell/cell, and cell/matrix communications and interactions in cellular organelles or multicellular organs.[16-18] Studying and utilizing the information from this natural “glyco-code” and exploiting the differences between healthy and malignant cells is a promising strategy for the diagnosis and treatment of cancer.[19]

Besides the biological origin of oligo- and polysaccharides and their important role in biological communication, their inherent hydrophilicity makes them even more attractive for biomedical polymer science. They are currently discussed as potential biodegradable substitutes for PEG, to reduce unspecific protein adsorption.[20] It has been reported, that hydroxyethyl starch (HES),[21-25] a synthetically modified starch derivative, but also dextrin[26-28] or other saccharides[29,30] can reduce the protein

adsorption on nanocarriers and prolong their circulation time in the blood stream similar to PEG. This protein-repellent property, together with their active biological function to interact with certain proteins/ cell surfaces, renders carbohydrates very promising elements for the construction of future therapeutics.

Another feature that renders carbohydrates interesting for drug delivery, for example, is their biodegradability. This does not only ensure the eventual body clearance of the materials, but is an additional handle to trigger drug release or activation by certain enzymes.[24-28] HES, for example, allows adjusting degradation kinetics, depending on the degree of hydroxyethylation.[24,25] In summary, the i) biological activity, combined with ii) the potential stealth properties, and iii) the enzymatic stimulus makes carbohydrates interesting materials for the design of nanocarriers for biomedical applications. Both, surface-modification of preformed nanoparticles with carbohydrates or the direct construction of the nanocarriers from mono-, oligo-, or polysaccharides have attracted considerable attention during the last decade over the borders of single disciplines, as can be seen in Scheme 1.

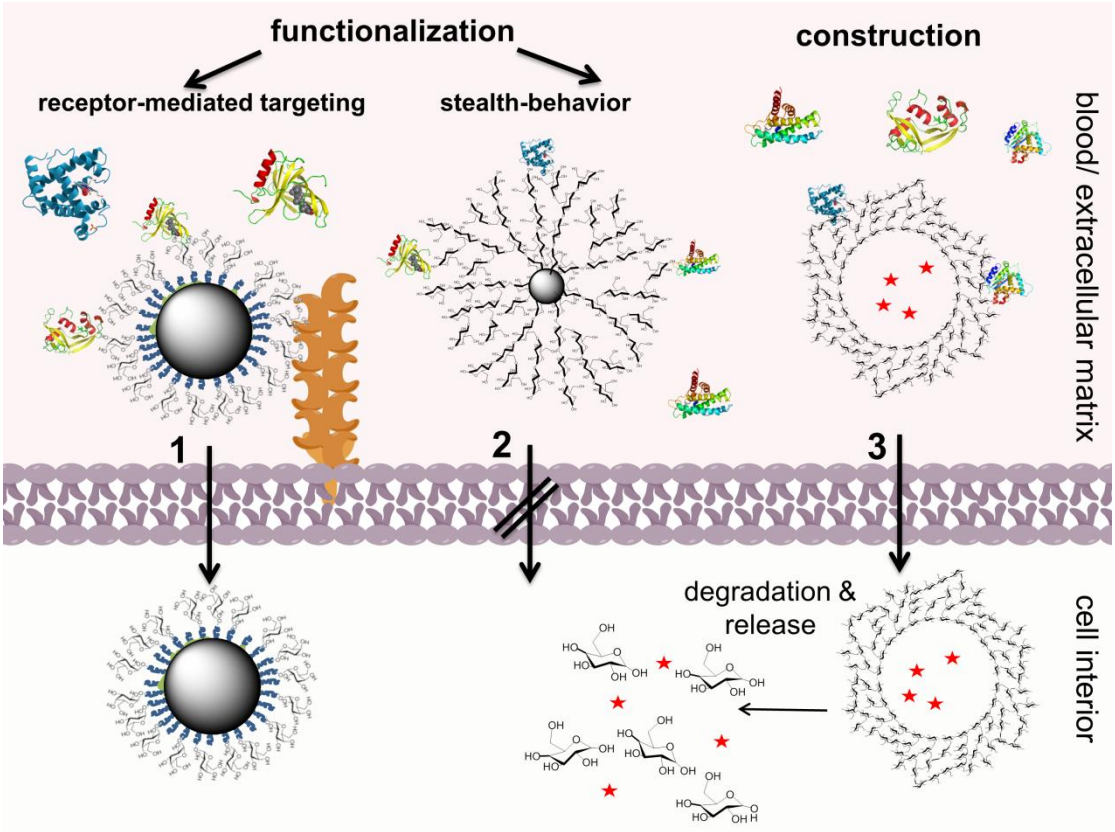

Scheme 1. *Schematic summary of the potential roles of sugar in nano-medicine. 1). Surface modification of the nanocarriers by certain sugars, e.g. mannose, can*

enhance the receptor mediated uptake of the nanocarrier. 2). Surface modification of the nanocarriers with other saccharides, e.g. dextrin (polysaccharide of glucose), can decrease the unspecific uptake of the nanocarriers by cells. 3). Nanocarriers made of saccharides can be degraded by cells, which will result in the release of the payload.

In this work, sugar based nano-capsules will be prepared in a water-in-oil miniemulsion system, their encapsulation efficiency of the payload will be systematically evaluated (Figure 1 gives an overview on the structural relations of carbohydrates, which are discussed herein). Furthermore, the interaction with plasma protein and different cell lines will be studied, together with the pharmaceutical behavior (in-vivo plasma halftime) and the specific targeting effect. In the end, the possibility to prepare the capsule by bio-orthogonal chemistry will be investigated.

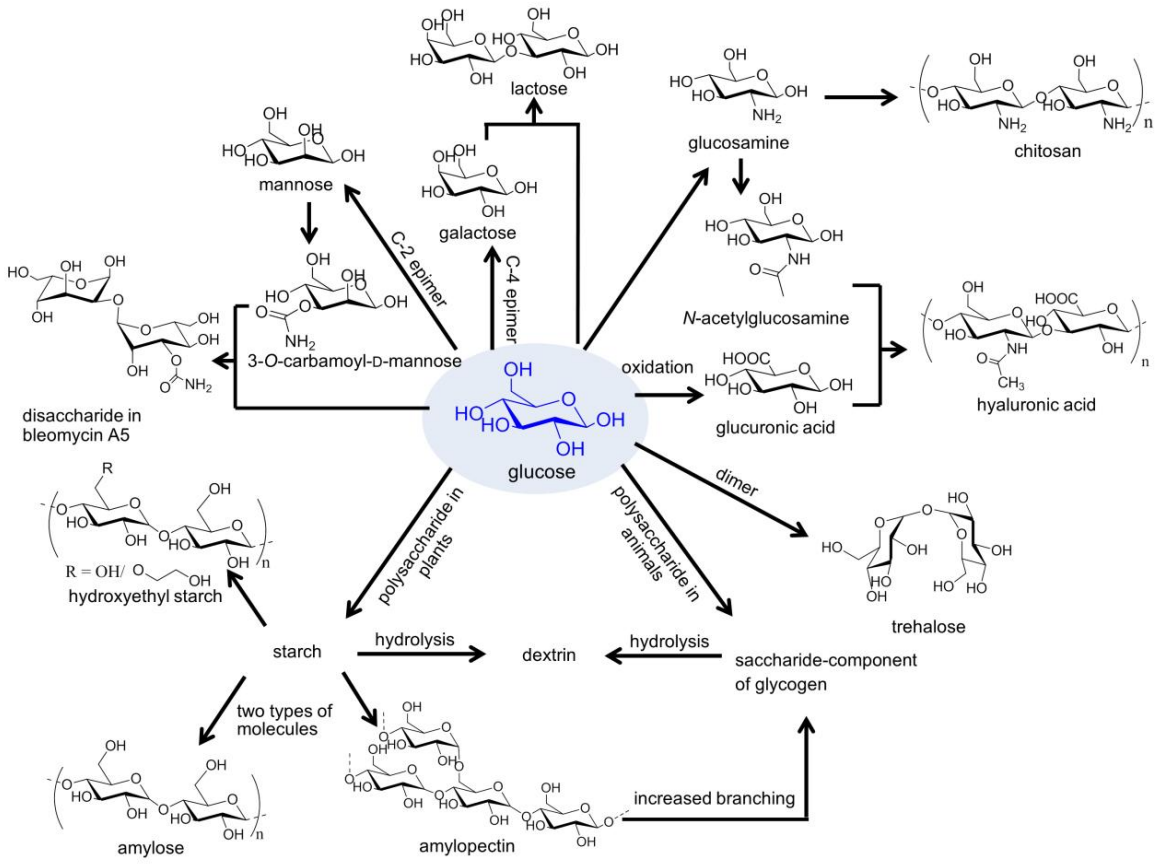

Figure 1. *Relations between different common carbohydrates.*

2. Theoretical background

2.1 Recognition of saccharides by cell surface receptors and the use for targeting of specific cells.

Cells of higher organisms are in constant communication and interaction with their environment. In order to survive and maintain the appropriate functions, external signals must be received by the cell-surface, and subsequently delivered into the cell's interior.[31] While many of these different types of biological information are encoded and delivered by protein-protein interactions, carbohydrates also play a significant role.[19,32,33] Carbohydrates act as recognition markers in different pathological and physiological processes, most of them occurring on the surfaces of cells. Three classes of proteins serve as receptors for the carbohydrate ligands: enzymes (for the synthesis, remodeling and degradation of carbohydrate), immunoglobulins and, most importantly, lectins[34] which are membrane-bound receptors and assist during the process of endocytosis.[35]

Through the binding with these receptors, many types of carbohydrates, including mono-, oligo-, and polysaccharides have been found to specifically bind to certain cell types. Mono/oligosaccharides like mannose derivatives exhibit strong binding to the C-type lectin DC-SIGN on the surface of dendritic cells,[36] C-type lectin receptors on alveolar macrophages,[37] and the plant lectin concanavalin A.[38] Galactose can also bind selectively to C-type lectin receptors on alveolar macrophages[37] and carbohydrate receptors on E. coli cells.[39] Lactobionic acid can bind to asialoglycoprotein receptors (ASGP-R) of hepatic tumor cells.[40] For rhamnose, a specific targeting effect to human skin cells was demonstrated.[41] Polysaccharides like hyaluronic acid or chitosan have been found to specifically bind to ocular mucosa.[42-44] Functionalized dextran has proven to specifically target vascular smooth muscle cells[45] and human endothelial cells.[46] Many cellular events are regulated by these sugar codes, including cell adhesion, proliferation, and cell death.[47-50]

Cancer still is one of the most prevalent deadly diseases worldwide and constitutes one of the two major causes of death in industrialized countries. While the complete eradication of malignant tumor is severely complicated by a tendency to form

metastases, all malignant cells have special biological signatures which distinguish them from their healthy counterparts.

Carbohydrates, in particular glycoconjugates, play an essential role for cancer metastasis and communication, through the interaction with endogenous lectins present on the cancer cells.[51-53] Presumably due to the fast metabolism of the tumor tissue, some of these lectins, e. g. galectins, are found expressed at an elevated level on malignant cells while they are not expressed detectably by their healthy counterparts.[13,54] Defined by their role as β-galactose receptors,[55] galectins have been reported as indicator for malignancies in stomach,[56] liver,[57] and the corresponding colon cancer.[58-60] A high galectin-1 level was reported in papillary carcinomas, but not in the healthy tissues.[61,62] A significant increase in the galecin-1 expression in adenocarcinoma cells was also reported, in contrast to the adjacent normal endometrium.[63] In addition, other carbohydrates, like hyaluronic acid also shows specific binding to CD44 receptors[64,65] which are expressed at low levels on hematopoietic, epithelial, and neuronal cells but at much higher levels in various tumor cells like lymphomas, melanomas, colorectal, and lung tumor cells.[66,67] Thus, many carbohydrate-related biomarkers have been developed which individually exhibit specific binding to different cancer cells,[68] and may open up possibilities to specifically target cancer cells by an appropriate carbohydrate functionalization of nanocarriers.

2.2 Protein repellent properties of carbohydrates

When a nanocarrier enters a biology fluid, e.g. is intravenously injected into the bloodstream, it will adsorb proteins on its surface, due to hydrophobic interactions and the high surface energy of most types of nanocarriers.[69,70] This procedure, known as opsonization, can lead to phagocytosis of the nanocarrier by the Mononuclear phagocyte system (MPS). The adsorbed proteins will determine the fate of the nanocarrier *in vivo* (this process is often called the formation of a "biological identity"),[69] typically resulting in the fast clearance of the nanocarriers from the blood. This makes any *in vivo* specific targeting a challenging task.[69] In order to prolong the *in vivo* plasma half-life times of the nanocarriers, the opsonization needs to be reduced, either by the material of the nanocarrier itself, or by surface modification (the dress of the nanocarriers). Currently, PEGylation is the "gold standard" to achieve long blood circulation times and reduced unspecific cellular uptake due to the hydrophilicity and the steric repulsion by PEG-modified surfaces and proteins.[71] PEGylation has achieved numerous successes in the past decades, and many PEG-related products both in consumer care and biomedical applications have improved the quality of life.[71,72] In spite of these achievements, recent studies reported several drawbacks of PEG. The occurrence of renal tubular vacuolization in animal models have raised concerns that a prolonged therapy with PEGylated drugs may lead to an accumulation of PEG in the cytoplasm of kidney cells as the polymer is not biodegradable.[73,74] In addition, PEG potentially forms toxic degradation products upon storage which could provoke adverse effects.[71] These setbacks of PEG could be circumvented by using polysaccharides as substitutes which often show low hypersensitivity even after chemical functionalization.[75] The structural similarity of many polysaccharides, for example HES or dextran, to the sugar component of glycogen, which is the form for the storage of sugar in animals, is a probable explanation why they lack immunogenicity. Moreover, the biodegradability of polysaccharides is advantageous over many other synthetic polymers that are currently discussed as alternatives for PEG.[76] Not only the post-injection clearance of the nanocarriers is enhanced by its biodegradability, but also enzymatic induced masking-unmasking or encapsulation-release cascades of the payload are possible. [24,26,27,38,77,78] However, care has to be taken depending

on the chemical modification, e.g. anchoring or polymerizable groups that may alter both the degradation process and the cytotoxicity of the carbohydrates.

Numerous studies have already proven that polysaccharide or their derivatives like HES[23,79-81] or dextran exhibit a low protein affinity.[82,83] Furthermore, the microbial polysaccharide pullulan, glycolipids, and dextran have shown their ability to decrease the uptake of nanocarriers into the MPS,[84,85] while HES has been proven to suppress the unspecific uptake of the nanocarriers *in vitro,*[86] and prolong the plasma halftime *in vivo*, the process of its attachment also being called HESylation.[24,77] While several mono- or oligosaccharides are responsible for the communication of biological information in the organism, some of them are capable of impeding the phagocytosis of native cells by the MPS. Sialic acid is one example of these saccharides and red blood cells without surface sialic acid are immediately removed from the blood by the MPS.[87] It has been proven, that when sialic acid is coupled to the surface of quantum dots, the *in vivo* plasma half-life time of the latter is prolonged.[88]

2.3 Glycoproteins: how nature uses carbohydrates

In nature, glycoproteins, i.e. glycosylated polypeptides, are of high importance and function as hormones,[89] antibodies,[90] antifreeze proteins,[91] and proteins in the cell membrane.[15] After glycosylation, the attached (oligo)saccharides provide additional properties for the protein, such as facilitating the protein folding and stabilizing the conformation of the peptidic backbone,[92] protection,[93] elongation of the *in vivo* plasma halftime,[94] communication with the immune system,[95] and adhesion to cognate receptors on other cell surfaces.[96,97]

Inspired by these natural strategies, various researchers have prepared neoglycoproteins for diverse applications. Pharmacologically active peptides have been used for the treatment of various diseases.[72,98] A major drawback, however, is their usually rapid degradation *in vivo*. To optimize the pharmacokinetic properties of such drugs, artificial polymers are frequently coupled to their surface. Typically PEG is used for this purpose but in modern literature, an increasing percentage of biodegradable biopolymers are coupled to proteins to optimize their therapeutic performance. For example, hyaluronan-functionalized insulin showed a prolonged and enhanced hypoglycemic effect, demonstrating the potential of hyaluronan for increasing the plasma half-life of peptides.[99]

Anakinra, a synthetically generated interleukin-1 antagonist, is used for the treatment of rheumatic arthritis, but has a plasma halftime of only 108 min; after conjugation with HES its blood circulation time was increased by a factor of 6.5.[100]

Dextrin (a glucose polymer) with a molecular weight of 7,700 and 47,200 g/mol and degree of succinoylation of 9–32 mol % was used to functionalize trypsin (a serine protease) and thus masking its activity. The activity of the enzyme can be restored after degradation of the polysaccharide by α-amylase.[26-28] Also hyaluronic acid was used for the functionalization of trypsin, resulting in an increase of its activity to 145% over the native protein, while exhibiting a 52% higher stability in the presence of elastase (a protease).[101] Although these works are beyond the scope of this work, the idea of mimicking nature to utilize the advantageous properties of different sugars is identical.

2.4 Carbohydrate-functionalized Nanocarriers

Being a C-2-epimer of glucose, mannose is an important monosaccharide for the glycosylation of proteins. Mannose-containing glycoproteins are produced in the liver and secreted into the blood, hence mannose is distributed throughout the body.[102] Many mannose-binding proteins, like the C-type lectins, are crucial for cell-surface recognition and other communication events.[103] Recently, mannose has been applied to functionalize mesoporous silica nanoparticles,[38] magnetic nanoparticles,[19] gold nanoparticles,[36] and polyanhydride nanoparticles[37] (Table 1, entry 1) to specifically target cells; distinct biological functionalities have been achieved in each case.

When thiol-functionalized mannose is reacted with alkenyl-terminated silanes in a radical thiol-ene addition (Table 1, entry 1, a), surface functionalization of mesoporous silica nanoparticles can be achieved, whose pores can be sealed by adding concanavalin A, a carbohydrate-binding protein, to the dispersion. The pores can be re-opened under acidic conditions (pH < 5.5) or in a glucose-rich environment. Release of the payload in the tumor tissue, where the pH value is typically lower than that in healthy tissue, or under high blood sugar level is thus possible.[38] In another work, mannose-functionalized silica nanoparticles have been prepared, which showed specific binding to MCF-7 human breast cancer cells.[104]

Carboxylated derivatives of mannose (Table 1, entry 1, b), galactose (Table 1, entry 2, a), fucose (Table 1, entry 3), and sialic acid (Table 1, entry 4, a) have been coupled to amino-functionalized magnetic nanoparticles via an amide linkage. When these nanoparticles were incubated with different malignant and non-malignant cells and investigated via magnetic resonance imaging, it was shown that the malignant cells can be differentiated by the changes of T_2 relaxation time (% ΔT_2) [19], as shown in Figure 2. Similar work was conducted using sialic acid-functionalized magnetic nanoparticles to detect the levels of β-amyloid, which is a pathological hallmark of Alzheimer's disease, both *in vitro* and *ex vivo*.[105]

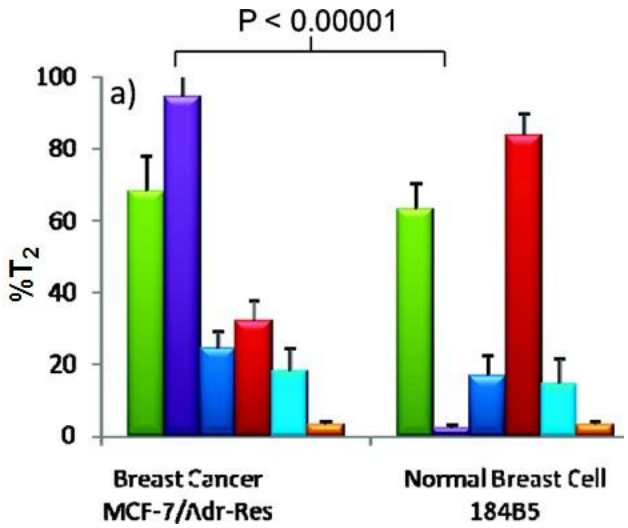

Figure 2. *Discrimination of the breast cancer cells from their healthy counterparts by the changes of T_2 relaxation time (% ΔT_2) in magnetic resonance imaging, by magnetic particles functionalized with: mannose (green), galactose (violet), fucose (dark blue), sialic acid (red), glucose (light blue), compared to unmodified magnetic particles (orange), (adapted with permission from reference[19]. Copyright 2010 American Chemical Society).*

Different (oligo)mannosides have also been functionalized with thiols and coupled to gold nanoparticles.[36] The obtained glycosylated gold nanoparticles show stronger binding to DC-SIGN (a C-type lectin) on the surface of dendritic cells compared to gp120, which is a protein essential for the entry of HI virus into cells, and thus could serve as a potential carbohydrate-based drug against HIV (Table 1, entry 1, c). Similar glycosylated gold nanoparticles have also been prepared in another work and observed to cross the blood−brain barrier (BBB) nearly 3-fold faster / more efficiently than unmodified gold nanoparticles.[106]

Both, α-1,2-linked dimannose (Table 1, entry 1, d) and galactose (Table 1, entry 2, g) have been coupled to polyanhydride nanoparticles through an amidation reaction via 1-ethyl-3-(3-dimethylaminopropyl)-carbodiimide hydrochloride (EDC) as the coupling agent. The obtained mannose surface-functionalized particles, which were termed “pathogen-like” nanocarriers, exhibited specific binding to alveolar macrophages through the surface C-type lectin and enhanced the expression of the macrophage mannose receptor.[37]

It is the concern of some recent publications that the protein adsorption after contact

with blood will hamper all specific targeting of nanocarriers due to shielding of targeting groups, which might reduce the efficiency of “targeted” drug delivery systems remarkably.[107-114] A current challenge is to understand the interaction of blood proteins with nanocarriers which carry additional targeting groups. The adsorption of plasma proteins onto the targeting agent could hinder the recognition of the targeting agent by the respective cells and hence could make any *in vivo* targeting impossible.[69] The interactions of mannose-functionalized nanocarriers with plasma proteins have been studied to address this problem. It turned out that, in comparison to a PEGylated nano-carrier, additional functionalization of the PEGylated nanocarrier with mannose did not significantly change its protein corona formation. Furthermore, these mannose functionalized nanocarriers showed the same binding affinity to dendritic cells (DCs) both in the presence and absence of the plasma protein corona.[115]

Galactose is the C-4 epimer of glucose and is for example essential for the antigen structure of red blood cells which is the determinant of the blood type. For O and A antigens, two galactose units are contained in the saccharide portion while for the B antigen, three galactose units are contained.[116] Galactose functionalized with an azide group at the C1-position, was coupled to pillar[5]arene by a Huisgen-type cycloaddition, while the latter is self-assembled into nanorods (Table 1, entry 2, c), which have proven a high affinity for the carbohydrate receptors on E. coli. as well as low toxicity, and can be utilized as excellent cell glues to agglutinate these bacteria.[39] In another work, different statistical glycol-dithiocarbamate copolymers were prepared and used to functionalize gold nanoparticles on the surface, which were further coupled with gold(I) triphenylphosphine as an anticancer agent. Among these glyconanoparticles, the galactose-functionalized ones were found to be 4-fold more cytotoxic to HepG2 cells, in comparison with glucose and lactose functionalized particles.[117]

Sialic acid is a monosaccharide, which is widely distributed in animal tissues and mostly bound in form of glycoproteins.[118] It plays an important role in recognition and communication with the immune system,[119-121] which is also proven by the fact that red blood cells without sialic acid on the surface are immediately removed from

blood by the MPS.[87] Ketone-functionalized sialic acid is reacted with aminooxy-functionalized quantum dots, namely phosphorylcholine self-assembled monolayer-coated quantum dots (PC-QDs), and their *in vivo* half-life times are extended compared to quantum dots functionalized by other monosaccharides (Table 1, entry 4, b; and Figure 3).[88]

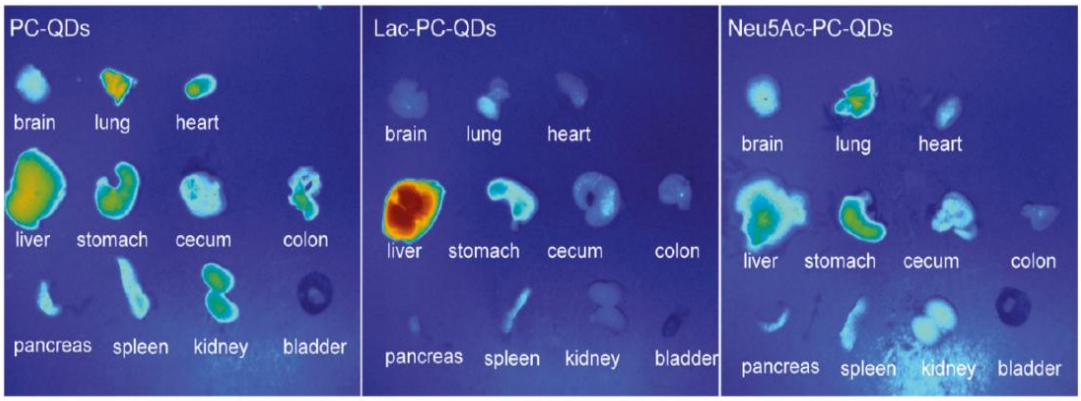

Figure 3. *Images of major organs isolated from three tested mice, 2 h after the administration of phosphorylcholine quantum dots (PC-QDs), lactose- functionalized quantum dots (Lac-PC-QDs), and sialic acid-functionalized quantum dots (Nue5Ac-PC-QDs). (Reprinted with permission from reference[88]. Copyright 2011 American Chemical Society).*

Sialyl-Lewis^x is very important antigen for blood groups, which displays on the terminus of glycolipids that are present on the cell surface, has been used to functionalize superparamagnetic silica nanoparticles (Table 1, entry 4, c), with the functionalization strategy shown in Figure 4. These nanoparticles have diameters of around 18 nm and carry NH_2-groups.[122] Subsequent functionalization of these particles with an NHS-ester allows coupling to amino-functionalized Sialyl-Lewis^X. The obtained glycosylated nanoparticles bind specifically to the inflammation-associated endothelial transmembrane proteins E and P selectin, both cell adhesion molecules. *In vivo* studies have shown an accumulation in the brain vasculature by measuring the relaxing time of the nanoparticles via MRI.[122]

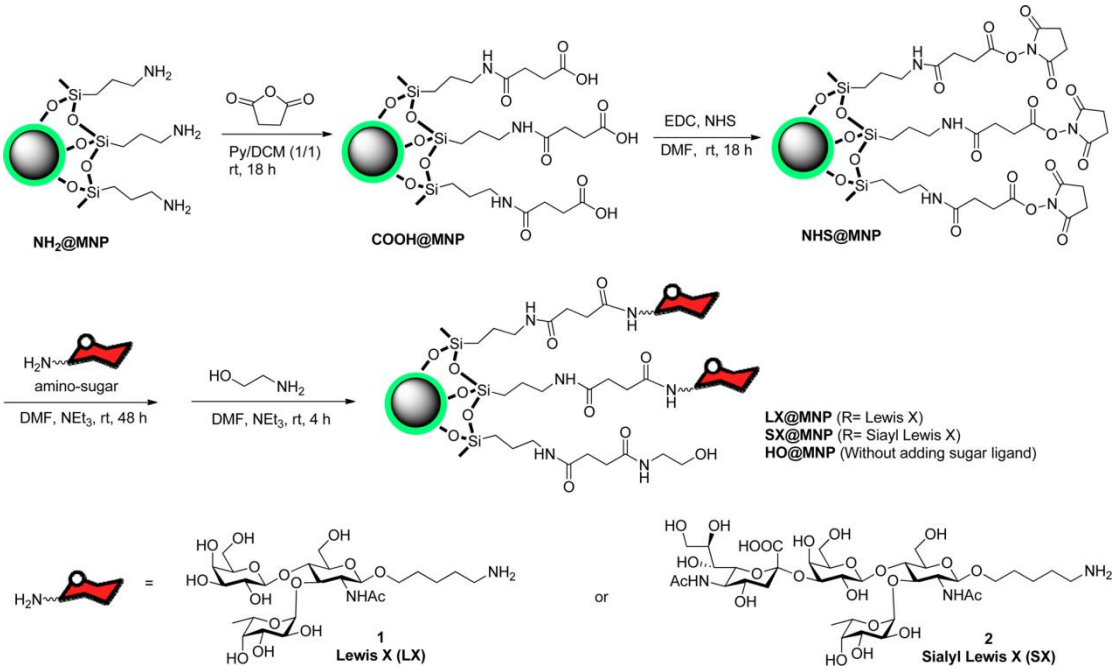

Figure 4. *Functionalization of superparamagnetic nanoparticles with a silica core by Sialyl-Lewis^X. (Reprinted with permission from reference[122]. Copyright 2014 American Chemical Society).*

Lactobionic acid (4-O-β-D-galactopyranosyl-D-gluconic acid, (Table 1, entry 6)) specifically bind to hepatocytes.[123] Thiolated lactobionic acid was used to functionalize block copolymers, which were prepared by the ring-opening copolymerization of ε-caprolactone and a pyridyl disulfide containing cyclic carbonate, followed by post polymerization modification with thiolated lactobionic acid via the thiol-disulfide exchange reaction. The post-modified block copolymers then self-assembled into micelles with lactobionic acid on the surface. These micelles were shown to target liver cancer through asialoglycoprotein receptors (ASGP-R), furthermore, the saccharide shells is cleavable under a reductive environment mimicking the interior of a cell.[40]

Rhamnose is a mannose-related 6-deoxy hexose which naturally occurs in the L-form. It is found mainly in bacteria and plants and is often present in the cell walls and is essential for the survival of bacteria.[124] Phosphonated rhamnose has been prepared (Table 1, entry 7) and anchored to magnetic nanoparticles through the strong binding of phosphonates groups to metals. The rhamnose-functionalized magnetic nanoparticles exhibited targeting effect to human skin cells. Since the iron

oxide nanoparticles are superparamagnetic, they can be used as MRI contrast agent with specific cell targeting.[41]

Bleomycin is a glycopeptide-type antibiotic, bleomycin (BLM, Figure 5), has strong antitumor abilities and is used for the treatment of malignant lymphomas and squamous cell carcinomas.[125,126] Additionally, BLM also has shown a specific tumor cell targeting effect, and hence has been used for tumor imaging.[127] In order to understand the origin of the tumor targeting effect, it has been split into the BLM-analogue deglycobleomycin (devoid of the disaccharide moiety) and the disaccharide moiety itself. The difference for the ability for specific tumor targeting of these two derivatives has been investigated, and the disaccharide motif was found to be responsible for selective binding to MCF-7 human breast carcinoma cells and BxPC-3 pancreatic cancer cells, while having their healthy counterparts not being targeted.[128] In contrast, deglycobleomycin (*Bleomycin* without the disaccharide moiety) did not show any specific targeting. Furthermore, after coupling the disaccharide moiety to the surface of microbubbles (Table 1, entry 8), which consist of an empty core and a lipid shell, and originally used as contrast agents for ultrasonography,[129] specific targeting of MCF-7 human breast carcinoma cells has been observed. Furthermore, the subsequent study verified that it is a single sugar unit from this disaccharide, namely the carbamoylmannose moiety, which is responsible for the tumor cell specific targeting effect.[130]

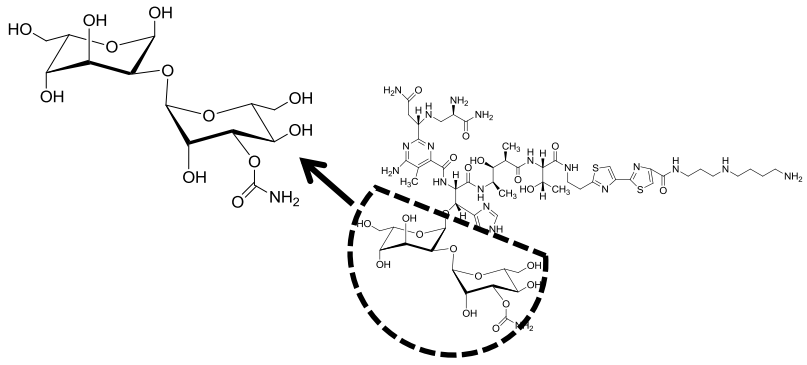

Figure 5.*Structure of Bleomycin A_5, and its disaccharide moiety.*

Trehalose (α-D-glucopyranosyl-(1→1)-α-D-glucopyranoside) is composed of two α-glucose units which are linked by an α,α'-1,1-glucosidic bond. It is widely found in animals, plants, and microorganisms. It is the blood-sugar of many insects, including locust, butterflies and bees. It is believed to transfer into a gel phase under

dehydrating condition, protecting the cell internal organelles and hence the whole cells against desiccation.[14] A monomer, namely methacrylamido trehalose (Table 1, entry 9) was polymerized followed by chain extension with aminoethyl methacrylamide (AEMA). The obtained polymer was used to complex siRNA to polyplexes which carry trehalose on the surface. These polyplexes show high stability in the presence of high salt concentrations and serum proteins and are specifically internalized into a brain tumor cell line (U-87 cells) as can be seen in Figure 6.[131]

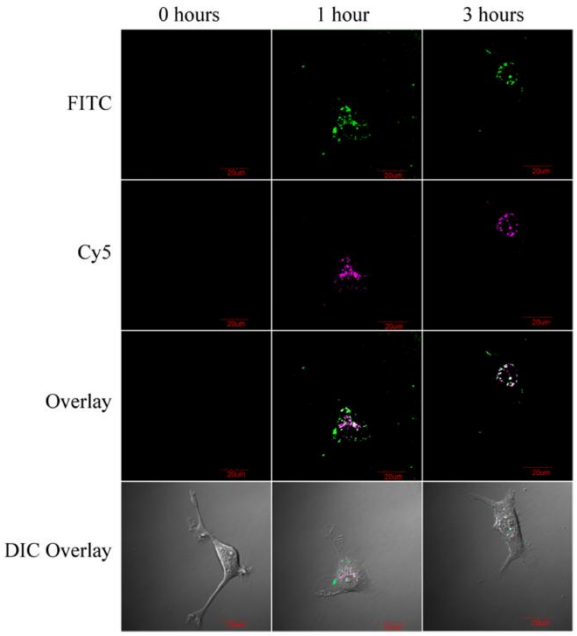

Figure 6. *Confocal microscopy of U-87 cells transfected with siRNA containing polyplexes, both fluorescent intensity from Cy5-labeled siRNA (magenta) and FITC-labeled poly(methacrylamidotrehalose) is detected (Reprinted with permission from reference[131]. Copyright 2013 American Chemical Society).*

Table 1: Carbohydrates used for surface-functionalization of nanocarriers.

#	Type of sugar		Chemical structure	Nanocarrier	Properties	Chemistry	note	ref
1	mannose	a	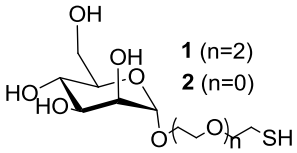	mesoporous silica nano-particles	pore closure by coupling of mannose with concanavalin A	thiol-ene reaction	re-opening of the pore controlled by pH or glucose level	38
		b	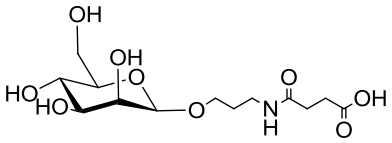	magnetic nanoparticles	increased binding affinity with different cell surface	amidation	selective binding to cancer cells	19
		c	Different (oligo)mannosides functionalized with thiol groups	gold nanoparticles	inhibition of DC-SIGN/gp120 binding	reaction between the thiol group and gold surface	a potential anti-HIV system	36
		d	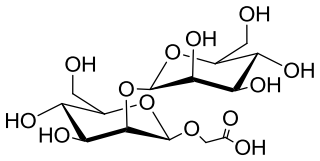	poly-anhydride nanoparticles	targeting C-type lectin receptors on alveolar macrophages	EDC coupling	enhanced expression of mannose receptor	37

2	galactose	a		magnetic nanoparticles	increased binding affinity with different cell surface	amide coupling reaction	differentiates normal cells from cancer cells	19
		b		polyanhydride nanoparticles	targets C-type lectin receptors on alveolar macrophages	EDC coupling	enhanced expression of galactose lectin	37
		c		self-assembled nanorods	high binding affinity to carbohydrate receptors on E. coli.	Huisgen azide alkyne cycloaddition	decreasing the toxicity of the nanorods	39
3	fucose			magnetic nanoparticles	Increased binding affinity with different cell surfaces	amidation	distinction between isogenic sublines of cancer cells	19
4	Sialic acid	a						

		b	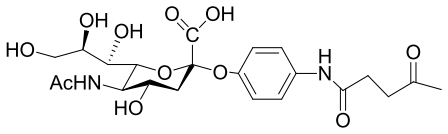	quantum dots	prolonged *in vivo* lifetime	Huisgen azide alkyne cycloaddition		88
		c	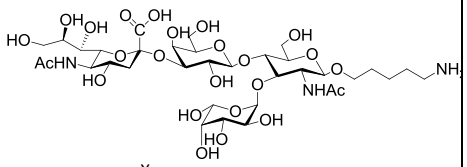 Sialyl-Lewis^X	core shell silica magnetic nanoparticle	bind specifically to the endothelial transmembrane inflammatory proteins E and P selectin	coupling between amine and NHS ester	nanoparticles accumulated in the brain vasculature	122
5	glucose		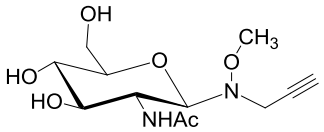	magnetic nanoparticles	Increased binding affinity with different cell surfaces	Huisgen azide alkyne cycloaddition		19
6	lactobionic acid		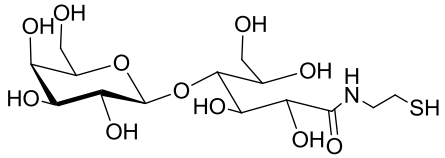	Micelles	targeting liver cancer cells through asialoglycoprotein receptors (ASGP-R)	thiol-disulfide exchange reaction	un-coating in a reductive environment (mimicking the cell interior)	40

7	Rhamnose	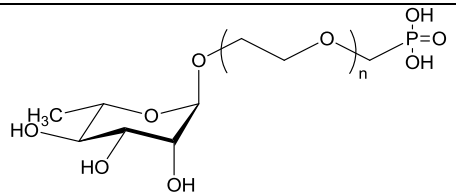	Fe_3O_4 nanoparticles	targeting of human skin cells	binding of phosphonate to Fe oxide		41
8	Disaccharide Moiety of Bleomycin A_5	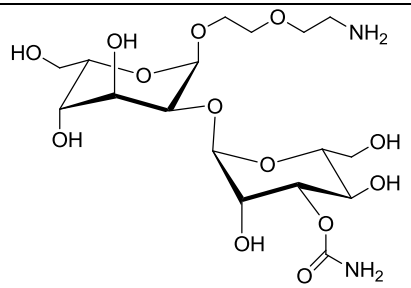	Microbubbles	selective binding to different cancer cell types	reacted with a NHS-ester coupled Cy5 dye		128
9	trehalose	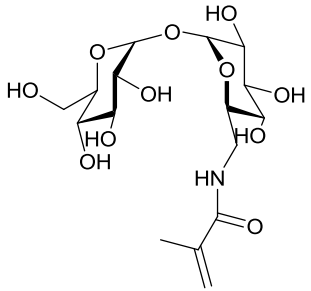	block copolymer self- assembly and siRNA complex	colloidal stability of polyplexes at high salt concentrations and specific internalization into glioblastoma cells	RAFT block copolymerization, with aminoethylmethacrylamide	the amount of siRNA delivered can be controlled	131

10	starch		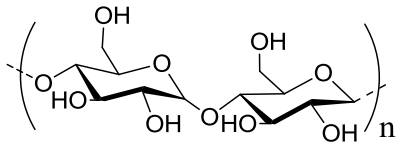	copper nanoparticles	lower toxicity	reduction of copper nitrate solution by ascorbic acid, starch as stabilizer for the nano-particle	excellent bactericidal action	132
11	Hydroxyethyl starch (HES)		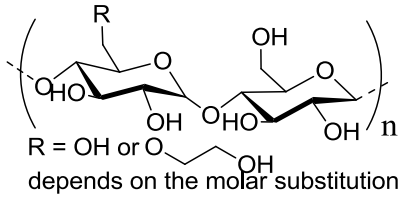 R = OH or depends on the molar substitution	DNA-polyplexes micelles	reduced unspecific cell uptake	Schiff base formation and reductive amination	deshielding of the nanocarrier possible	24,77
12	chitosan	a	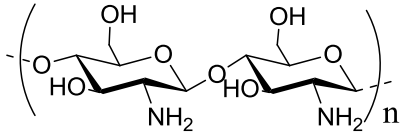 $M_w \sim$ 47kDa	poly lactic-*co*-glycolic acid nanoparticle	significantly increased (>5-fold) uptake by MCF-7 cells	electrostatic interactions		133
		b	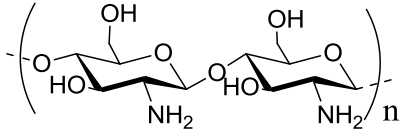 Molecular weight of 100,000 g/mol	hyaluronic-paclitaxel nanoparticle	protection of the payload	electrostatic interactions	pH responsive release of paclitaxel	134

		c	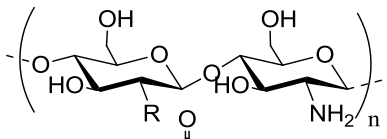 R = NH_2 or HN(C=O)CH_3 depends on the deacetylation degreeN > 75% deacetylated	silver nanoparticle	lower toxicity	chitosan as a stabilizer during preparation	higher rate of killing cancer cell compared to PEGylated gold nanorod	135
		d	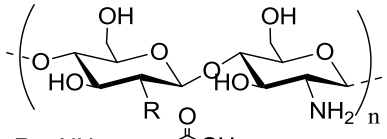 R = NH_2 or HN(C=O)CH_3 depends on the deacetylation degreeN degree of deacetylation=82.7%; M_W = 250,000	gold nanoparticles	low unspecific cell uptake, enhanced stability and tumor targeting ability	glycol-modified chitosan is used as reducing agent for Gold(III) chloride *in situ*	tomography of liver tissues with metastatic cancer	136
13	Hyaluronic Acid	a	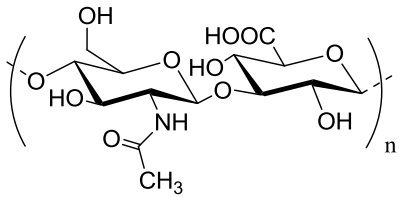	micelles prepared from branched poly (ethylene imine)	Increased transfection efficiency and decreased cytotoxicity	reductive amination		137
		b	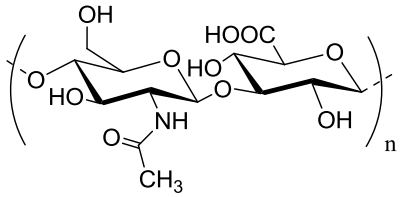	re-constituted high density lipoprotein loaded with	lower accumulation in liver and higher atherosclerotic	electrostatic interactions	efficiently suppressed the advancement	138

				lovastatin	lesions targeting efficiency		of atherosclerosis	
		c		gold nanocage	specific binding to cancer cells via interaction with CD44, release in lysosome	Au-catechol bonds	near-infrared irradiation accelerates the release	139

Starch is a polysaccharide based on glucose as the monomer, which is coupled via glycosidic linkages. Two forms of starch are found in nature: amylose, a linear and helical polysaccharide with α-1,4-glycosidic bonds, and amylopectin, a branched poly(glucose) with 1,4- and 1,6- glycosidic bonds. It is the energy storage medium of green plants and the most common carbohydrate in human diets.[140] The sugar part of glycogen, as another glucose polymer, is used to store glucose in animals with a similar structure as amylopectin, but with a higher degree of branching. Starch is used as the stabilizer during preparation of copper nanoparticles, while ascorbic acid is used as reducing agent, and copper nitrate as the source of copper (Table 1, entry 10), which will result in starch-functionalized copper nanoparticles with a reduced toxicity, while retaining high antibacterial potential against both gram negative and gram positive strains.[132]

Hydroxyethyl starch. For some applications, the degradation kinetics of starch is too fast; starch is rapidly hydrolyzed by plasma amylases. In order to balance the biodegradability and stability, hydroxyethyl starch (HES) was introduced. It is prepared by ethoxylation of the hydroxyl groups with ethylene oxide, resulting in decreased biodegradation kinetics. The degree of hydroxyethyl-substitution is expressed by the molar substitution, which is the mean number of hydroxyethyl groups per glucose unit, and ranges between 0 and 3. The higher the molar substitution, or the higher the C2/C6 ratio of hydroxyethylation, the lower the rate of metabolization.[75] Moreover, HES exhibits low hypersensitivity[75] and depressed protein adsorption[23,79-81] rendering it an interesting substitute for PEG for the preparation of stealth nanocarriers. HESylation of proteins and nanocarriers is of high potential for future drug delivery vehicles as it combines adjustable degradation with stealth properties.[141] HES with different molecular weights and degrees of substitution were coupled to poly(ethylene imine) via Schiff base formation and reductive amination (Table 1, entry 11). Subsequent complexation of the polymer with DNA generated so called DNA-polyplexes, which presented HES on their surface. These polyplexes proved to exhibit stealth properties, as the nanocarrier is protected against α-amylase. The effect of deshielding is also affected by the degree of substitution of HES, as can be seen in Figure 7.[24,77]

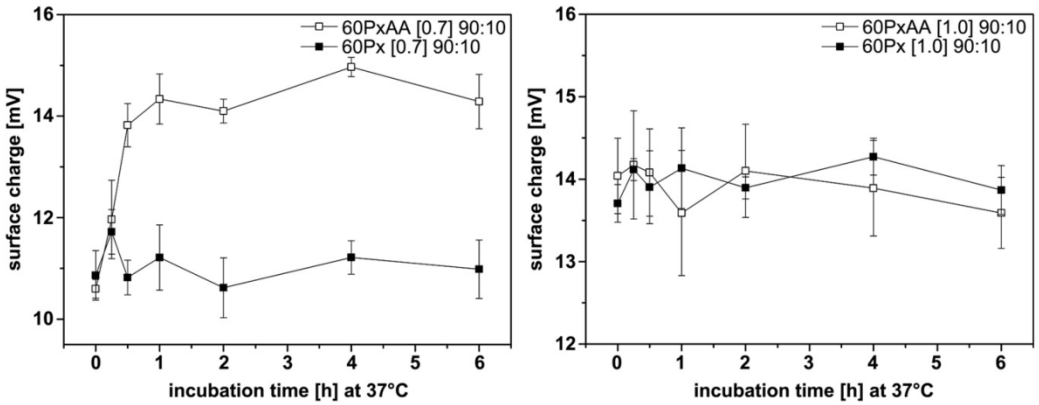

Figure 7. *The effect of alpha amylase (AA) on biophysical characteristics of HESylated polyplexes. Two different HES species are coupled with poly(ethylene imine) (Px). Both of them have the molecular weight of 60 kDa, and the molar substitution of 0.7 and 1.0 respectively. The surface charge of HES60[0.7]-shielded (left) and HES60[1.0]-shielded (right) DNA-polyplexes under the effect of AA as a function of time at 37 °C (Reprinted with permission from reference 19).*

Chitosan is a linear cationic polysaccharide, mainly prepared from the shells of shrimps or other crustaceans, composed of randomly distributed *N*-acetyl-D-glucosamine (acetylated unit) and glucosamine (deacetylated unit), with the ratio being referred as the degree of deacetylation.[142] Due to the cationic charges of chitosan, it can be electrostatically anchored onto the surface of anionically charged polymers or particles, such as poly(lactic-*co*-glycolic acid) nanoparticles (Table 1, entry 12, a). Compared to the unmodified nanoparticles, the chitosan-coated particles proved a significant increased (>5-fold) uptake by MCF-7 cells, while the proapoptotic effect of chitosan providing synergistic cytotoxic activity with docetaxel, an anti-mitotic chemotherapeutic.[133] In another work, chitosan was adsorbed to the surface of nanoparticles, which were formed by the self-assembly of hyaluronic-paclitaxel conjugates, by electrostatic interaction (Table 1, entry 12, b). This enables the protection of the ester bond between hyaluronic acid and paclitaxel at acidic pH, and allows a controlled *in vitro* release of paclitaxel from the nanocarrier, which makes it suitable for oral administration.[134]

Nanoparticles based on effective Au and Ag photothermal transducers can be used to trigger localized hyperthermia of tumors. Chitosan has been used for the surface functionalization of silver nanoparticles (Table 1, entry 12, c), and gold nanoparticles (Table 1, entry 12, d). To a mixture of aqueous solutions of trisodium citrate, ascorbic acid, chitosan, and preformed Ag nanoparticles, a solution of $AgNO_3$ was added dropwise, and chitosan surface functionalized Ag nanoparticles are obtained. These Ag nanoparticles show a lower toxicity compared to PEGylated gold nanorods, which are a common hyperthermia agent.[135] Ethylene glycol-modified chitosan is used as reducing agent to produce gold nanoparticles along the polymer chain by reducing gold (III) chloride trihydrate *in situ*, as can be seen in Figure 8. The obtained gold nanoparticles exhibited stealth properties, enhanced stability and tumor targeting ability.[136]

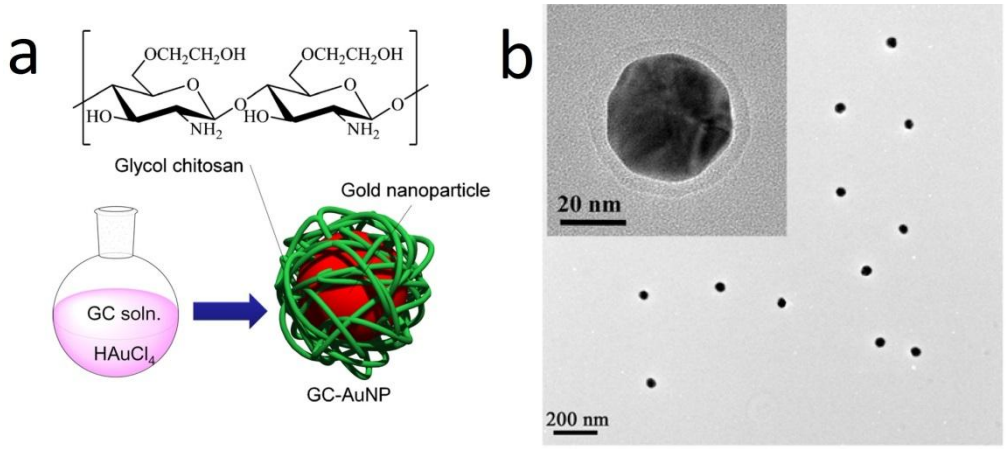

Figure 8. *(a) Chemical structure of glycol chitosan (GC) and surface-modified AuNPs (GC-AuNP). (b) TEM images of GC-AuNP (inset : magnified images). (adapted from ref.[136] with permission).*

Gum Arabic is the dried gum of acacia tree branches and stems. As a mixture of polysaccharides and proteins, it is mainly composed of galactose (44%), rhamnose (13%), arabinose (27%), glucuronic acid (16%) and peptides (2-3%),[143] and possesses excellent emulsifying properties.[144] Gum Arabic capped gold nanoparticles (GNP) have been prepared by using the leaf extract of *Vitex negundo* as a reducing agent and gum Arabic as a capping agent.[145] Epirubicin was encapsulated in the GNP, while the surface of the GNP was functionalized by folic acid. These GNP showed increased stability at pH 7.4, together with enhanced cytotoxicity against A549 cells in comparison to free epirubicin. In another work, in-

vivo studies of gum Arabic functionalized GNP resulted in significant alterations in lung tumors in mice upon laser irradiation, including cyto-toxicity, apoptosis, decreased inflammation and angiogenesis, and enhanced lipid peroxidation.[146]

Hyaluronic acid is a polysaccharide distributed widely in all tissues and body fluids of vertebrates and is most abundantly found in the connective tissues, serves many physiological functions, including lubrication, filtering, water homeostasis, and regulation of plasma protein distribution. It is metabolized by receptor-mediated endocytosis, and subsequent lysosomal degradation.[147] Hyaluronic acid was conjugated with branched poly(ethylene imine) via reductive amination (Table 1, entry 13, a). Then, the polymer was self-assembled into micelles which were surface-modified by hyaluronic acid and proved increased transfection efficiency and decreased cytotoxicity.[137] A reconstituted high density lipoprotein loaded with lovastatin (a statin which blocks the de novo-synthesis of cholesterol) was functionalized by hyaluronic acid (Table 1, entry 13, b), through electrostatic adsorption of hyaluronic acid to a cationic lipid core of the nanoparticle. After surface-modification, the nanocarrier has lower accumulation in liver and better atherosclerotic lesions targeting efficiency, and efficiently suppressed advancement of atherosclerosis.[138] Dopamine coupled hyaluronic acid has also been used to surface functionalize a gold nano-cage (Table 1, entry 13, c), as can be seen in Figure 9.

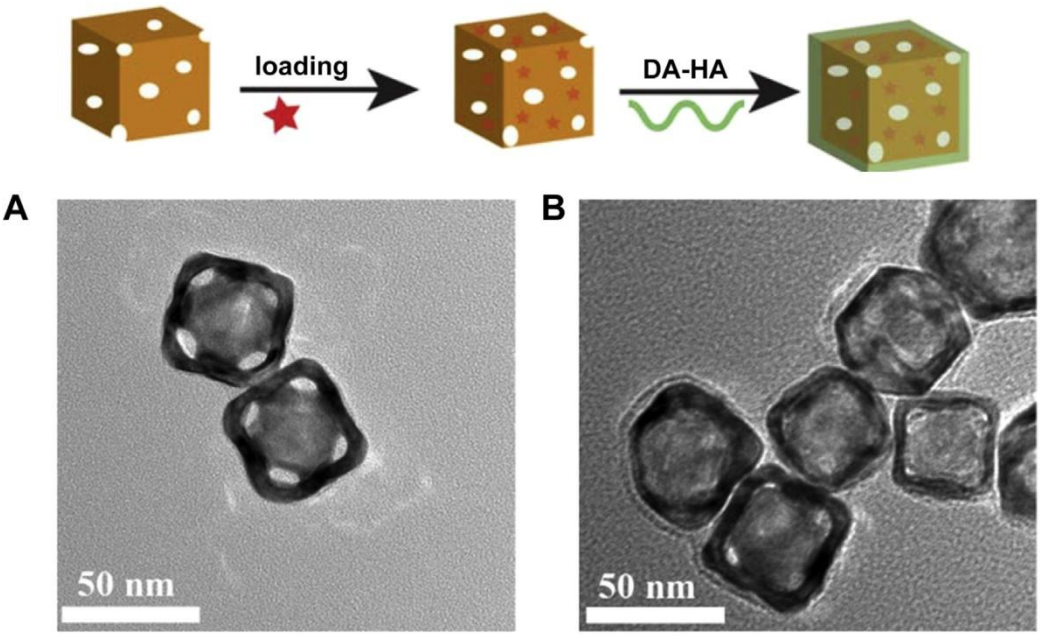

Figure 9. *Schematic representation of the coating of doxorubicin loaded gold nano-cage with hyaluronic acid, and the TEM image of the gold nano-cage before (A), and after (B) hyaluronic acid coating (adapted from reference [139] with permission).*

The hyaluronic acid layer can seal the nanoporous in the gold nanocage to protect the encapsulated dopamine, while the interaction between hyaluronic acid and the excess CD44 acceptors on the cancer cells can lead to specific cellular internalization of the nanocage.[139] After the functionalized gold nanoparticles enter the lysosomes, the degradation of the hyaluronic acid layer *in situ* will result in the release of the payload, furthermore, the release can be accelerated upon near-infrared (NIR) irradiation.

2.5 Carbohydrate-constructed Nanocarriers

Due to their outstanding biocompatibility, biodegradability, high diversity of chemical functionalities, and versatile biological functions, carbohydrates are also useful for the construction of nanocarriers for biomedical applications.

Amphiphilic dendrimers carrying both long alkyl chains and mono- or disaccharides as the hydrophilic part (Table 2, entry 1a, 2 and 3 with mannose, galactose, and lactose, respectively) can be formulated into vesicles by the addition of their THF or ethanolic solution into water. So called “glycodendrimersomes” (Figure 10) are generated via self-assembly of the amphiphile. They exhibited multivalent binding with lectins from both plants and humans.[148]

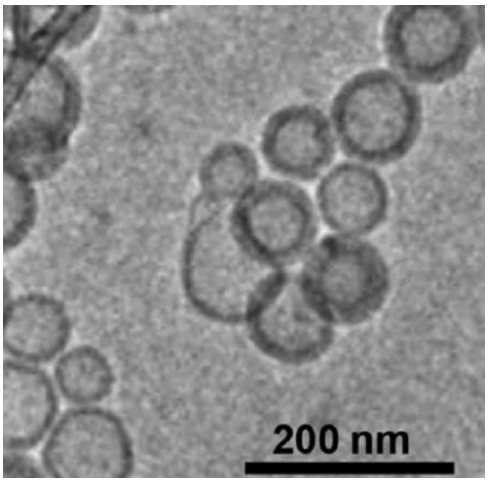

Figure 10. *Cryo-TEM images of glycodendrimersomes assembled from amphiphilic glycodendrimer composed of mannose (adapted with permission from reference[148]. Copyright 2013 American Chemical Society).*

Apart from self-assembly, emulsion techniques are interesting and versatile methods for the *in situ* formation of carbohydrate-based nanocarriers: Nanocapsules can be prepared in an inverse miniemulsion (i.e., a stable dispersion of water droplets in an organic solvent, compare Figure 11) by the polyaddition of the sugar-hydroxyls (dissolved inside the aqueous droplets) at the interface to strong electrophiles. Mannose-nanocapsules were prepared by the polyaddition of mannose to toluene diisocyanate (TDI) which occurs exclusively at the interface of a water-in-oil

miniemulsion (Table 2, entry 1, a). By the inverse miniemulsion technique, hydrophilic guests can be encapsulated with high efficiencies in the aqueous core of the capsule if they do not take part in the polyaddition reaction. After intravenous injection mannose nanocapsules are preferentially deposited in the lung.[149]

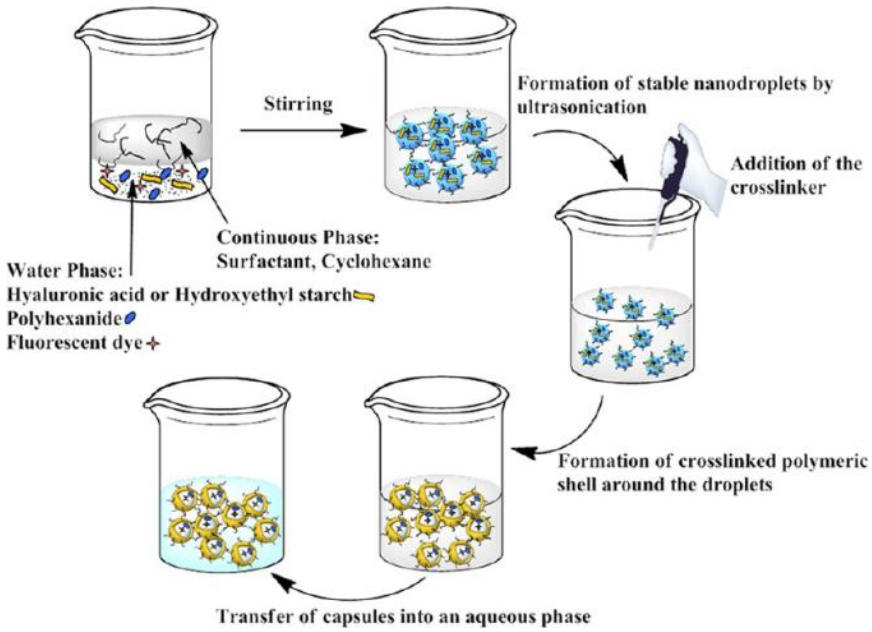

Figure 11. *Schematic illustration of the nanocapsule formation through interfacial polyaddition in the inverse miniemulsion system with hyaluronic acid as the polyol component and toluene diisocyanate (TDI) served as the bifunctional electrophilic crosslinker (Reprinted with permission from reference[150]. Copyright 2013 American Chemical Society).*

Water-soluble potato starch has been used to prepare nanocapsules (Table 2, entry 7a) by the above mentioned inverse miniemulsion technique, while silver nanoparticles were generated *in situ* in the core to serve as an antibacterial agent.[151]

HES with a molecular weight of M_w = 200,000 g·mol^{-1} and a degree of substitution of 0.5 has also been used to prepare nanocapsules through the inverse miniemulsion technique. The obtained HES nanocapsules (HES-NCs) showed a suppressed uptake into HeLa cells[86] and a preferential deposition in the liver (Table 2, entry 9).[149]

The *in vivo* plasma half-life times of the HES-NCs obtained by this strategy can be further tailored by different surface functionalization methods. PEGylation of the capsule surface by isocyanate-terminated PEG results in increased plasma half-life times with 20% and 5% of the nanocapsules remaining in the blood plasma after 24 h and 72 h, respectively.[152]

Despite the straightforward reaction setup, this strategy has limited feasibility, when used to encapsulate and protect pharmaceutical agents, which often contain nucleophiles like amines, thiols, or alcohols, and consequently will participate in the polycondensation reaction with the diisocyanate electrophile. Recent work presents strategies to use bioorthogonal reactions to generate the nanocarriers allowing the encapsulation of more complex molecules.

Two different strategies have been developed to meet this demand so far. In the first strategy, the copper-catalyzed azide-alkyne cycloaddition (CuAAC) is utilized in an oil-in-water miniemulsion: an aqueous solution of azide-functionalized sucrose and a miglyol solution of a dialkyne (bis- (propargyloxy)butane) as oil phase were allowed to react at the interface of surfactant-stabilized hydrophobic droplets.[153] Sucrose was functionalized with azide groups under Mitsunobu conditions (Table 2, entry 5). The obtained nanocapsules have a diameter below 200 nm, and a core filled with miglyol, as can be seen in Figure 12, allowing loading of the nanocarriers with hydrophobic molecules. However, the removal of the copper catalyst may be problematic with this protocol and copper-free click chemistry could be used in future studies to prevent this, which was demonstrated for non-carbohydrate systems in miniemulsion recently.[154]

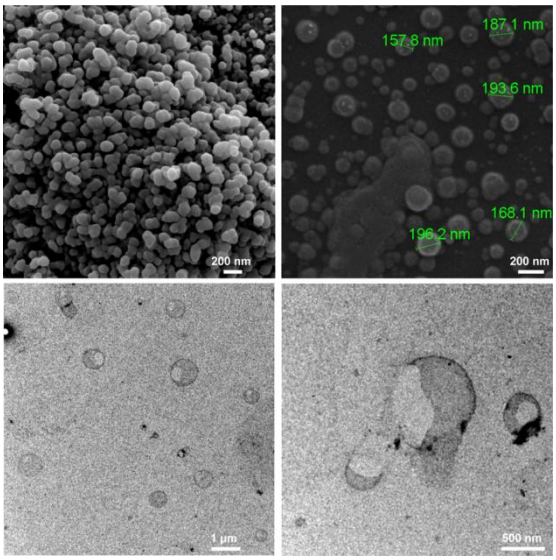

Figure 12. *SEM (top) and TEM (bottom) images of the sucrose nanocapsules generated by interfacial CuAAC polyaddition. (Reprinted with permission from reference[153]. Copyright 2012 American Chemical Society).*

In the second strategy, ofefin cross metathesis was carried out in a water-in-oil miniemulsion by the reaction of acrylated dextran dissolved in water droplets and dispersed in a cyclohexane solution of phenyldi(undec-10-en-1-yl)-phosphate as the oil phase (Table 2, entry 6).[155] The TEM and SEM images of the obtained capsules can be seen in Figure 13. The ruthenium catalyst for the olefin metathesis can be easily removed by centrifugation as it is only soluble in the continous (outer) phase. These nanocapsules offer the possibility to be degraded by enzymes that cleave dextran or the phosphate crosslinkers and in addition by pH changes due to ester cleavage.

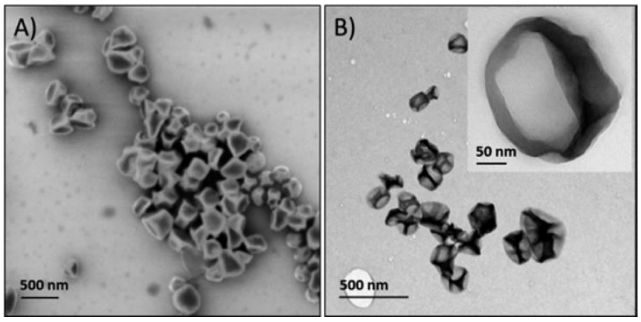

Figure 13. *(a) Scanning electron microscopy image and (b) transmission electron microscopy image of the nanocapsules prepared in a minimulsion process by olefin cross metathesis. (Reprinted with permission from reference[155]. Copyright 2014 American Chemical Society).*

Another emulsion technique has been used to encapsulate hydrophilic guests (e.g. proteins) into inverse micelles of trehalose (Table 2, entry 4, Figure 14): Dioctyl sodium sulfosuccinate (AOT) is dissolved in isooctane as the oil phase, while different proteins are dissolved together with trehalose in the water phase. After mixing of the two phases, stable water-in-oil micelle dispersions will be obtained, which can be subsequently freeze-dried by flash-freezing, and result in AOT-coated sugar-glass nanoparticles. The surfactant coating on the nanoparticle surface provides colloidal stability in organic solvent–polymer solutions. The trehalose, which transfers into gel phase under dehydrating conditions, protects the cell internal organelles and hence protect the cells in desiccation, serves to protect the protein from chemical and physical degradation during storage.[156]

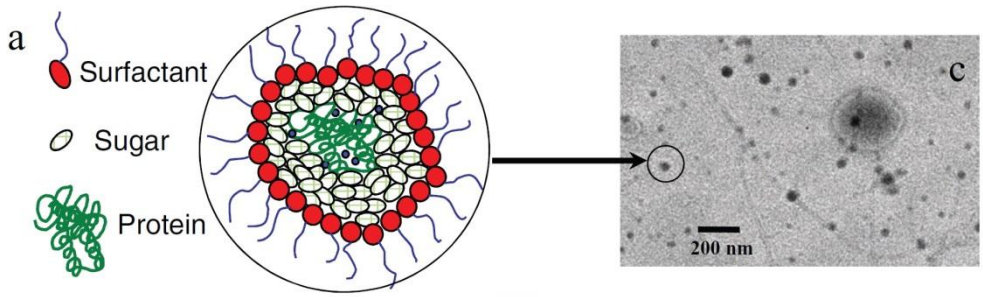

Figure 14. *Schematic representation and TEM image of sugar–glass nanoparticles. (Reprinted with permission from reference*[156]*)*

Table 2. Application of (poly)saccharides to construct nanocarriers.

#	Type of sugar		Chemical structure	nanocarrier	Properties	Chemistry	note	Ref.
1	mannose	a	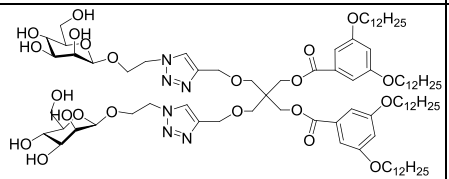	glyco-dendrimersome	multivalent binding with human and plant lectins	self-assembly in water into glycodendrimersomes	controlled over the size by adjusting the concentration	148
		b	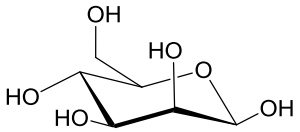	nanocapsule	encapsulation of hydrophilic guest in the core of the capsule	polycondensation with diisocyanate in a miniemulsion system	a preferential deposition in the lung	149
2	galactose		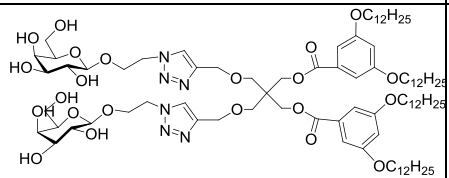	glyco-dendrimersome	multivalent binding with human and plant lectins	self-assembly in water into Glycodendrimersomes	controlled over the size by adjusting the concentration	148
3	lactose		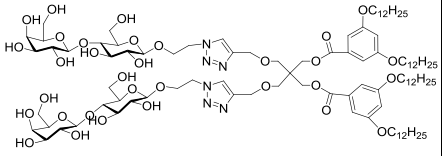	glyco-dendrimersome	multivalent binding with human and plant lectins	self-assembly in water into Glycodendrime	controlled over the size by the concentration	148

					rsomes		
4	trehalose	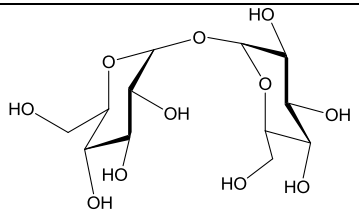	nanoparticle	protect the protein from chemical and physical degradation during storage	self-assembly into inverse micelles		156
5	sucrose	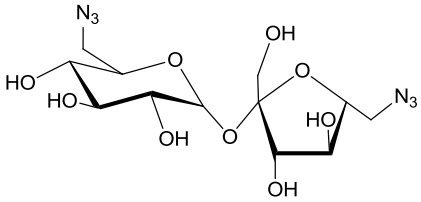	nanocapsule	encapsulation of hydrophobic guest in the core of the capsule	Huisgen azide alkyne cycloaddition	prepared by bio-orthogonal reactions	153
6	dextran	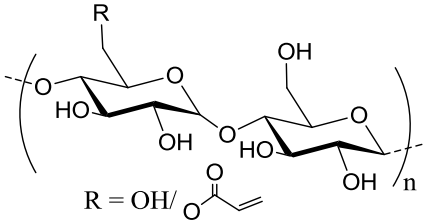 R = OH/ depends on the degree of substitution	nanocapsule	encapsulation of hydrophilic guest in the core of the capsule	olefin cross metathesis on the interface of miniemulsion	prepared by bio-orthogonal reactions	155
7	starch	a 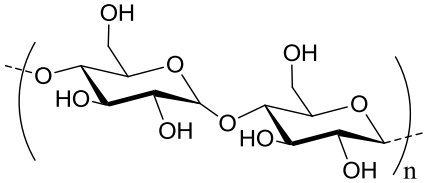 water-soluble potato starch MW 15,000 g mol^{-1}	nanocapsule	encapsulation of water soluble guests in the core and functionalization of the shell possible	polycondensation with diisocyanate in a miniemulsion system	silver nano particles in the aqueous core, as antibacterial agent	151

		b		multilayered polysaccharide vesicle	the amylase treatment of the nanoparticles allows the presence of a void / hollow inner core (resulting from the degradation starch molecules) within the fabricated particles	rehydration of a thin film of hyaluronate-starch to form vesicles		157
		c		siRNA complex	protect siRNA from enzymatic degradation	self-assembled with siRNA to form nanocarriers	efficiently induced P-glycoprotein gene silencing in the human ovarian adenocarcino macell line	158

8	Hyaluronic Acid	a	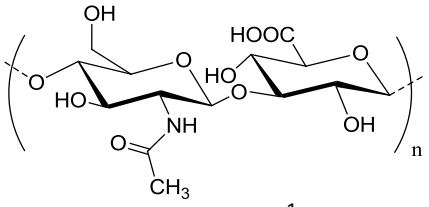 M_w =140 000 g·mol^{-1}	nanocapsule	encapsulation of polyhexanide in the core of the capsule	polycondensation with diisocyanate in a miniemulsion system	release of polyhexanide upon the contact with bacterial	150
		b	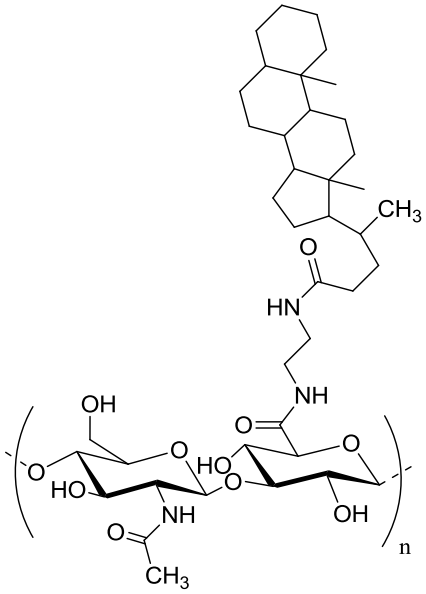	nanoparticle	specific uptake by SCC7 cancer cells, Encapsulation of doxorubicin and camptothecin	amphiphilic HA-CA is self-assembled to nanoparticles in PBS	size can be tuned between 237–424 nm , rapid drug release in the presence of enzyme Hyal-1	159-162
		c	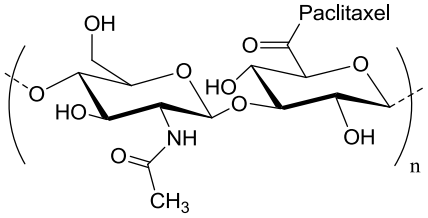	nanoparticle	higher cellular uptake than free paclitaxel in HepG2 cells	hyaluronic - paclitaxel self-assemble in water to	paclitaxel could accumulate remarkably	134

						form the nano-particles	into tumor sites after oral administration	
		d		nanoparticle	binding of the particle with CD44 over-expressed cancer cells	self-assembled in water into nanoparticles	higher therapeutic potential in the presence of a green tea polyphenol, epigallocatechin-3-gallate	163
		e		multilayered polysaccharide vesicle	incubation with hyaluronidase contributed to accelerate the release	rehydration of a thin film of hyaluronate-starch to form vesicles	drug release in the presence of hyaluronidase	157

9	HES	a	M_w = 200,000 g·mol^{-1}	nanocapsule	encapsulation of hydrophilic guest in the core of the capsule	polycondensation with diisocyanate in a miniemulsion system	suppressed unspecific uptake into HeLa cells, preferential deposition in the liver	[86], [149]

Multilayered polysaccharide vesicles are generated from starch as the core and hyaluronic acid (HA) as the shell (Table 2, entry 7b). The hydroxyl groups of starch were activated by succinic anhydride and then reacted with an excess of cysteamine by Steglich esterification (i.e. *N,N*-dimethylamino pyridine (DMAP), dicyclohexyl carbodiimide (DCC), and *N*-hydroxy succinimide (NHS) in dimethyl sulfoxide (DMSO)) to produce amino-functionalized starch with additional disulfide bonds. The amines were then reacted with the activated ester groups of HA. Rehydration of a thin film of this core-shell HA-starch conjugate in PBS will result in self-assembled nanoparticles with starch core and hyaluronic acid shell, which are subsequently treated by amylase, and result in vesicles with a hollow inner core in the end. Proteins/peptides can be encapsulated in these vesicles, when they are dissolved in the PBS buffer used. In addition, the enzymatic degradation of the HA shell by hyaluronidase (HYAL) enzyme contributed to accelerate the release of the payload.[157] In another work, starch modified with ammonium groups is complexed with siRNA by electrostatic interaction to self-assemble into nanocarriers (Table 2, entry 7, c), the starch can protect the siRNA from enzymatic degradation on its delivery route. It has high cellular uptake into a human ovarian adenocarcinoma cell line and efficiently induced P-glycoprotein (P-gp) gene silencing.[158]

Antibacterial nanodevices are interesting for coatings and wound dressings if the release of antibacterial agents can be triggered by the presence of bacteria. HA-nanocapsules (Table 2, entry 8a) containing the antimicrobial agent polyhexanide were prepared by the interfacial polycondensation with TDI in an inverse miniemulsion. They can be specifically cleaved in the presence of the enzyme hyaluronidase, a factor of pathogenicity and invasion for bacteria like *Staphylococcus aureus* and *Escherichia coli*.[150]

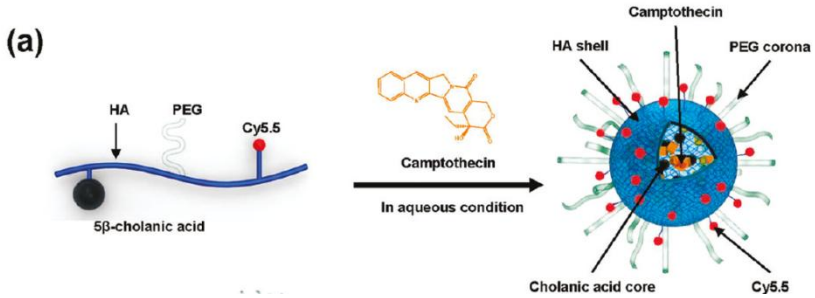

Figure 15. *Schematic illustration of the formation of drug-loaded HA-NPs. (Reprinted with permission from reference.*[160] *Copyright 2011 American Chemical Society).*

Hyaluronan-cholanic acid conjugates (HA-CA conjugates) were synthesized by the chemical conjugation of the hydrophobic bile acid (a steroic acid) to the hydrophilic HA backbone through amide formation (Table 2, entry 8b, Figure 15). The amphiphilic HA-CA can self-assemble into nanoparticles and can be loaded with doxorubicin and camptothecin, both strongly cytotoxic compounds, and exhibited an efficient intracellular uptake into SCC7 cancer cells. The size of the nanoparticles was varied between 200 and 400 nm by varying the degree of substitution. Enzyme-triggered drug release was induced by the enzyme Hyal-1, as can be seen in Figure 16.[159-162]

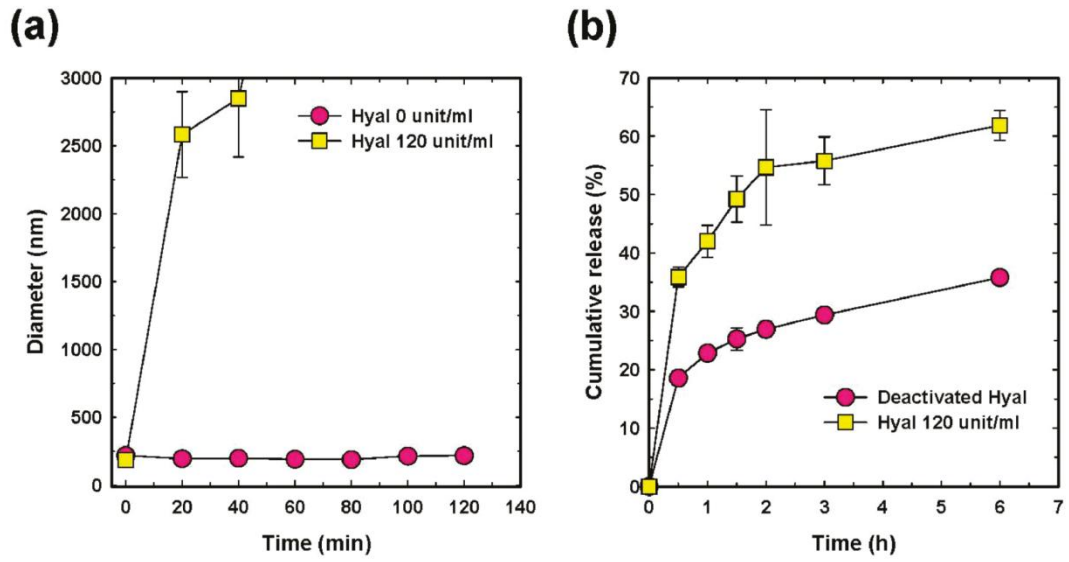

Figure 16. *(a) Particle size changes of P-HA-NPs and (b) release patterns of CPT from P-HA-NPs in the presence and absence of Hyal-1. Error bars represent the standard deviation (n = 5). (Reprinted with permission from reference[160]. Copyright 2011 American Chemical Society).*

Esterification between hyaluronic acid and paclitaxel, a mitotic inhibitor used in cancer chemotherapy, was conducted via dicyclohexyl carbodiimide (DCC) coupling in anhydrous DMSO (Table 2, entry 8c). These conjugates then self-assemble in water to nanoparticles, which demonstrated higher cellular uptake than free paclitaxel against HepG2 cells, a human liver carcinoma cell line. The oral administration of this nanoparticles can result in remarkable accumulation of paclitaxel into the tumor (Figure 17).[134]

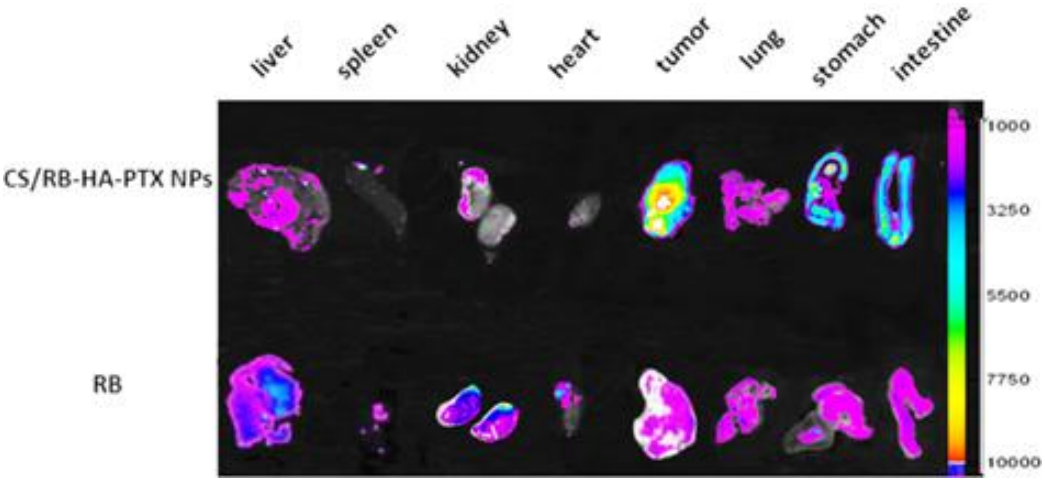

Figure 17. *Ex vivo fluorescence intensity images of the tumors and major organs after oral administration of rhodamine B labelled hyaluronic acid-paclitaxel nanoparticles (CS/RB-HA-PTX CNPs) and free Rhodamine B (RB). (Taken from reference [134] with permission).*

Amphiphilic hexadecylated polysaccharides were synthesized (Table 2, entry 8d) and self-assembled in water into nanoparticles. Doxorubicin can be encapsulated in these nanoparticles, which showed specific binding with CD44 over-expresseing cancer cells. Higher therapeutic potential in the presence of a green tea polyphenol, epigallocatechin-3-gallate, was also observed for this nanoparticle system.[163]

Other polysaccharides like cellulose and chitin, which intrinsically are water insoluble, have also been used to construct nanocarriers. In some cases, their water solubility has been increased by chemical modifications, for example, carboxymethylation. Carboxymethyl cellulose has been conjugated with docetaxel and Poly(ethylene glycol) through acetylation, self-assembled into nanoparticles, which was stable against dilution, and induced significantly higher toxic effects against EMT-6 murine mammary carcinoma cells and murine Pan02 tumors cells.[164] Carboxymethyl chitin nanoparticles have also been prepared by crosslinking of the polysaccharide with $CaCl_2$ and $FeCl_3$.[165] The obtained nanoparticle showed anti-bacterial activity by itself, and a sustained and controlled release of the payload. While different functions are enabled by cellulose and chitin, the intrinsic low water solubility and poor bio-degradability in animals rendered them to be used more as wound dressing, scaffolds for tissue engineering and medical implants.[166,167]

It is the aim of this work to prepare sugar based nano-capsules, systematically evaluate their encapsulation efficiency of the payload, the interaction with plasma protein and different cell lines, the pharmaceutical behavior (in-vivo plasma halftime), the specific targeting effect, and the possibility to prepare the capsule by bio-orthogonal chemistry.

3. Tailoring the stealth properties of biocompatible polysaccharide nanocapsules

A part of this work in this chapter has been published in Biomaterials (Kang B, Okwieka P, Schöttler S, Seifert O, Kontermann RE, Pfizenmaier K, Musyanovych A, Meyer R, Diken M, Sahin U, Mailänder V, Wurm FR, Landfester K, Biomaterials. 2015;49:125-34)[168] and altered for this thesis with permission. I developed the synthesis, prepared all the related samples, and conducted the characterization concerning DLS, SEM, TEM, NMR, release, fluorescamine assay; the in-vitro, in-vivo characterization and the protein adsorption assay were conducted by the collaboration partners, which are acknowledged after each corresponding contribution.

Introduction

As a rapid growing interdisciplinary research field, nanomedicine has extended the number of possible therapeutic methods, including nanobiosensors[169], nanovaccination[170,171], nanoparticle related imaging[172], nanodrug carriers[173,174], etc. Among these many potential applications, nanocarriers for targeted drug delivery are a major research field due to promising therapeutic effects, e.g. specific cell targeting, protecting the drug simultaneously on its way to the desired site, and the controlled release of the delivered cargo[175,176]. Of utmost importance for targeted delivery and release are the functional properties of the nanocarrier itself: unspecific cell-uptake has to be prevented, and the carrier needs to exhibit long blood circulation half-life in order to achieve enrichment and selective, targeted activity at the diseased tissue. High drug loading capacity is needed to maximize therapeutic effect. In addition, the nanocontainer should be biodegradable, but only subsequent to uptake and release of the bioactive principle at the target site. Finally, of equal important is the precise quantification of the chemistry of nanocarrier synthesis, to allow systematic investigation and understanding of the factors, which influence the performance of the system. Many studies have so far addressed the question of suitable targets and provide a large toolbox of targeting structures[177-189]. In contrast,

information on the development of new synthesis mechanisms for the nanocarrier platform itself is sparse. The performance of the whole targeting system is often hindered by properties of the nanocarrier itself[190-193], which often possesses one or more of the setbacks like low stability, cytotoxicity, no precise quantification (of functional groups, drug loading, etc.), unspecific interaction with healthy cells, and short plasma half life time.

In this study, miniemulsion was chosen as the preparation method, due to its outstanding performance to generate nano-objects with tunable sizes, various surface functionalization possibilities, and efficient encapsulation of a payload[194]. Nanoparticles with diameters between 50 nm to 500 nm have been successfully prepared by miniemulsion, through different reaction mechanisms, including radical polymerization[195], polycondensation[196], oxidative polymerization[197], and click chemistry[198].

HES is a starch derivative, whose hydroxyl groups at the C2 or C6 positions of each glucose unit are partially functionalized with a hydroxyethyl group. It is approved for clinical application, where in most cases it is used as a volume expander for the treatment of a hypovolemic shock[199]. Due to the presence of hydroxyethyl groups, the enzymatic degradation of HES is much slower compared to native starch, while the biocompatibility is rather unchanged[200]. Furthermore, it has been shown that, when HES is attached on the surface of micelles, i.e. “HESylation”, it shows similar properties as membrane-grafted poly(ethylene glycol) (PEG), i.e. “PEGylation”, with respect to prolonged blood circulation times or reduced unspecific cell uptake, often called “stealth effect”[24,25].

In the present study, we investigated the combination of both strategies: first, HES-NCs have been prepared by interfacial polyaddition in an inverse (water-in-oil) miniemulsion with diameters ranging from 150 to 250 nm. Then, the surface of these polysaccharide nanocapsules was further functionalized with PEG via different chemistries: either the coupling of PEG was conducted within the organic phase directly after the polyaddition, or the bare HES-nanocapsules were transferred into an aqueous dispersion and subsequently PEGylated. Both strategies were compared with respect to toxicity, stability in long time storage, protein adsorption, cell uptake *in vitro*, and plasma half life time *in vivo*. In addition, a detailed

investigation of every step in the reactions was carried out to allow a precise quantification of functional groups and added PEG chains on the nanocontainers.

3.1 Results and discussion

Synthesis and Characterization of HES-NCs.

An inverse miniemulsion (water-in-cyclohexane) was used to prepare hollow nanocontainers based on crosslinked HES. These nanocontainers can be loaded with high efficiency with hydrophilic substances. The formation of a crosslinked polymer shell around the aqueous droplet template was achieved by the efficient nucleophilic addition of HES's hydroxyl groups with the electrophile toluene diisocyanate (TDI) (Scheme 2).

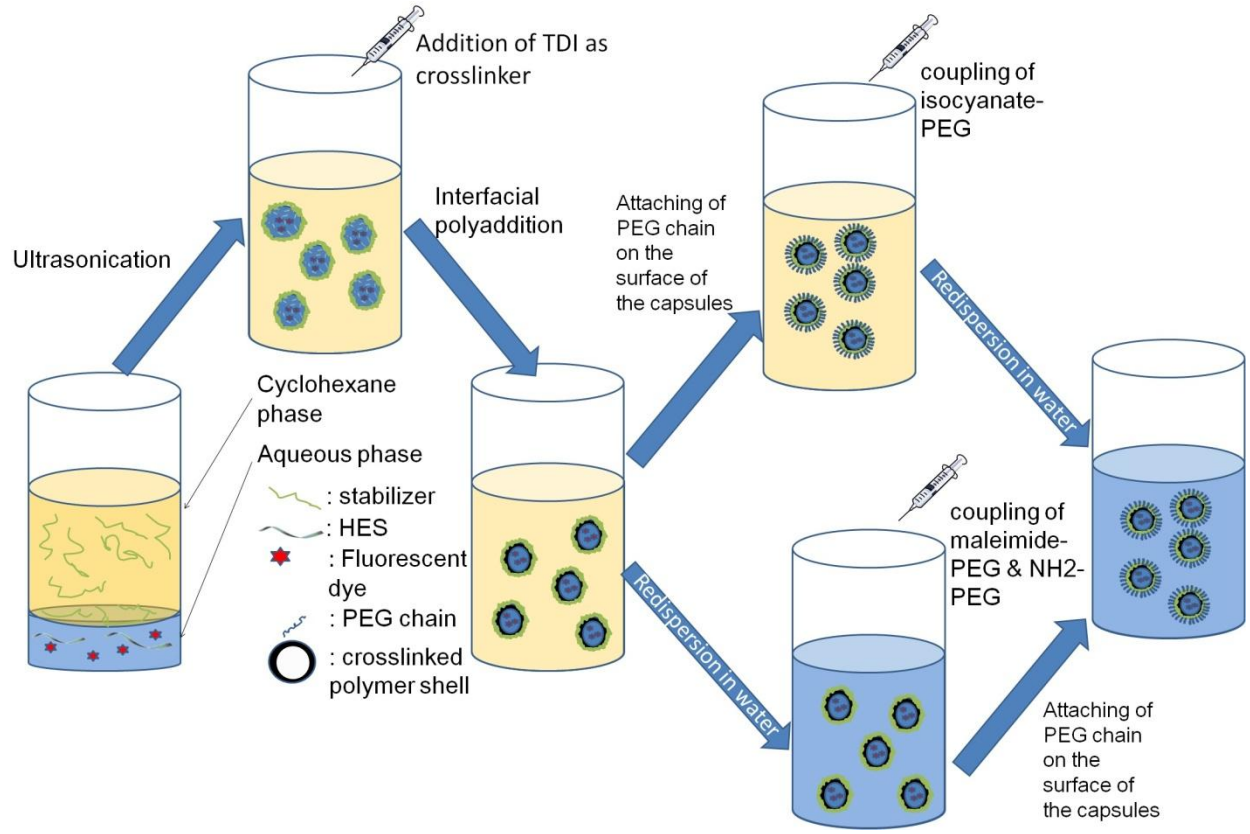

Scheme 2. *Illustration of the procedure for preparation of HES-NCs, followed by different PEGylation strategies.*

HES and the model drug (here SR101) were dissolved in water and dispersed via ultrasonication in the organic phase to form stable nanodroplets. To this stable

miniemulsion, TDI was added slowly as a crosslinker over a period of several minutes; the reaction between hydroxyl groups of HES and the isocyanate groups leads to the polyaddition of these two monomers at the droplet's interface and the formation of a crosslinked polysaccharide shell. As shown in Table 3, Figure 18 and Figure 19, the obtained capsules have a large aqueous core to polymer ratio, and consequently a large payload which is usually loaded in a nearly quantitative manner.

Table 3. Nanocapsules prepared by different HES molecules.

#	Properties of the HES		Radius/nm (size distribution)	Fluorescent dye leakage after one month of storage(%)
	Mn(kDa)	Degree of substitution		
1	42.41	1.0	201(28.1%)	9.1
2	8.3	1.0	190(26.2%)	5.6
3	22.02	1.0	201(24.7%)	7.4
4	66.58	1.0	193(31.8%)	8.1
5	94.16	1.0	200(28.9%)	9.9
6	196.6	1.0	206(30.6%)	8.0
7	441.7	1.0	213(22.3%)	7.8
8	78.08	0.4	217(31.7%)	7.6
9	62.23	0.7	193(25.2%)	7.3
10	55.97	1.3	199(21.1%)	8.0
11	24.99	0.2	204(32.9%)	6.4

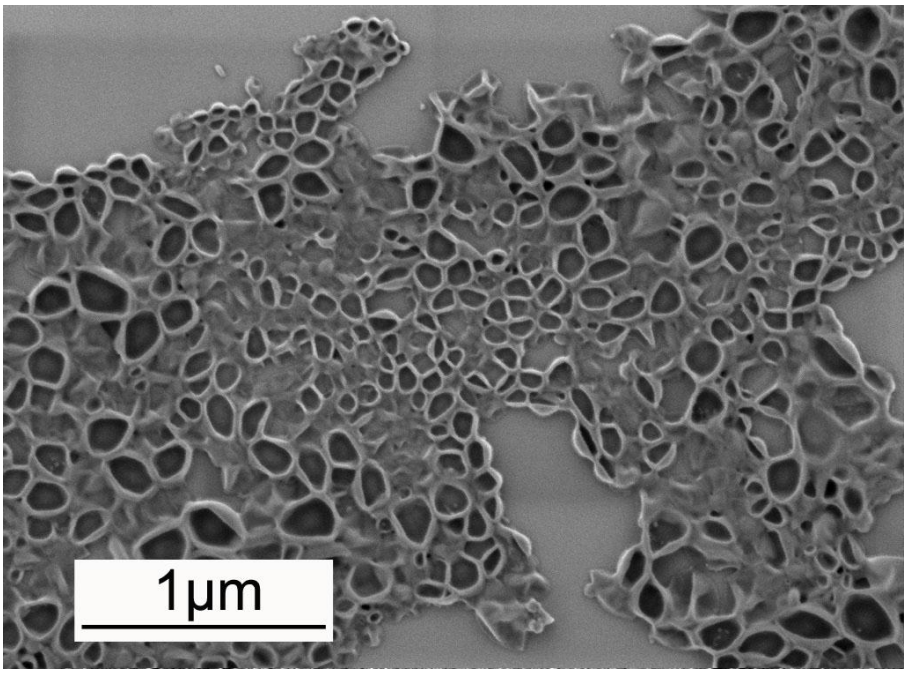

Figure 18. *SEM image of as prepared HES capsules from the cyclohexane phase.*

HES of different molecular weight and degrees of substitution were studied, and the obtained capsules are characterized regarding size, encapsulation efficiency, and permeability of the shell. It was found that the size of the capsules after redispersion in water is independent of the degree of ethoxy-hydroxylation of HES (compare Table 3). A sulforhodamine derivative (SR101), was dissolved in the water phase together with HES before the formation of capsules and the encapsulation efficiency as well as leakage of the capsules was determined (Figure 19).

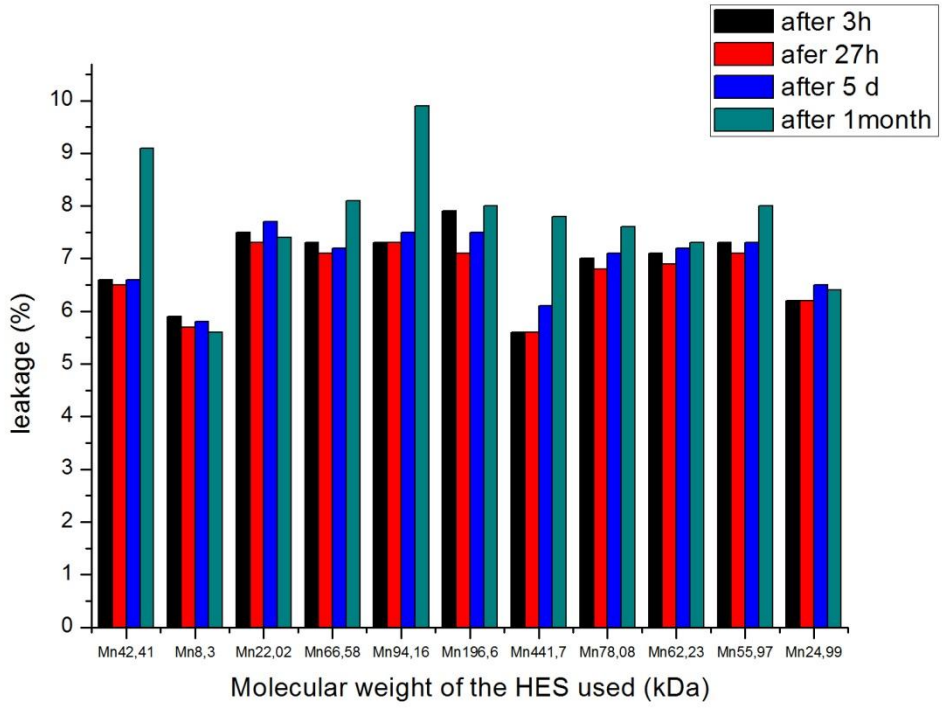

Figure 19. *Permeability of capsules prepared by using different HES molecules.*

There was a certain initial leakage detectable after 3 h storage of nanocapsules in aqueous medium after redispersion, which was probably due to the disruption of some nanocapsules during the redispersion procedure. For all nanocapsules prepared herein, the initial leakage was, however, always below 10%, which stands for an encapsulation efficiency greater than 90% in all cases. After one month storage at room temperature, the maximum increase in leakage for all capsules was around 3%, proving a high density of the nano-membrane surrounding the cargo. For further studies, HES with a molecular weight of 66.58 kDa is used. Table 4 lists the sizes and functionality of these capsules, which were used for further biological study.

Table 4. The composition and characterization of synthesized HES capsules.

Sample name	Average Diameter /nm, (SD)	Number of primary amine groups per capsule	Functional end group of the used PEG	Number of PEG chains attached
HES-1	252 (22%)	N.D.	--	--
HES-2	140(35%)	N.D.	--	--
HES-Mal	170(52%)	2000	maleimide	1300
HES-NH2	164(22%)	2000	Primary amine	2000
HES-Iso-1	172(19%)	N.D.	isocyanate	34000
HES-Iso-2	172(19%)	N.D.	isocyanate	59000
HES-Iso-3	180(22%)	N.D.	isocyanate	59000

The size of nanocarriers for drug delivery systems is usually requested to be smaller than 200 nm in order to avoid phagocytosis by the mononuclear phagocyte system (MPS)[201]. The HES-NCs prepared by the literature-reported method are usually larger than this size limit[86,202]; to lower the size of the nanocarriers, an additional ultrasonication step, as explained in the experiment part, was introduced before the addition of the cross-linker. This straightforward pre-emulsion, sonication, dilution, second sonication protocol allowed to prepare reproducibly HES-NCs with diameters below 200 nm (typical diameters from DLS and TEM are 140-150 nm, see Table 4 and Figure 20, respectively).

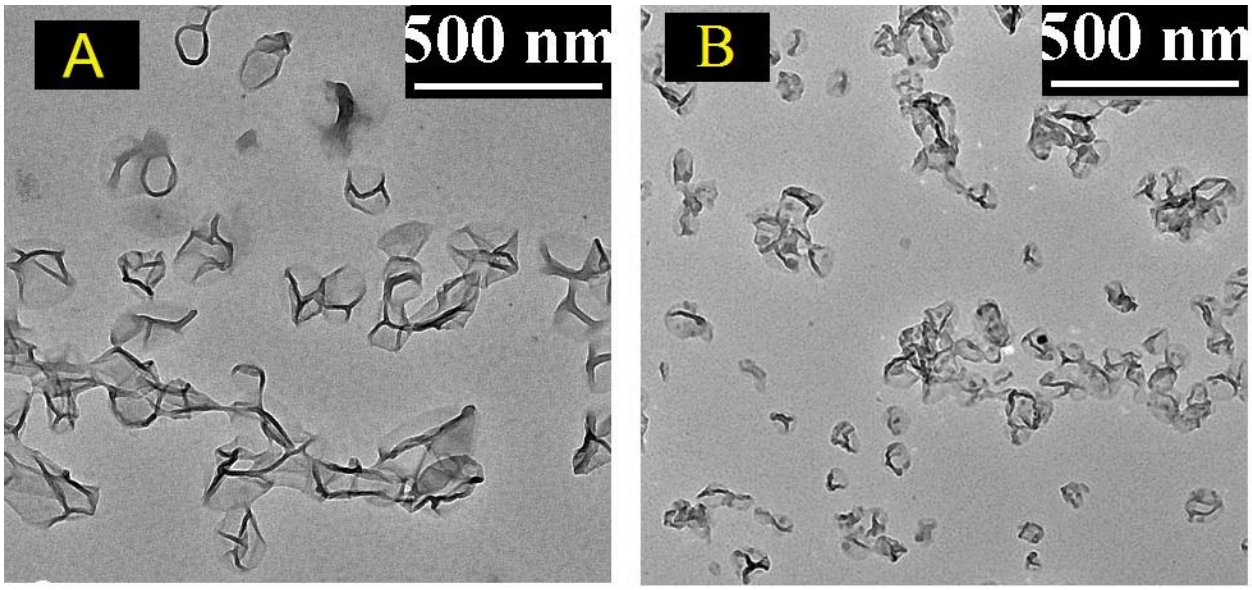

Figure 20. *TEM images of synthesized capsules: A) HES-1; B) HES-2 which has an additional sonication step to reduce the size of the nanocapsules.*

Both DLS and TEM measurement showed a decreased of radius of nanocapsules prepared via this optimized protocol (in Table 4 only HES-1 was prepared with a single sonication step).

PEGylation of HES-NCs in water.

After the shell of the nanocapsule was generated, part of the isocyanate groups of TDI were found unreacted on the surface of the nanocapsules in the cyclohexane phase. During the redispersion process into aqueous environment, these isocyanate groups will be hydrolyzed into primary amine groups. These nucleophilic groups were first used as anchors to attach poly(ethylene glycol) chains to the capsule surface by different chemistries. The number of amine groups, which come from the hydrolysis of unreacted isocyanate groups, per nanocapsule was quantified by the fluorescamine assay (as shown in Figure 21). After reaction of fluorescamine with primary amines a highly fluorescent product is generated and can be detected by UV/Vis spectroscopy[203]. A standard working function is established by taking hexylamine as a reference (Figure 22).

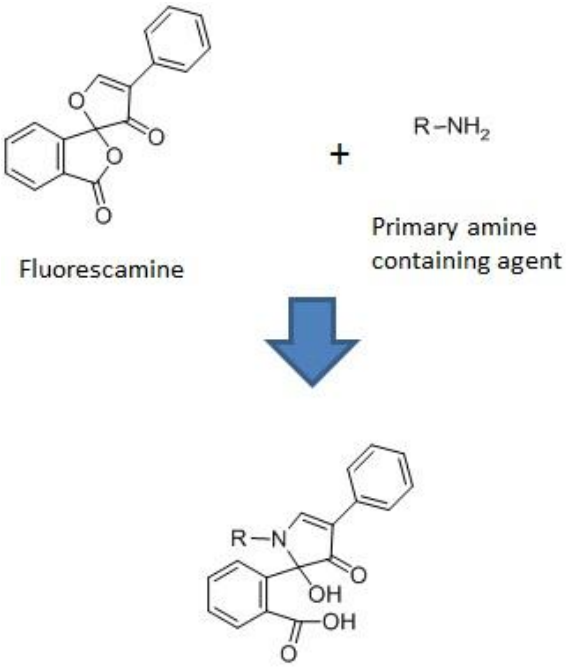

Figure 21. *Reaction scheme for the fluorescamine assay.*

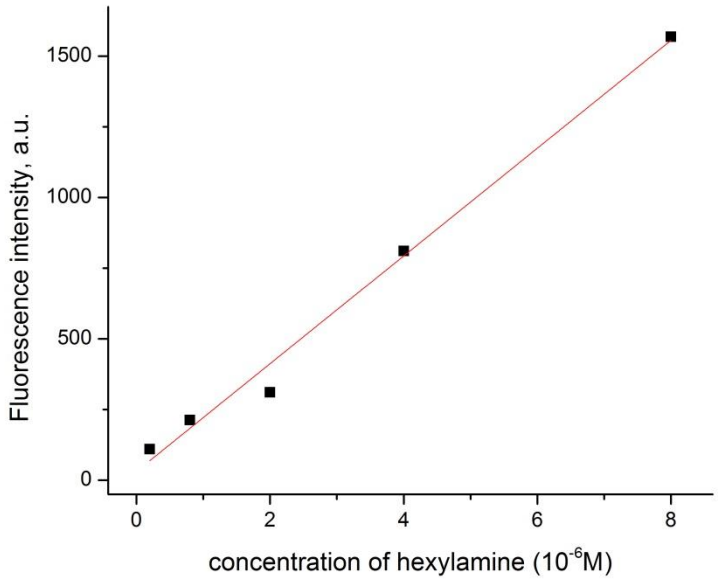

Figure 22. *Calibration curve developed from the reaction between fluorescamine and hexylamine at various concentrations.*

As can be seen in Scheme 3, two different methods have been used to couple PEG to the surface of the capsule in water phase, by using maleimide or primary amine functionalized PEGs respectively, whereby glutaraldehyde was used as linker for the latter case. The number of PEG chains per nanocapsule was quantified by ^{1}H NMR spectra of the nanocapsule dispersion compared to an internal standard (see Experimental Part for details). The number of PEG chains per capsule is listed in Table 4.

By using maleimide-PEG, ca. 1,300 PEG chains per nanocapsule (HES-MAL) were attached, while ca. 2,000 PEG chains were coupled onto the surface for NH_2-PEG via glutaraldehyde (HES-NH_2). Notably, for the small capsule prepared by two sonication steps, the number of primary amine groups per capsule was determined to be 2,000 per capsule, which means that the coupling of NH_2-PEG through glutaraldehyde was highly efficient and quantitatively reacted with all available primary amines on the surface of the capsule.

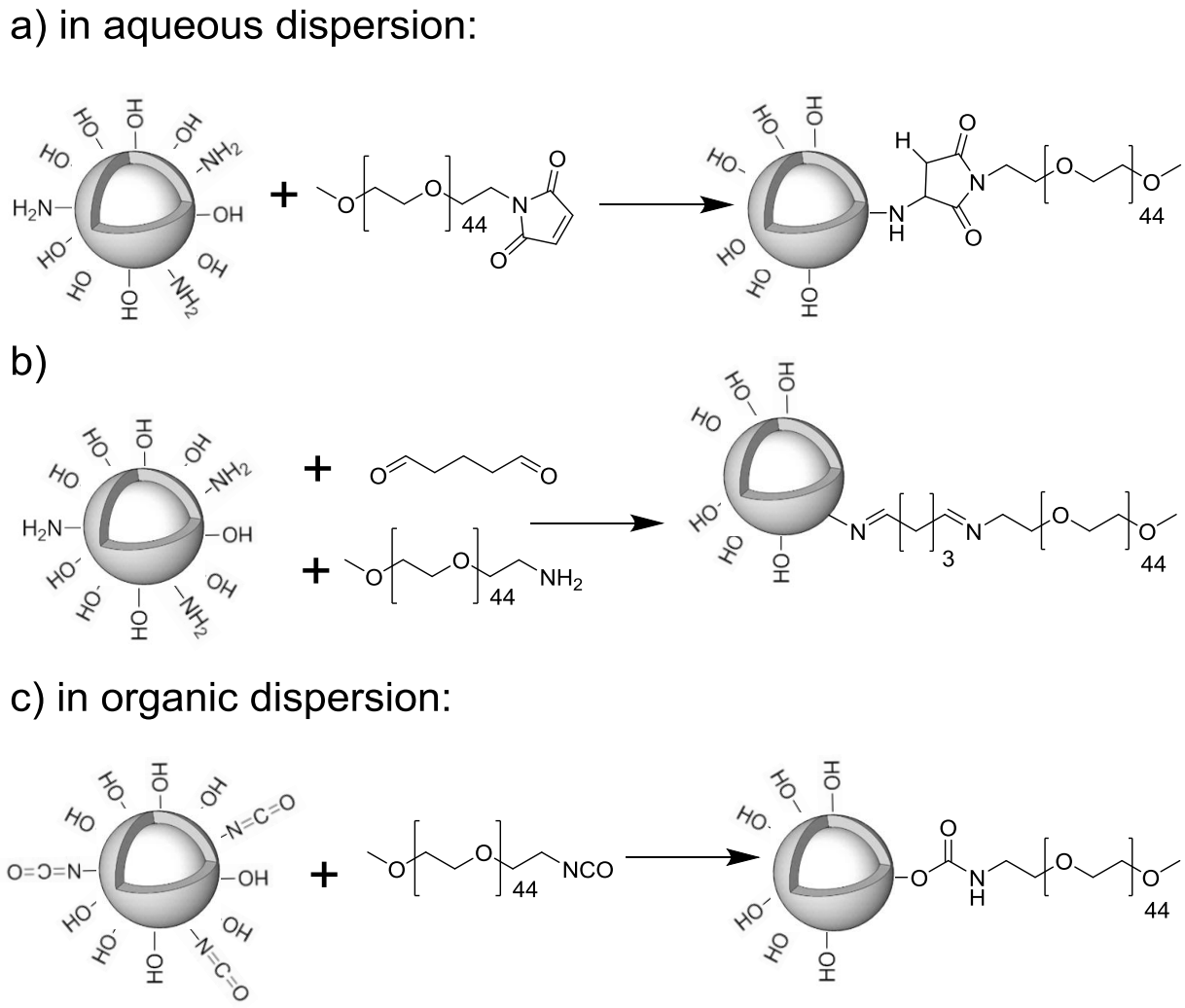

Scheme 3. *Schematic representation of three different PEGylation methods for HES-NCs. a) Functionalization of HES-NCs with maleimide-PEG. b) Functionalization of HES-NCs with NH_2-PEG. C) Functionalization of HES-NCs with isocyanate-PEG.*

PEGylation of HES-NCs in cyclohexane.

As a second approach to introduce PEG chains as a stealth layer on top of the HES-NCs, we investigated the PEGylation in organic phase via isocyanate chemistry to increase the absolute number of PEG chains on the nanocapsules surface. The residual hydroxyl groups on the surface of the capsule were used to attach monoisocyanate-functionalized PEG (Scheme 3, c). The coupling reaction is carried out under anhydrous conditions to avoid unwanted hydrolysis. In order to increase the solubility of PEG in the organic phase, it was diluted with anhydrous acetone. The percentage of acetone in the oil phase turned out to be very important for an efficient coupling reaction: a too low percentage of acetone cannot provide enough solubility for PEG, which will result in an insufficient PEGylation, while a too high acetone content will partially dissolve and destroy the shells of the capsules, making it impossible to collect the PEGylated capsules by centrifugation. For all experiments, 20 wt% of acetone in the oil phase showed reproducible results (Table 4). PEG chains were successfully coupled to HES-ISO-1 and HES-ISO-2 by this method. Quantification after coupling via ^{1}H NMR showed that for HES-ISO-1, 34,000 PEG chains were coupled to each capsule, while for HES-ISO-2 59,000 per capsule which is a significantly higher amount than mentioned above and a high influence on the stealth properties is expected (see below, Figure 24). A TEM image of HES-ISO-2 was prepared (Figure 23), as can be seen, after attaching the PEG chains, the morphology of the capsule is kept, while the interference of electron beam with surface coupled polymer reduces the contrast of the image.

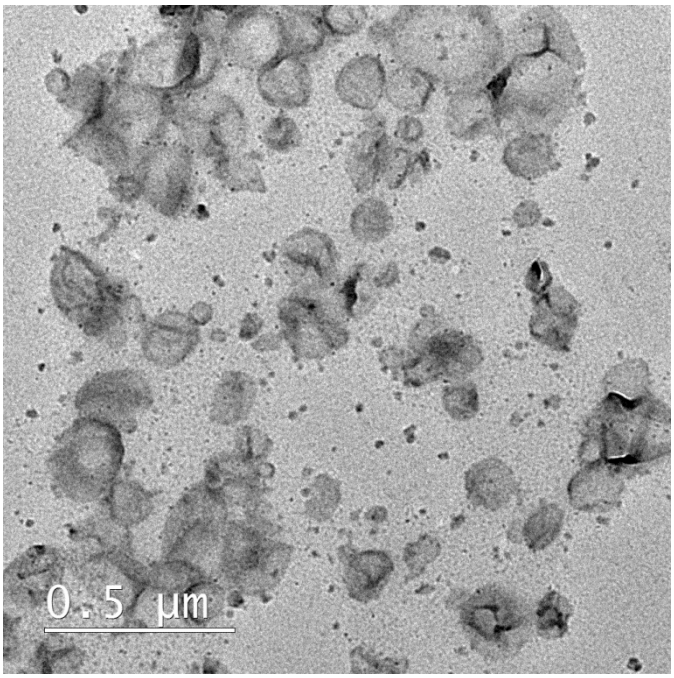

Figure 23. *TEM image of nanocapsules coupled with PEG and redispersed in water phase. The surface coupled poly(ethylene glycol) chains interference with the electron beam, and reduce the contrast of the image.*

In vivo plasma half-life.

Nowadays, HESylation is a common pathway to modify surfaces or micelles with stealth properties[24,25]. A detailed investigation of colloidal objects based on HES, however, is missing. Moreover, we sought to potentially improve these basic stealth properties of HES by additional PEGylation of HES capsules. Therefore, we compared the pharmacokinetic properties of unmodified HES-NCs with several samples of PEGylated HES-NCs (see above) and measured their plasma half-life time *in vivo*, as can be seen in Figure 24. Contrary to expectations of sufficient stealth properties of HES on its own, the unmodified HES-NCs were rapidly cleared from the blood plasma with less than 2% remaining after 2 h after the injection. This rather short plasma half-life of the unmodified nanocapsules could be due to the poor mobility of the HES chains after crosslinking or due to the presence of too many urethane bridges in the shell. To increase the plasma half-life, we combined the positive properties of HES such as biodegradability and easy handling concerning the formation of loaded- nanocapsules with the known stealth properties of PEG. As can be seen in Figure 24, compared to unmodified HES2, the circulation time of both HES-MAL and HES-NH_2 was significantly prolonged. Furthermore, when we compared the circulation time between HES-MAL and HES-NH_2, a trend of increased circulation time as a result of increased surface PEG density became apparent, too. In order to further increase the plasma half-life, a higher density of surface coupled PEG chains will probably be needed. Since the measured surface density of primary amines was also 2000 per capsule, we have consumed all the available primary amine groups for capsule HES-NH_2. Therefore, a new method is needed in order to further increase the plasma half-time of the nanocapsules.

Subsequent plasma half-life studies showed that the circulation time of HES-ISO-1 was substantially enhanced compared to HES-MAL and HES-NH_2, with 10% of the fluorescent capsule signal staying in the blood plasma after 24 h, and 72 h after injection, still 2% of capsules were detectable. With an increased surface PEG density, the plasma half-life of HES-ISO-2 was further prolonged, with 20% and 5% of capsules remaining in the blood plasma after 24 h and 72 h, respectively. To test the reproducibility of the long circulation capsules, HES-ISO-3 was prepared under the same condition as HES-ISO-2, and showed comparably good circulation time

too. These results show that, when the poly(ethylene glycol) chains are attached to the surface of the capsules in the right way and at the appropriate density, the combination of the biocompatible HES shell and the surface attached PEG chains can provide the system with a substantially enhanced plasma half-life, which makes the capsule system an ideal platform for targeted drug delivery.

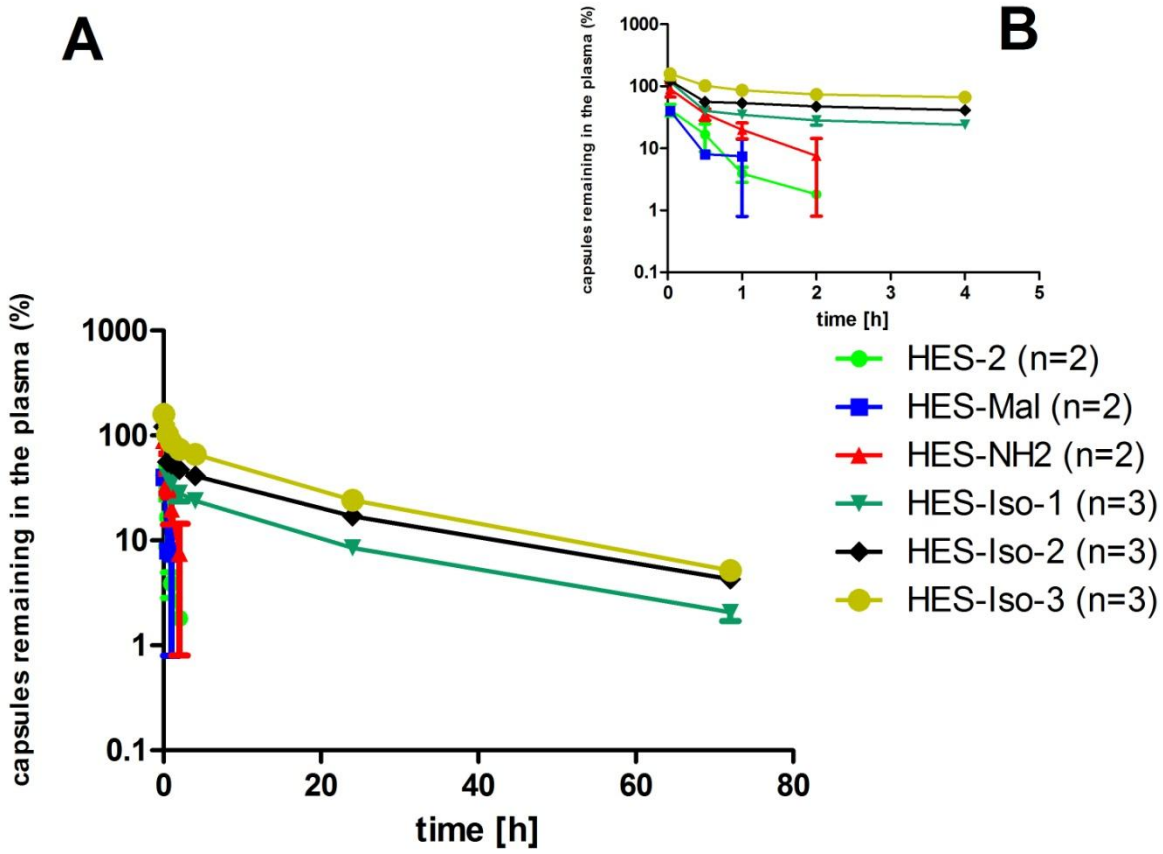

Figure 24. *Plasma half-time of different functionalized capsules. B) the zoom in of the figure is the first 4 h. HES2) the unmodified HES capsule, HES-Mal) HES capsule reacted with maleimide terminated PEG in water phase, HES-NH_2) HES capsules reacted with glutaraldehyde and amine terminated PEG in water phase, HES-ISO-1) HES capsules reacted with isocyanate terminated PEG in cyclohexane phase, HES-ISO-2) HES capsules reacted with increased amount of isocyanate terminated PEG in cyclohexane phase, HES-ISO-3) a repetition of HES-ISO-2 (experiments conducted by Oliver Seifert).*

Interactions of PEGylated nanocapsules with different immune cells in vitro.

One important prerequest for drug delivery systems is the depressed unspecific interaction with "normal", i.e. nonactivated/resting immune cells. In this study, different peripheral blood mononuclear cells (PBMC) were incubated *in vitro* with HES-Iso-2, and cell uptake of the nanocapsules was studied by flow cytometry under different conditions. The percentage of capsules bound to monocytes, NK cells, B and T cells is shown in Figure 25, and Figure 26, 27, 28. Monocytes are antigen-presenting cells that interact with and internalize microorganisms, e.g. bacteria, yeast, viruses, and other foreign materials such as particles, and clean them from the blood system. As can be see in Figure 25, and Figure 26, 27, 28, there is little binding between monocytes and capsule HES-Iso-2. These results not only explained the long circulation properties of these capsules, but also proved the stealth feature of the capsules avoiding unspecific interaction and uptake by immune cells.

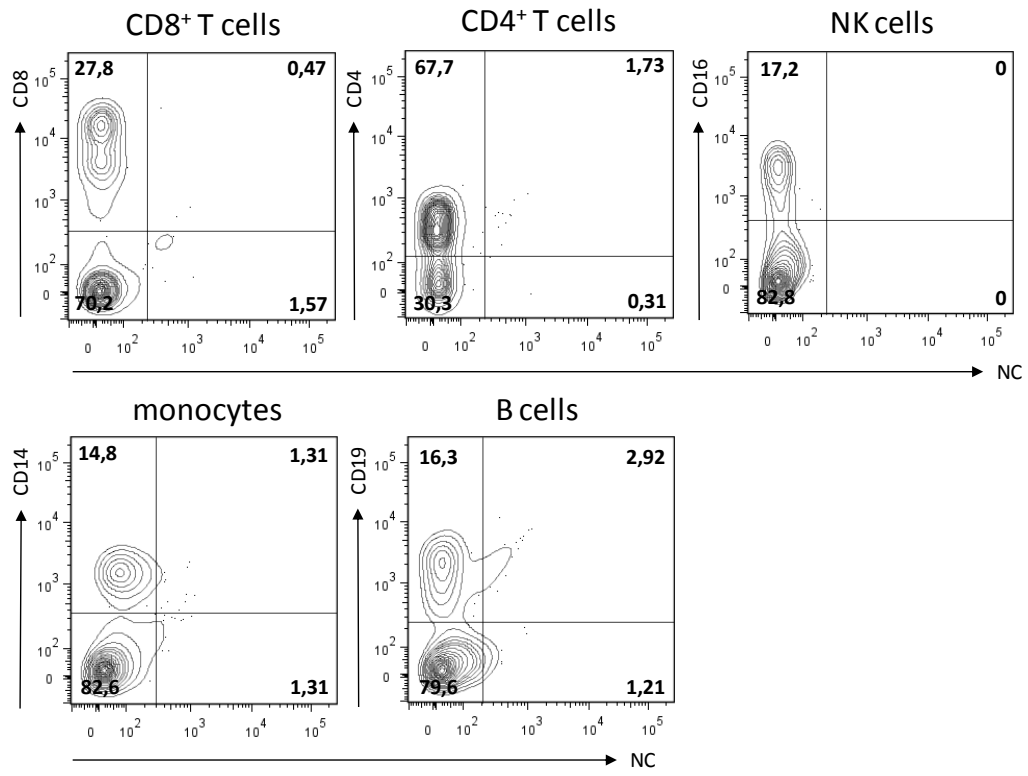

***Figure 25**. Flow cytometry analysis of HES-Iso-2 uptake into monocytes. Nanocapsule concentration was 50 µg/ml, incubated at 37 °C for 4 h (experiments conducted by Patricia Okwieka).*

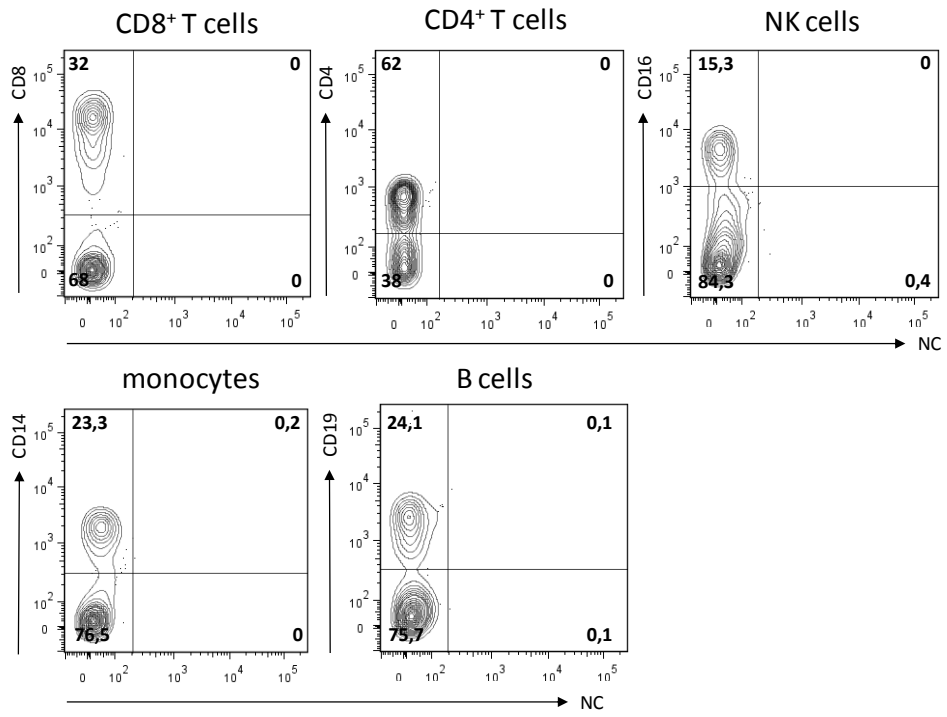

Figure 26: *Flow cytometry analysis of uptake of HES-Iso-2 into PBMCs. Nanocapsule concentration of 5 µg/ml, incubated at 37 °C for 4 h (experiments conducted by Patricia Okwieka).*

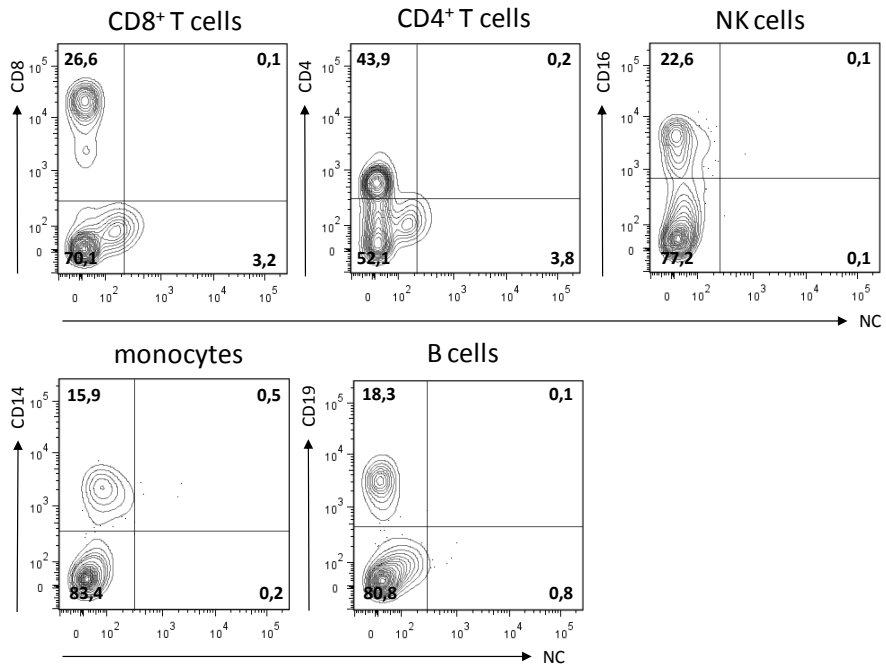

Figure 27: *Flow cytometry analysis of uptake of HES-Iso-2 into PBMCs. Nanocapsule concentration of 5 µg/ml, incubated at 37 °C for 24 h (Experiments conducted by Patricia Okwieka).*

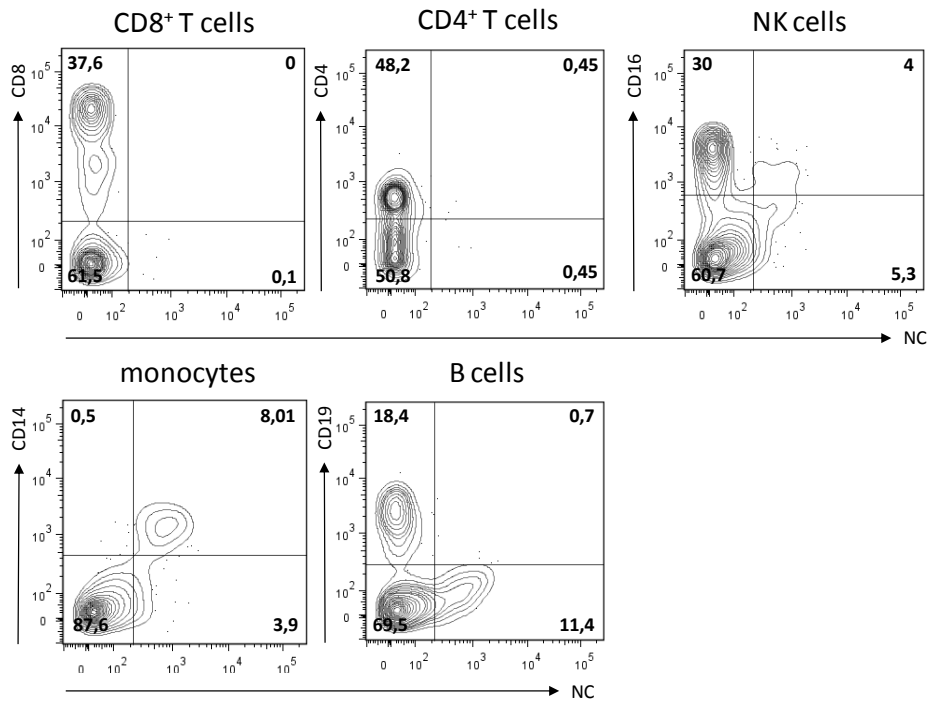

Figure 28: *Flow cytometry analysis of uptake of HES-Iso-2 into PBMCs. Nanocapsule concentration of 50 µg/ml, incubated at 37 °C for 24 h (Experiments conducted by Patricia Okwieka).*

Protein adsorption.

A quantitative analysis of proteins adsorbed to the surface of the HES capsules was performed. The capsules were incubated with human serum, thoroughly washed and the remaining proteins removed from the surface using a urea/thiourea-buffer. Quantification was then performed with Pierce 660 nm Assay (Thermo Scientific, Rockford, USA). The obtained protein amounts normalized to the nanocapsule surface area are shown in Figure 29. For the non-functionalized capsules, 1.071 mg per m^2 capsule surface were detected, whereas for the PEG-functionalized capsule the value decreased to 0.676 mg/m^2. This shows that the PEGylation of the capsule decreases protein adsorption by 37%.

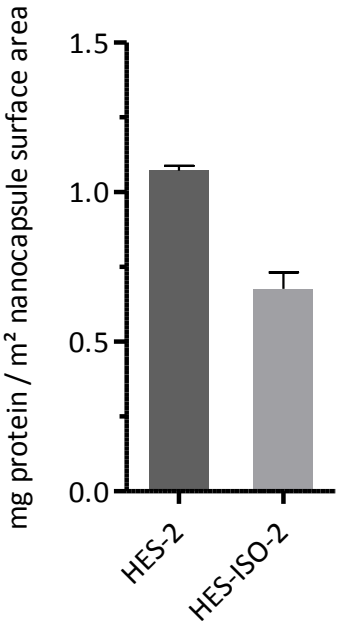

Figure 29. *Quantification of adsorbed proteins on HES-NCs with (HES-Iso-2) and without PEG (HES-2). Mean values (n=3), error bars (± SD) (experiments conducted by Susanne Schöttler).*

In-vivo biodistribution

The *in-vivo* biodistribution of both unmodified and PEGylated capsules were studied in healthy mice, as described in the experimental part. As can be seen in Figure 30, the unmodified capsules are largely trapped in the liver 30 min after intravenous injection, while PEGylated capsules remain distributed over the body through blood circulation, for more than 24 h, with relatively less accumulation in liver.

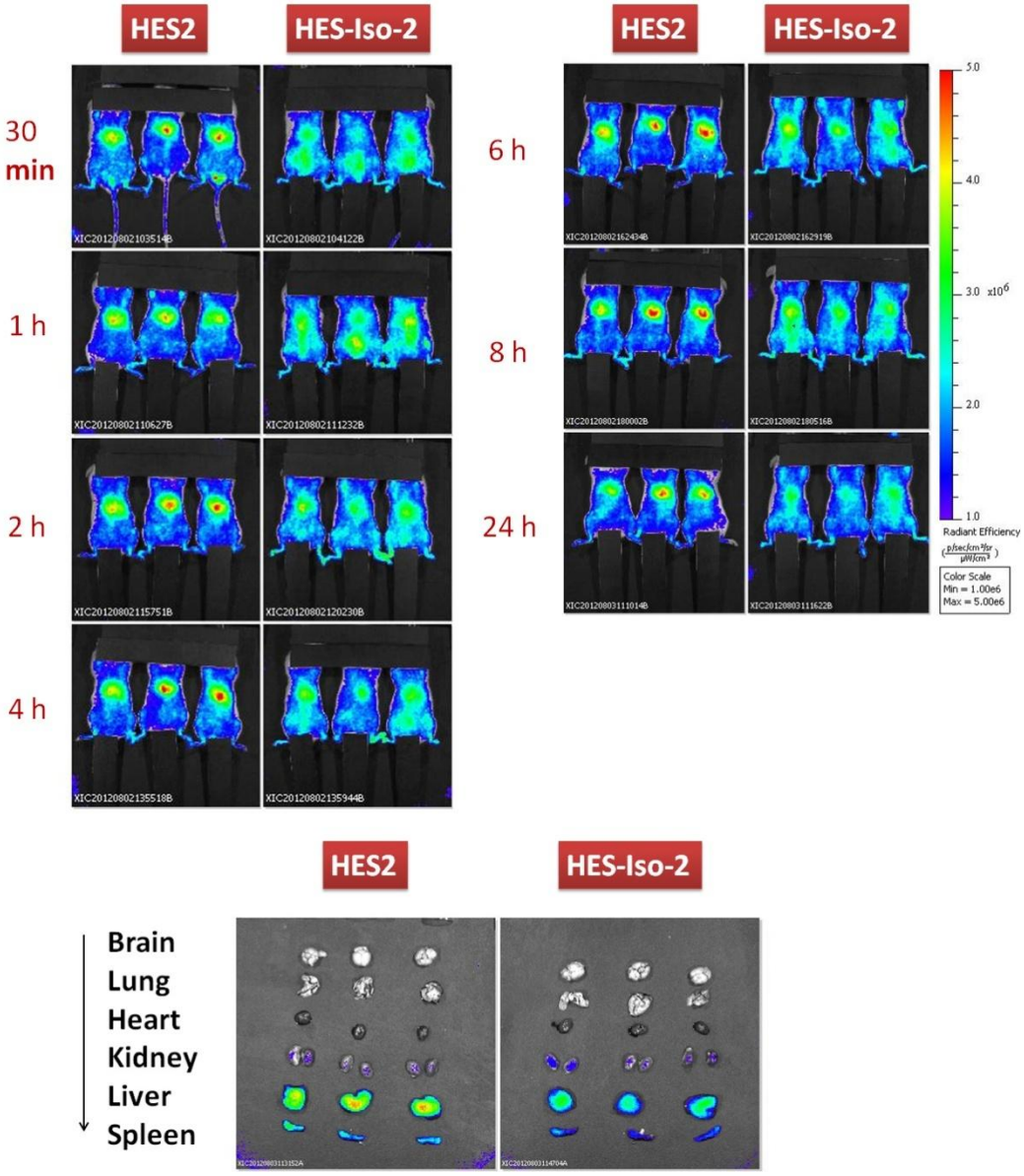

Figure 30. *Bio-distribution of unmodified (HES2) and PEGylated (HES-Iso-2) capsules. 1 mg of the capsules was injected intravenously and the fluorescent intensity was recorded after 30 min, 1 h, 2 h, 4 h, 8 h, and 24 h. The mice were sacrificed after 24 h and different organs were tested for their fluorescent intensity (experiments conducted by Mustafa Diken).*

As can be seen in Figure 30, the accumulation of capsules in liver and spleen was much lower for PEGylated sample, compared to unmodified capsules.

Discussion and conclusion

When attached to the surface of nanocarriers, HES has been proved, that it can provide stealth property[24,25]. It is due to this reason, we decided to take it as the building block for the nanocapsules. Previous work from our group[86] did show depressed unspecific uptake of HES capsules in HeLa cells. Stealth property of these HES capsules is expected, when they are injected intravenously into the blood system. However, the size of the HES capsule used in our previous publication[86], which is sample HES-1 in this work, is around 250 nm. According to the work from other groups, the size of the nanocarrier need to be small enough to avoid phagocytosis by the mononuclear phagocyte system (MPS)[201]. HES-2 is prepared for this purpose. By straightforward pre-emulsion, sonication, dilution, second sonication protocol, HES-NCs with diameters below 200 nm is prepared (typical diameters from DLS and TEM are 140-150 nm, see Table 4 and Figure 20, respectively), and this small HES capsule (HES-2) is sent for *in-vivo* plasma halftime test. Contrary to expectations of sufficient stealth properties of HES on its own, the unmodified HES-2 nanocapsules were rapidly cleared from the blood plasma with less than 2% remaining 2 h after the injection. This rather short plasma half-life of the unmodified nanocapsules could be due to the poor mobility of the HES chains after crosslinking, or due to the presence of too many urethane bridges in the shell.

To increase the plasma half-life, we combined the positive properties of HES such as biodegradability and easy handling, concerning the formation of loaded-nanocapsules, with the known stealth properties of PEG. The residual amine and hydroxyl groups on the surface of the capsules offer versatile functionalization possibilities. In this work we have coupled PEG to the capsule by reacting with both these groups. Namely, using maleimide and amine terminated PEG to couple with the amine groups on the capsule surface (HES-Mal and HES-NH_2), and using isocyanate terminated PEG to react with hydroxyl groups (HES-Iso-1, HES-Iso-2, and HES-Iso-3). It turned out that, by the coupling with amine groups we can attach maximum ca. 2000 PEG chains per capsule (HES-Mal), while the maximum density for the hydroxyl method is 59000 per capsule (HES-Iso-2). Subsequent *in-vivo* plasma halftime test showed, for the HES-NCs, an increased PEG density in this range can effectively increase the plasma halftime (see Figure 24). The HES-Iso-2 shows outstanding plasma halftime, after 24 h and 72 h, there are 20% and 5% of

capsules remaining in the blood plasma, respectively. The high plasma halftime of HES-Iso-2 is reproduced by HES-Iso-3. These results show that, when the poly(ethylene glycol) chains are attached to the surface of the HES capsules in the right way and at the appropriate density, the combination of the biocompatible HES shell and the surface attached PEG chains can provide the system with a substantially enhanced plasma half-life, which makes the capsule system an ideal platform for targeted drug delivery.

On the other hand, the plasma halftime of the PEGylated HES capsules is so outstanding, that we start to consider the possibility, whether the capsules are internalized in some of the blood cells, therefore, the fluorescent signal can stay in the blood plasma for such a long time. Based on these considerations, *in vitro* tests of HES-Iso-2 with different blood immune cells were initiated. Different peripheral blood mononuclear cells (PBMC) were incubated *in vitro* with HES-Iso-2, and the cell uptake of the nanocapsules was studied by flow cytometry. The percentage of capsules bound to monocytes, NK cells, B and T cells is shown in Figure 25, 26, 27, and 28. Monocytes are antigen-presenting cells that interact with and internalize microorganisms, e.g. bacteria, yeast, viruses, and other foreign materials such as particles, and clean them from the blood system. As can be see in Figure 25, there is little binding between monocytes and capsule HES-Iso-2. These results show that, there is little unspecific binding between HES-Iso-2 and different blood immune cells, and the origin of the long circulating properties comes from the advanced stealth property of the capsule itself.

Due to the hydrophobic interaction between the protein and the nano-particles, and the high surface tenstion of the nano-partcle itself, whenever nanoparticles enter biological fluoides like blood, proteins will spontaneously absorb on their surface, and consequently form a so called protein corona. Many researchers have proposed that the behavior of the nanocarriers in biological liquid, for example the stealth properties of nanocarrier in blood plasma, is often determined by the protein corona formed on the surface of them, instead of the intrinsic functionalization of the nanocarrier itself[204-211]. The protein corona formed on the nanocapsule self is compared between HES-2 and HES-Iso-2. The results demonstrate that we can decrease the protein absorption by 37% after PEGylation, from 1.071 mg per m^2 to 0.676 mg/m^2. By PEGylation we can decrease 37% of the protein absorption,

however, the plasma halftime is increased drastically. We believe that in this case, it is not the amount of protein absorpt, but the type of protein, which determines the stealth properties of the HES capsules. A study of the detailed composition of the protein corona on these capsules is under investigation with mass spectrometry, and will be discussed in another work in our group.

The *in-vivo* bio-distribution of HES-2 and HES-Iso-2 is compared. As can be seen in Figure 30, the accumulation of capsules in liver and spleen is depressed after PEGylation. This versatile chemical platform in combination with the outstandingly long circulation times makes the PEGylated HES nanocontainers ideal for further studies for targeted cell uptake and subsequent drug release.

In summary, interfacial polyaddition in an inverse miniemulsion system was used to prepare biodegradable, PEG functionalized nanocontainers with optimized pharmacokinetic properties suited for targeted drug delivery. In the work presented here, hydrophilic, biocompatible and biodegradable HES was reacted at the water-oil interface with TDI in order to generate a cross-linked nanocontainer that can be loaded with hydrophilic dyes or drugs. HES-NCs with different sizes and versatile chemical functionality were prepared, which have good shelf-life stability over long time storage, and are non-toxic. The surface of nanocarriers was functionalized with PEG via different chemical protocols producing nanocapsules with a variable and precisely determined PEG density. Hydrophilic drugs, fluorescent dyes, or other contrast agents can be encapsulated in the nanocontainer, which will be protected against degradation on the delivery route. The library of different PEGylated nanocapsules was investigated *in vitro* with respect to biocompatibility, protein interaction, cell uptake and *in vivo* plasma half-life time. Highly PEGylated nanocapsules did show a reduced protein adsorption and a very low unspecific cell uptake in several blood cells. As a result, these nanocontainers show a pronounced plasma circulation time in blood which is higher than typically applied liposomal formulations. This versatile chemical platform in combination with the outstandingly long circulation times makes the PEGylated HES nanocontainers ideal for further studies for targeted cell uptake, and the results will be discussed in the following sector.

3.2 Experimental Part

Materials

The isocyanate-PEG and isocyanate-PEG-isocyanate (PEG molecular weight of 5,000 g·mol^{-1}, 110 ethylene oxide units) were purchased from Nanocs Inc., USA. PBS buffer (pH 7.4, without Ca^{2+} and Mg^{2+}) was purchased from Gibco, Germany. Borate buffer (1M, pH 9.5) was produced by adjusting pH of boric acid (B6768 Sigma) water solution to the desired value by sodium hydroxide solution. HES (200k, 0.5 degree of substitution) was bought from Fresenius Kabi, dialyzed in the dialyzing tube with molecular cutting off of 14k againt MillQ water for 4 days, and subsequently freeze-dried for further synthesis. Oil soluble surfactant poly((ethylene-*co*-butylene)-*b*-(ethylene oxide)), P(E/B-b-EO), consisting of a poly(ethylene-*co*-butylene) block (M_w = 3,700 g·mol^{-1}) and a poly(ethylene oxide) block (M_w = 3,600 g·mol^{-1}) was synthesized starting from ω-hydroxypoly-(ethylene-*co*-butylene), which was dissolved in toluene after addition of ethylene oxide via anionic polymerization[212]. The anionic surfactant sodium dodecylsulfate (SDS) was purchased from Fluka. C-type-lectin (Galanthus nivalis snowdrop lectin fluorescein labeled 2 mg) was bought from BIOZOL Diagnostica Vertrieb GmbH. The fluorescent dye Cy5-oligo was purchased from BioChemica, Aldrich. DBCO-PEG4-NHS was bought from Jana Bioscience. Dimethyl sulfoxide (<50 ppm water content) was purchased from Acros Organics. Demineralized MilliQ water was used for the synthesis of nanocapsules. Polystyrene nanoparticles was prepared according to literature.[195] All the other chemicals were purchased from Sigma Aldrich, and used as received.

Characterization methods

Dynamic Light Scattering (DLS). The average size of the capsules is measured by DLS using a PSS Nicomp Particle Sizer 380. The capsule dispersion is diluted by MilliQ water to a solid content of 0.1%. The scattered light is detected at 90°, while the temperature is maintained at 25 °C.

Electron Microscopy. Scanning electron microscopy (SEM) measurements are carried out by using a LEO (Zeiss) 1530 Gemini device (Oberkochen, Germany). The samples are diluted to a solid content of 0.01% with MilliQ water, then 15 µL of the diluted sample is placed on the silica wafer and dried at room temperature overnight. Transmission electron microscopy (TEM) measurements are carried out by using Jeol 1400 device at 80 kV accelerating voltage. The samples are diluted in the same way as for SEM sample preparation. Then 2 µL of the diluted sample is placed on a copper grid, which is covered by a 5 nm thick carbon film.

Nuclear magnetic resonance (NMR) spectroscopy. ^{1}H NMR spectra of functionalized capsules are measured at 300 MHz on a Bruker Avance 300 Spectrometer.

General protocol for the synthesis of HES-NCs. HES-NCs were prepared in a water-in-oil miniemulsion system similarly to the previously published protocols.[86] An aqueous solution of HES is emulsified with cyclohexane containing a block copolymer, P(E/B-*b*-EO) as surfactant. In a typical reaction, 100 mg of the stabilizer is dissolved in 9.5 g of cyclohexane at 60 °C. The water phase consists of 1 mg of SR101 (dye acting as a model for a low molecular weight drug), 10 mg of NaCl, 100 mg HES and 590 mg of PBS buffer. 7.5 g of the oil phase are mixed with the water phase and are magnetically stirred at 1000 rpm for 30 min, followed by ultrasonication at 70% amplitude for 3 min, with a pulse of 20 s on and 10 s off (cooling the mixture with an ice bath), using a Branson Sonifier W-450-Digital and a ½" tip. Then, 85 mg of TDI is added into 2 g of the oil phase, and added dropwise (over a period of 2 min) into the formulated miniemulsion. The interfacial polymerization is allowed to proceed at 25 °C for 24 h. HES molecules with different molecular weight and degree of substitution is used, with the detailed composition listed in (Table 4).

HES capsules with sizes lower than 200 nm. The reaction is conducted in the same manner as described above, however, an additional amount of oil phase is added after the sonication step, followed by an additional sonication step before the addition of the crosslinker TDI. The oil phase is prepared by dissolving 160 mg of P(E/B-*b*-EO) in 14.5 g of cyclohexane. The water phase is mixed with 7.5 g of the oil phase, magnetically stirred at 1000 rpm for 30 min, followed by ultrasonication under the same conditions as for the preparation of larger HES-NCs. After ultrasonication, 5 mL additional oil phase is introduced into the system, and magnetically stirred for the other 30 min at 1000 rpm, followed by an additional ultrasonication step. To start the polyaddition, TDI is added into 2 g of the oil phase, and added dropwise into the miniemulsion system. The interfacial polymerization is allowed to proceed at 25 °C for 24 h.

Redispersion of HES-NCs in water. 1.5 g of the nanocapsule dispersion in cyclohexane is centrifuged at 4000 rpm for 30 min, and the precipitate is redispersed in 400 µL of fresh cyclohexane by pipetting up and down. Then, a 0.3wt% SDS solution is prepared, and filtered (sterile, with 0.2 µm pore size). 5 mL of this SDS solution is gently shaken in a sonication bath (Bandelin Sonorex, type RK 52H), while the nanocapsule dispersion in cyclohexane is added slowly. Then the whole dispersion is magnetically stirred at 1000 rpm at room temperature overnight, in an open vial, to allow evaporation of cyclohexane. The obtained dispersion is ultrafiltrated using Amicon Centrifugal Filter (Ultra-0.5, Ultracel-100 Membrane, 100 kDa), in order to remove the excess of SDS and used for further measurements.

Quantification of primary amine groups at the surface of nanocapsules. The fluorescamine (FA) assay[203] is used to quantify the available primary amine groups at the surface of the nanocapsules. A stock solution of FA is prepared by mixing 2 mg of FA and 1.5 mL of anhydrous acetone. A standard working function is established from an aqueous hexylamine solution as reference. For a typical quantification step, 25 µL of the nanocapsule dispersion in water (1wt% solid content) are added into 725 µL of boric buffer (pH 9.5), followed by the addition of 200 µL of the FA stock solution. The mixture is vortexed (Heidolph REAX2000 at maximum speed) for 30 s, and the fluorescence intensity is measured by a Tecan plate reader at 25 °C by excitation at 410 nm and detecting the emission at 470 nm. All fluorescence measurements are repeated three times.

Functionalization of HES capsules with maleimide-PEG. 12 mg of maleamide-PEG (MeO-PEG_{44}-Mal, with M_n=2,000 g·mol^{-1}) are dissolved in 1 mL of MilliQ water. 5 mL of the nanocapsule dispersion in water (1wt% solid content) are magnetically stirred, while the maleimide-PEG solution was added in one portion. The system is stirred at room temperature overnight, Millipore ultrafilter with a molecular cut off of 100 kDa is used to remove the free PEG chain after coupling.

Functionalization of HES capsules with NH_2-PEG. To 5 mL of the nanocapsules dispersion in water (1wt% sold content) 3µL of a glutaraldehyde stock solution (50% water solution) are added. After 2h at room temperature, the unreacted glutaraldehyde is removed by ultrafiltration, and 12 mg of MeO-PEG_{44}-NH_2 with M_n=2000g·mol^{-1} in 1 mL of MilliQ water are added. The reaction is allowed to proceed overnight, and the free PEG is removed by ultrafiltration.

Functionalization of the surface of HES-NCs with monoisocyanate-PEG. For a typical coupling reaction, 2 mL of the nanocapsule dispersion is centrifuged at 4000 rpm for 30 min to remove the excess of surfactant. The upper phase is discarded, while the precipitate is redispersed in 2.5 g of anhydrous cyclohexane by pipetting up and down. 16 mg of monoisocyanate-PEG (MeO-PEG_{44}-NCO, with M_n=2,000 g·mol^{-1}) was dissolved in 0.63 g (800 µL) of anhydrous acetone and added dropwise into the capsule dispersion, which is magnetically stirred at 500 rpm. The reaction is allowed to proceed for 5 h, and centrifuged at 4000 rpm (Eppendorff centrifuge 5417C) afterwards to remove non-coupled PEG. The precipitate is redispersed in 400 µL of cyclohexane and used for further analyses.

Quantification of PEG chains on HES-NCs. ^{1}H NMR spectroscopy was used to determine the number of PEG chains coupled to HES-NCs. A glass capillary tube containing 5% of dichloromethane (DCM) in deuterated DCM was used as a constant internal reference for all samples, as can be seen in Figure 31. The PEGylated capsule dispersion is freeze-dried, redispersed in D_2O, and set for NMR measurement with the internal reference inside a second glass vial, as can be seen in Figure 31. Integration of the resonance corresponding for poly(ethylene glycol) units (at 3.5 ppm) is compared with that of DCM (at 5.5 ppm) to quantify the number of PEG chains in the dispersion. The number of capsules in the dispersion can be calculated through the solid content of the dispersion, the average diameter of the

capsules, and the polymer to water ratio in the capsule, by taking the assumption that the density of the shell is 1 g/cm^3.

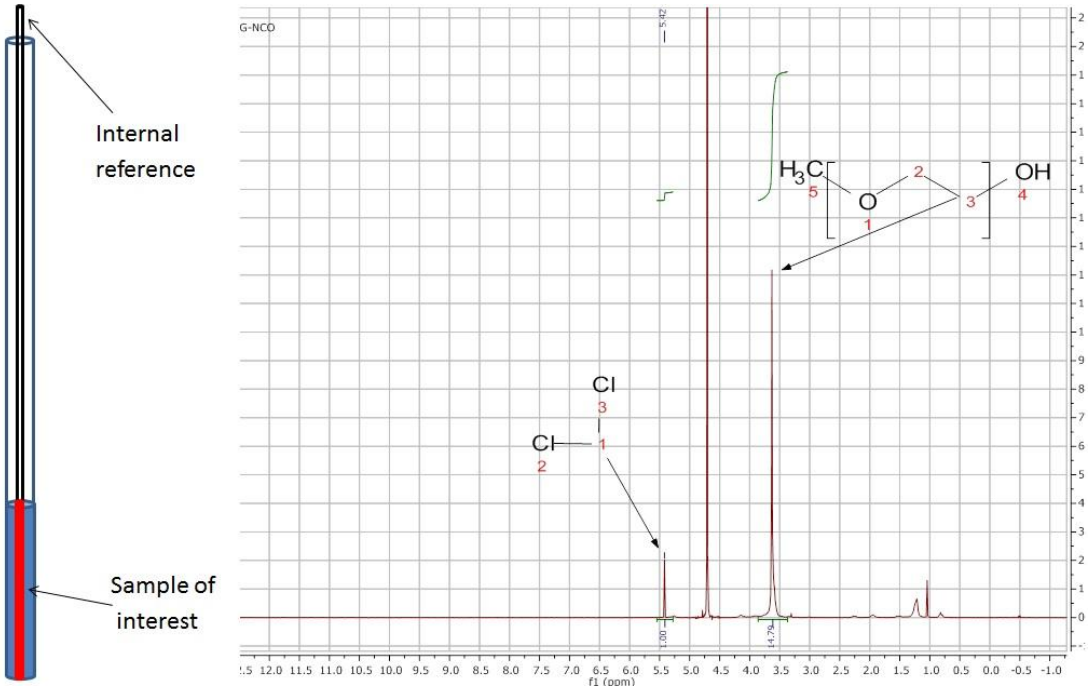

Figure 31. *Schematic representation of the method used for the quantification of surface attached PEG by ^{1}H NMR in D_2O (250 MHz, 298K).*

***In-vitro* test** *(experiments conducted by Patricia Okwieka).*

Nanocapsule incubation with human serum and protein quantification.

The nanocapsule dispersions were diluted with ultrapure water to a total particle surface area of 0.05 m^2 in 150 µL and incubated with 1 mL human serum for 1 h at 37 °C under constant agitation. The particles were separated from the supernatant by centrifugation at 15,000 g for 1 h. The nanoparticles were washed with phosphate-buffered saline (PBS; Gibco) in three centrifugation/redispersion steps at 15,000 g for 1 h. To elute the adsorbed proteins, the particle pellet was re-suspended in 7 M urea, 2 M thiourea and 4% CHAPS, and the nanoparticles were again pelleted. The supernatant was then used for protein quantification. Protein concentrations were determined using Pierce 660 nm protein Assay (Thermo Scientific, Rockford, USA) according to manufacturer's instructions with BSA as a standard. Each sample was measured in triplicate.

Preparation of peripheral blood mononuclear cells (PBMC)

PBMC were isolated from healthy human donor buffy coats using standard Ficoll density centrifugation. Donor blood was obtained according to the declaration of Helsinki.

Incubation of nanocapsules with PBMC

For nanocapsule treatment cryopreserved PBMC were thawed in AIM-V containing 10% human serum. 5 x 10^6 PBMC per well were seeded in a 48 well plate and incubated with 50 µg/ mL of nanocapsules for 4 h at 37 °C/ 5% CO_2. Afterwards cells were harvested with cold PBS and stained against several expression markers.

Antibody staining of PBMC for flow cytometry analysis

Potential NC uptake by PBMC was analyzed using a LSR-Fortessa FACS analyzer equipped with FACSDivaTM software (both Becton Dickinson). A 586/15 nm bandpass filter with excitation by a 100 mW/561 nm laser was used to detect the fluorescent dye SR101 of the NC. PBMC were stained against several markers: CD3, CD4, CD8, CD14, CD16, CD19, CD45, and CD56. The following fluorochrome-

conjugated monoclonal mouse anti-human antibodies were used: CD3-V450 (BD), CD3-FITC (Beckmann Coulter), CD4-APC-H7 (BD), CD8-APC (Beckmann Coulter), CD14-V450 (BD), CD19-APC (BioLegend), CD16-Pacific Blue (BioLegend), CD45-FITC (Beckmann Coulter), CD45-APC (Beckmann Coulter), CD45-V450 (BD), CD45-APC-H7 (BD), and CD56-APC (BD). Cells were incubated with antibodies for 15 min at 4 °C, washed with PBS/ 0.1% BSA, centrifuged (5 min, 1500 rpm) and resuspended in 500 µL PBS/ 0.1% BSA. Conjugates were excited using a 100 mW/ 488 nm laser (filter 530/ 30 nm), a 40 mW 640 nm laser (filter 670/ 30 nm and 780/ 60 nm) and a 100 mW 405 nm laser (filter 450/ 50 nm). For analysis, cells were gated on a forward scatter/ sideward scatter dot plot to exclude debris. The selected events were then further analyzed for the mentioned cell markers.

In-vivo test

Pharmakokinetic studies for plasma half-life studies *(experiments conducted by Oliver Seifert).*

Female SWISS (Janvier, CD1, 8 weeks old animals per construct) received an intravenous (i.v.) injection of 300 µg of the capsule in a total volume of 100 µL (in PBS). Blood samples (50 µL) were taken in the time intervals of 2 min, 30 min, 1 h, 2 h, 4 h, 6 h, 1 day and 3 days, incubated with heparin and stored at 4°C. Using Li-COR, fluorescence intensity of the blood samples was measured to analyze the concentration of the functionalized capsules. Comprising standard curve and weight of animals, the percentage of injected doses was calculated. $T_{1/2}\beta$ and area under the curve (AUC) were calculated with Excel.

In vivo / Ex vivo Fluorescence Imaging for the bio-distribution of the capsules *(experiments conducted by Mustafa Diken).*

Six to eight-week old female BALB/c mice were obtained from Charles River. All mice were kept and handled in accordance with federal and state policies on animal research.

In vivo/ ex vivo fluorescence imaging of fluorescently labeled unmodified or PEGylated HES-NCs was performed using the IVIS Spectrum Imaging system (Perkin Elmer). Upon intravenous injection of nanocapsules (1 mg), BALB/c mice (n = 3) were anesthetized with isofluorane at different time points (30 min, 1 h, 2 h, 4 h, 6 h, 8 h, 24 h) and placed in the light-tight chamber of the IVIS instrument. Fluorescence emission was visualized by using the light source and filters with excitation at 745 nm and emission at 800 nm for an exposure time of 3sec. 24 h after injection, mice were sacrificed and fluorescence signal from isolated organs such as brain, lungs, heart, kidneys, liver and spleen were collected *ex vivo* using the same filter set and exposure time. Fluorescence images were presented as superimposed to black & white photos of mice/organs and the fluorescence intensity was depicted with a pseudocolor scale.

4. Surface modification of HES-NCs for cell-specific targeting

The work in this chapter concerning the surface modification of HES capsules by mannose, the study of interaction of the nanocapsules with blood plasma protein, and the influence of the protein corona on the targeting efficient has been published in Angewandte Chemie International Edition (Kang, B.; Okwieka, P.; Schöttler, S.; Winzen, S.; Langhanki, J.; Mohr, K.; Opatz, T.; Mailander, V.; Landfester, K.; Wurm, F. R. Angew. Chem. Int. Ed. Engl. 2015, 54, 7436.)[213] *and altered for this thesis with permission. The manuscript concerning the surface modification of HES-NCs with Microbody, scFv antibody, and Dec205 is in preparation. I synthesized the nanocarriers and developed all the surface modification methods, synthesized the 2-aminoethyl α-D-mannopyranoside, and conducted the characterization concerning DLS, SEM, TEM, NMR, fluorescamine assay, anthracene azide assay, and the c-type-lectin binding assay; the in-vitro, ITC characterization and the protein adsorption assay was conducted by the collaboration partners, which are acknowledged after each corresponding contribution.*

Introduction

In the last decades, the application of synthetic nanocarriers for the targeted delivery of drugs is termed as a promising therapy against cancer, due to its ability to reduce the side effect of the traditional chemotherapy. While the specific targeting of the tumor tissue can be achieved passively by the enhanced permeability and retention effect (EPR),[214] surface modification of the nanocarriers by targeting agent, which can actively bind to the malignant cell line, will not only increase the targeting effect to the tumor tissue, but also be able to target the tumor cells in metastases.

When synthetic nanocarriers enter biological fluids, it is known that, due to the high surface energy and hydrophobic interactions, they strongly adsorb plasma proteins.[70,215] Many researchers proposed that the *in vivo* fate of any nanocarrier is determined by this protein "corona" formation post injection, instead of the intrinsic properties of the mostly polymeric nanocarrier itself.[204-211,216] PEGylation is the state of the art approach to depress the unspecific interaction with plasma proteins and often referred to the term "stealth effect".[11,217] However, the stealth effect alone is not

enough: specific targeting agents have to be attached additionally in order to reach the place of action and avoid opsonization.[215] But how does this additional moiety interact with plasma proteins? A new corona could be generated around the carriers, consequently altering the *in vivo* performance by covering and deactivating the targeting group.

While the protein corona formation for single component nanoparticles, such as polystyrene[206,210,218], zinc oxide[219], silica[210,219,220], gold[221], and titanium dioxide[219] has been extensively studied, no study has been conducted comparing protein interactions of a PEGylated nanocarrier before and after the attachment of an additional targeting group. Hence, no information on the combination of stealth properties of the PEGylated carrier and the specific targeting after "on-top attachment" of the targeting group is known. Herein, for the first time, we compare PEGylated stealth nanocarriers with subsequently modified analogues carrying mannose targeting moieties with respect to protein adsorption. Isothermal titration calorimetry (ITC), dynamic light scattering (DLS), and cell-uptake studies before and after incubation with human plasma have been performed and the influence on the targeting efficiency to dendritic cells is evaluated.

4.1 Results and discussion

Surface functionalization of HES-NCs with mannose

A working strategy for specific targeting is the attachment of various small biomolecules, such as folic acid[86,222], glucose[223], mannose[224,225], galactose[224], or dissacharides[226] to the nanocarriers. Coupling of these targeting agents to the nanocarriers often involves several reaction steps, furthermore, quantification of the attached groups is challenging especially when the nanocarrier itself is biocompatible and vulnerable against chemical transformations. In this work we present a robust and general protocol for the coupling of such small biomolecules to the surface of nanocarriers, and a corresponding characterization method, which can quantify the number of the coupled biomolecules very precisely.

We have been studying hydroxyethyl starch nanocapsules (HES-NCs) as biodegradable nanocarriers intensively.[86] They are prepared via an inverse miniemulsion protocol and diameters can be adjusted precisely (Table 4). More recently, well-defined PEGylation of HES-NCs was accomplished via different protocols.[227] Herein, we extend these protocols to generate NCs which can be further functionalized "on-top" with specific targeting groups. Diisocyanate-PEG (OCN-PEG_{110}-NCO, M_n = 5000 g·mol^{-1}) reacts both with the surface hydroxyls of the polysaccharide and subsequently with targeting groups. After one of the isocyanate groups has reacted with the surface, the reactivity of the other one will decrease drastically due to the steric hindrance and loss of mobility. An excess of diisocyanate-PEG has to be used, which will further reduce the formation of cycles, and keep the second isocyante group available. Monoisocyanate-PEG (MeO-PEG_{110}-NCO, M_n = 5000 g·mol^{-1}) has been used to prepare PEGylated capsules as negative control for further studies. Quantification of the HES-NCs by NMR spectroscopy after PEGylation revealed that 5*10^5 PEG chains have been coupled to the surface for both PEGs (cf. Table 5), which is a first indication that the diisocyanate-PEG did not form cycles and reacted rather selectively at one end.

Two methods have been used to couple mannose to the PEGylated HES-NCs (Scheme 4). Route 1 is a combination of techniques with mannose carrying an azide

group at C-1, and coupling to the capsules via metal-free click chemistry: The HES-NCs, which were PEGylated by diisocyanate-PEG, were redispersed in water, and the mixture is magnetically stirred in an open vessel to evaporate cyclohexane. During this procedure, the isocyanate groups can be hydrolyzed to release primary amine groups. The number of amine groups was determined by a fluorescence assay (reference, support info); however, only a rather small amount of 1,000 groups per NC was detected. The large discrepancy between the number of available NCO-groups and the number of amines per NC can be reasoned due to the fast reaction of already hydrolyzed amines with remaining isocyanate groups to form a urea linkage. The reaction speed between isocyanates amines is ca. thousand times faster than the hydrolysis of the former,[228] hence most of the primary amine groups will be consumed by the cyclization with other PEG chains. The available amines were activated for the Huisgen-click reaction by amidation with an *N*-hydroxy succinimidyl ester carrying dibenzocyclooctyne (DBCO) (Scheme 4, Route 1). The DBCO groups are used since they react with azides in the absence of any metal catalyst due to their ring strain, which is a great advantage for bioapplications.[229,230] The number of DBCO groups per HES-NC was quantified after quantitative click reaction with anthracene methylazide and found to be approx. 1000 (experimetal part). 2-Azidoethyl α-D-mannopyranoside was then reacted with DBCO-modified NCs, and after purification, the number of remaining DBCO groups was quantified as well. No DBCO was detected after the addition of azidomannose. Therefore, both the coupling of DBCO to the amine groups and the subsequent coupling of azide mannose to DBCO have achieved quantitative yield by this method, however, the total number of targeting groups remained rather low.

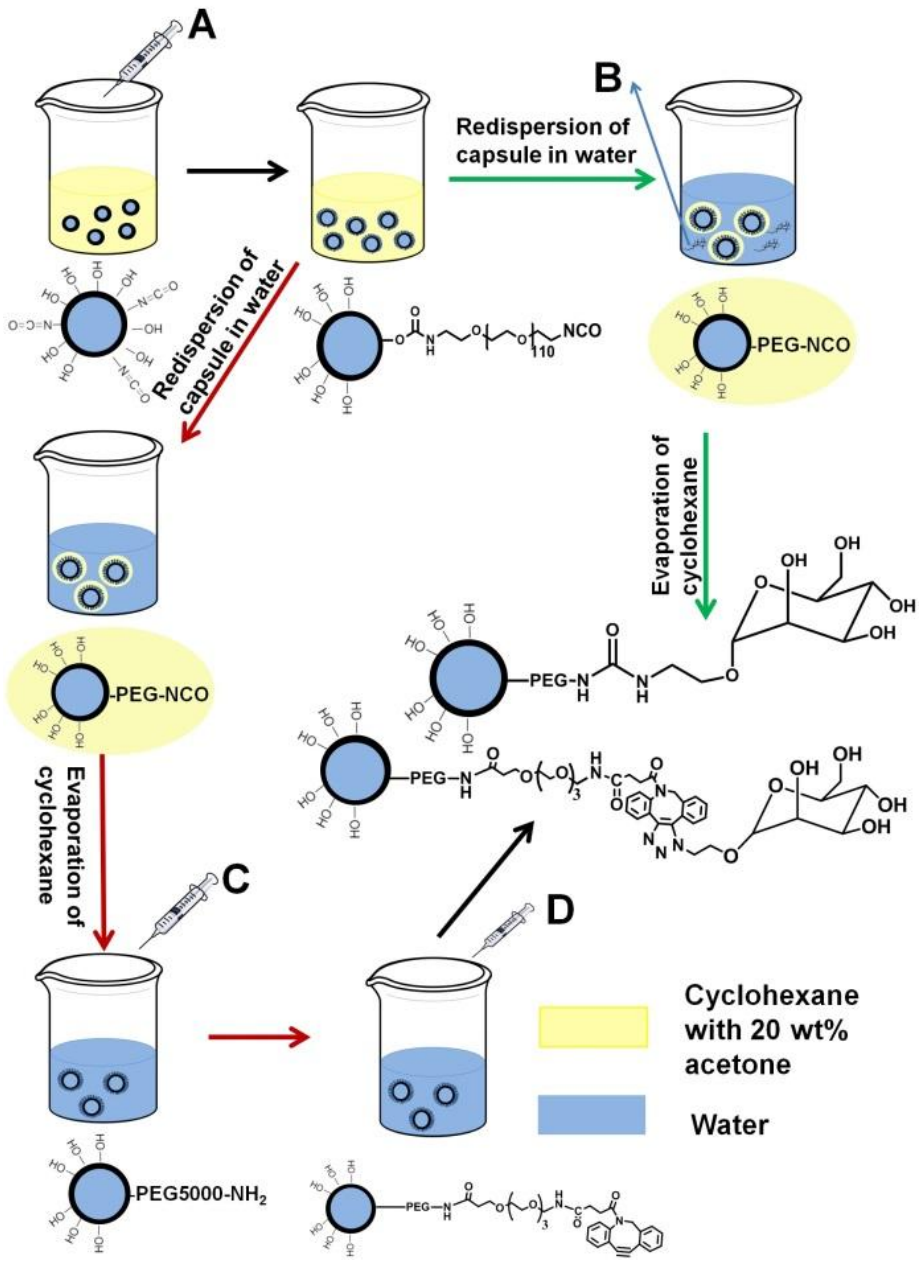

Scheme 4. *Preparation of HES nanocarriers with specific targeting to dendritic cells: Different coupling protocols to attach the mannose targeting group. ROUTE 1: Combination of isocyanate, active ester and copper-free click chemistry. ROUTE 2: Pure isocyanate chemistry. Reactants: A: diisocyanate-PEG (OCN-PEG110-NCO, Mn=5,000 g·mol^{-1}) in acetone; B: D-mannosamine or 2-aminoethyl α-D-mannopyranoside is coupled in water, followed by evaporation of cyclohexane and dialysis; C: DBCO-PEG4-NHS, D: 2-azidoethyl α-D-mannopyranoside is coupled by click reaction followed by dialysis.*

A second route utilized amine-functionalized mannose derivatives which are directly coupled to the available NCO-groups during the redispersion procedure (Scheme 4, Route 2). Namely, amino-derivatives of mannose are dissolved in water, before the redispersion process. The mixture is magnetically stirred in an open vessel, to evaporate the cyclohexane and produce a stable dispersion of PEGylated and mannose-funcionalized HES-NCs. Due to the high reaction kinetics of isocyanates with amines, the amino-sugars will preferably react with the nanocarriers, before hydrolysis of the isocyanates occurs. The amount of amine-functionalized mannose in water (before the addition of NCs) can be quantified by the fluorescamine assay[203]. After the coupling reaction, the NCs are precipitated by centrifugation, and the remaining amine-functionalized mannose in the upper phase is quantified by the same method. By comparing both amounts, the precise number of mannose units which are attached to the NCs is available. Two different mannose derivatives were used, D-mannosamine and 2-aminoethyl α-D-mannopyranoside, with the amine groups at the C-2 or the C-1 position (the functionalized HES-NCs are named HES-PEG5000-C2-Man and HES-PEG5000-C1-Man accordingly). With this easy and fast protocol ca. $2 \cdot 10^5$ (Table 5) mannose units can be attached to the NCs in both cases. Compared to the first method, this method is a single step coupling reaction, produces a 200 times higher mannose density, allows a precise quantification and omits expensive intermediates. This general protocol can be used for any type of small biomolecule, as long as it carries an amine group.

Table 5. Characterization of unmodified HES nanocarriers and HES nanocarriers functionalized with mannose by different methods.

Sample name	PEG per NC[a]	Mannose per NC (S.D.)	Diameter (S.D.) /nm
HES	0	0	165 (25%)
HES-PEG5000	$5 \cdot 10^5$	0	166 (27%)
HES-PEG5000-DBCO-Man	$5 \cdot 10^5$	1000 (3.5%)[b]	172 (21%)
HES-PEG5000-C2-Man	$5 \cdot 10^5$	$2 \cdot 10^5$ (3.3%)[c]	168 (32%)
HES-PEG5000-C1-Man	$5 \cdot 10^5$	$2 \cdot 10^5$ (3.3%)[c]	176 (30%)

[a] The standard deviation (S.D.) is 7.5% for all the samples, comes from the standard deviation, when the fixed internal reference is quantified in the NMR spectroscopy. [b] The standard deviation comes from the standard working function for the fluorescence assay with 9-(azidomethyl)anthracene, which was used to quantify the number of DBCO groups. [c] The standard deviation comes from the standard working function for the fluorescence assay with fluorescamine, which was used to quantify the number of amine groups.

The binding affinity of all mannose-functionalized HES-NCs with immature dendritic cells (iDC) has been investigated by fluorescence aided cell sorting (FACS, Figure 32). In a recent study our group demonstrated that unmodified HES-NCs have a suppressed unspecific cell uptake.[86] This result is also confirmed in this work, however, the subsequent PEGylation of the NCs' surface even further reduces the uptake into iDC (Figure 32). Also, HES-PEG5000-DBCO-Man exhibited a similar low binding affinity to dendritic cells as the HES-PEG5000. This is attributed to the rather low density of targeting units per capsule (0.0028 mannose per nm^2). The interaction between the receptor and single carbohydrate molecule is inherently weak, which has a binding constant in the range of 10^3-10^4 $Lmol^{-1}$. By increasing the surface density of mannose, the binding constant will increase drastically, to 10^6-10^7 $Lmol^{-1}$.[231,232] HES-PEG5000-C2-Man, the density of sugar is 200 times higher compared to HES-PEG5000-DBCO-Man and thus exposes ca. 0.55 mannose units per nm^2. Interestingly, the binding affinity with iDC is still lower compared to the unmodified

HES-NCs (Figure 32B). The reason for this could be that the free hydroxyl group at C-2 position of the mannose molecule is essential for interaction with protein acceptor.[233] Only, when 2-aminoethyl α-D-mannopyranoside (with the amine at the C-1 position) was used, a much stronger binding of HES-PEG5000-C1-Man with iDC compared to unmodified and PEGylated capsules was detected (Figure 32C). These results clearly demonstrate that, when mannose is attached via a PEG linker to HES-NCs, a multivalency effect is achieved, combining the stealth behavior of a PEGylated nanocarrier with on-top mannose functionalization.

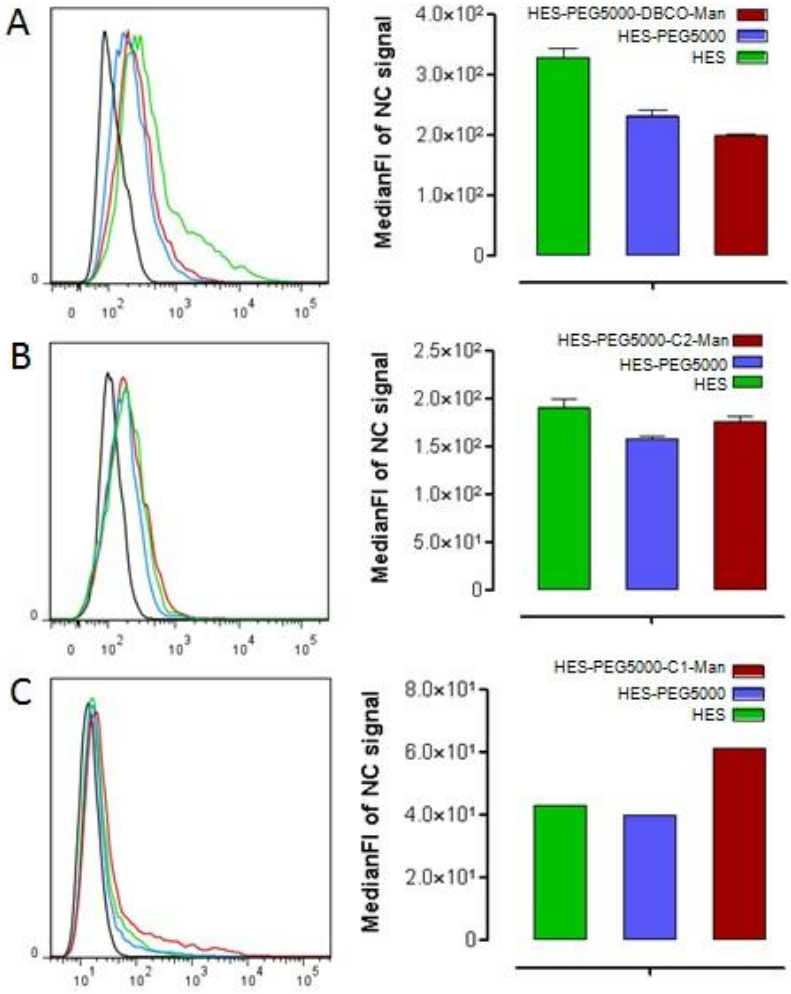

Figure 32. *In-vitro binding of HES-NCs with dendritic cells before incubation with human plasma protein. Immature dendritic cells were incubated with 50 µg mL^{-1} of each NC for 16 h at 37 °C. Black lines in histogram (left): untreated iDC; green line: HES; blue line: HES-PEG5000; red lines: various mannose functionalized NCs (cf. main text and Table 5 for sample codes (experiments conducted by Patricia Okwieka).*

Surface functionalization of HES-NCs with different antibodies

Route 1 (labeled with red arrows) in Scheme 4, which involves the coupling of NHS ester linked DBCO groups to the end of PEG and the subsequent coupling of azide functionalized molecules to the DBCO groups, turned out to be insufficient when used to couple mannose to the capsule for DCs targeting, since the maximum number of mannose coupled is limited to be 1000 per capsule, which is not enough to activate the multivalent interaction with the cells. However, this method demonstrated many advantages at the same time, including of the ease of functionalization of a PEGylated interface with additional targeting agent, the great advantage for bio-applications due to the catalyst-free click reaction involved, and the well-established quantification methods, which allows functionalizing the nanocapsule with targeting agent in a quantitative manner. Other than mannose, some of the targeting agent, especially antibodies, have much higher individual binding affinity with cellular accepters, hence can be used via route 1 to surface modify the HES-NCs for cell-specific targeting. The general strategy of surface functionalization of HES-NCs with different antibodies is shown in Scheme 5.

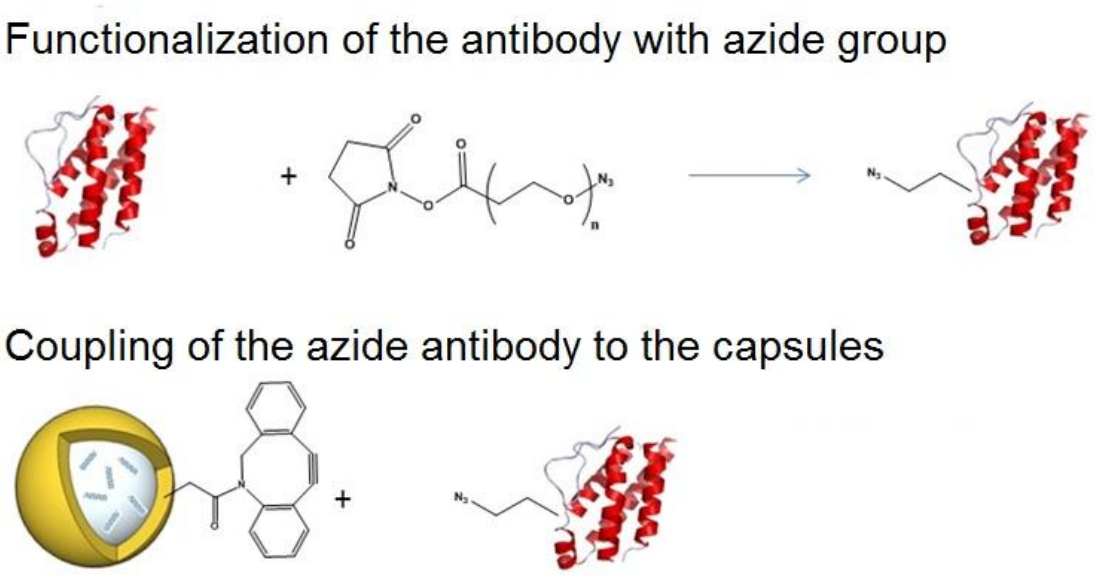

Scheme 5. *Surface functionalization of HES-NCs with proteins. Two steps are involved, including the functionalization of the protein with an azide group, and the coupling of azide functionalized antibody to the DBCO- functionalized nanocapsule.*

Two microbodies have been used to functionalize the HES-NCs. The first is integrin αVβ3 binding microbody named as 2.5D. The second is a melanocortin 1 receptor (MC1R) binding microbody, named as MC-ME-030. Both microbodies can specifically target B16-F10 murine melanoma cells, and are functionalized by an azide group.

Firstly, the interaction between non functionalized, but PEGylated HES-NCs with the B16-F10 murine melanoma cells was investigated (Figure 33). No binding of PEGylated HES-NCs with the cells was detected, which is in accordance with the results demonstrated in Figures 25-28 (binding of PEGylated HES NCs with different immune cells in blood), and further proved the low unspecific interaction of the PEGylated HES-NCs with different cells lines.

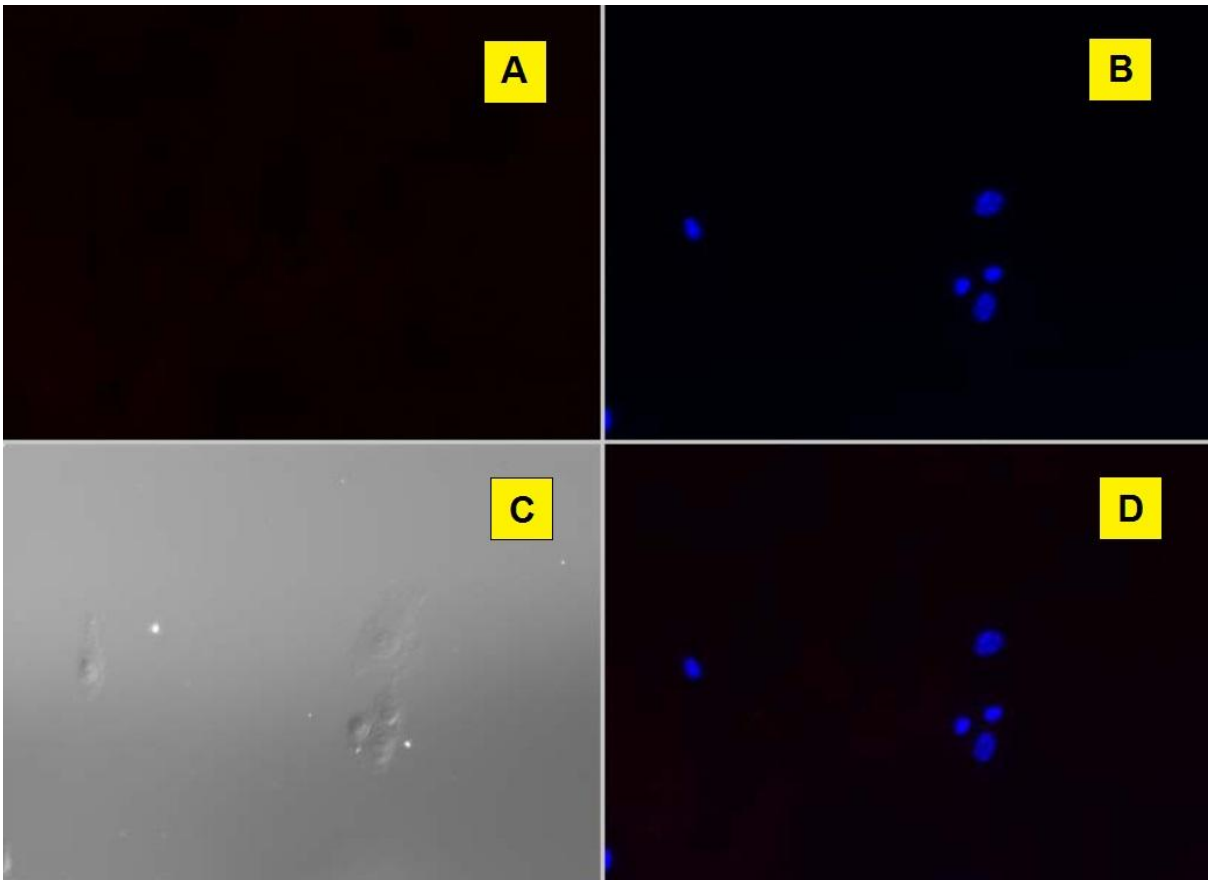

Figure 33. *Binding of PEGylated HES-NCs without additional functionalization with the B16-F10 murine melanoma cells. A) stain of the capsules, B) stain of the cell nuclear, C) dark field, D) Merge of other three channel (Experiments conducted by J. Wüstehube-Lausch).*

Secondly, the coupling efficiency between the azide-modified microbody and the DBCO functionalized HES-NCs was evaluated. The number of DBCO groups per capsule was quantified to be ca. 300 per capsule, after the addition of 300 equivalents of the modified microbody (azide- 2.5D) to the DBCO functionalized HES-NCs dispersion, the click reaction was allowed to proceed overnight, the capsules were precipitated by centrifugation, while the supernatant of the first and second washing step was analyzed by HPLC in order to identify remaining non-coupled, i.e. free microbodies(Figure 34).

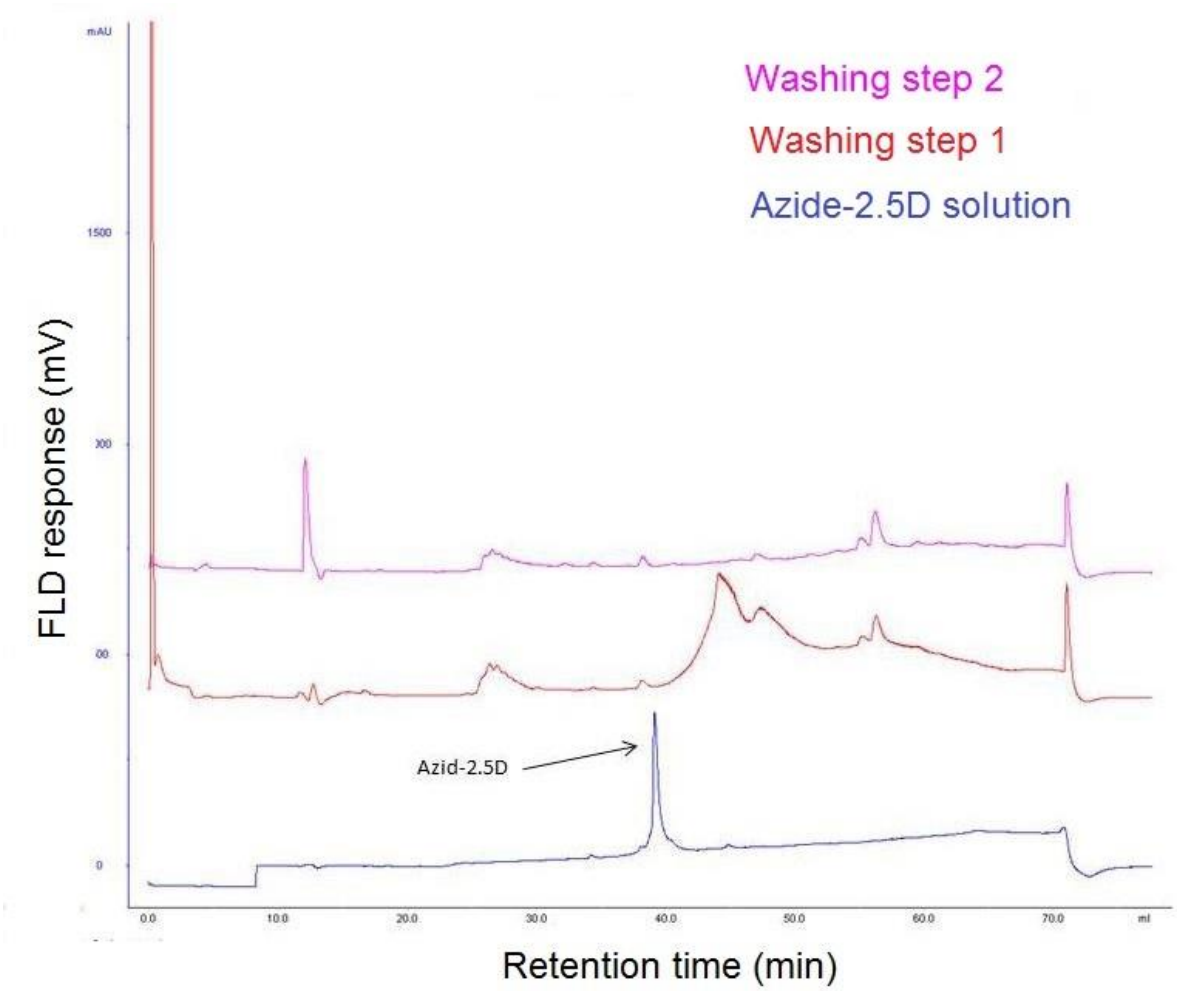

Figure 34. *Quantification of free microbodies by HPLC. No detectable free azide 2.5D was found in the supernatant of the first and the second washing step, which stands for a quantitative coupling efficiency for the click reaction between the azide groups from 2.5D and the DBCO groups on the surface of the HES-NCs (experiments conducted by Martin Daneschdar).*

The HPLC data from the supernatant of the first and second washing step show no free microbody (azide 2.5D), which means the catalyst free click coupling of Microbody to the nanocapsule is a quantitative reaction with nearly 100% efficiency.

Different equivalents of both microbodies were then coupled to the HES-NCs with different surface densities, as can be seen in Table 6, and their targeting efficient to B16-F10 murine melanoma cells was evaluated by fluorescence microscopy.

Table 6 List of microbody-functionalized PEGylated HES-NCs.

Sample name	Type of microbody coupled	Number of microbody per capsule
HES+PEG+2.5D a	2.5D	300
HES+PEG+2.5D b	2.5D	600
HES+PEG+2.5D c	2.5D	40
HES+PEG+2.5D d	2.5D	5
HES+PEG+MC a	MC-ME-030	300
HES+PEG+MC b	MC-ME-030	1000
HES+PEG+MC c	MC-ME-030	50
HES+PEG+MC d	MC-ME-030	5

At first, 2.5D was used to modify the HES-NCs with a surface density of 300 per capsules, which is named as "HES+PEG+2.5D a" in Table 6. The subsequent study of the binding of these capsules with the B16-F10 murine melanoma cells is shown in Figure 35.

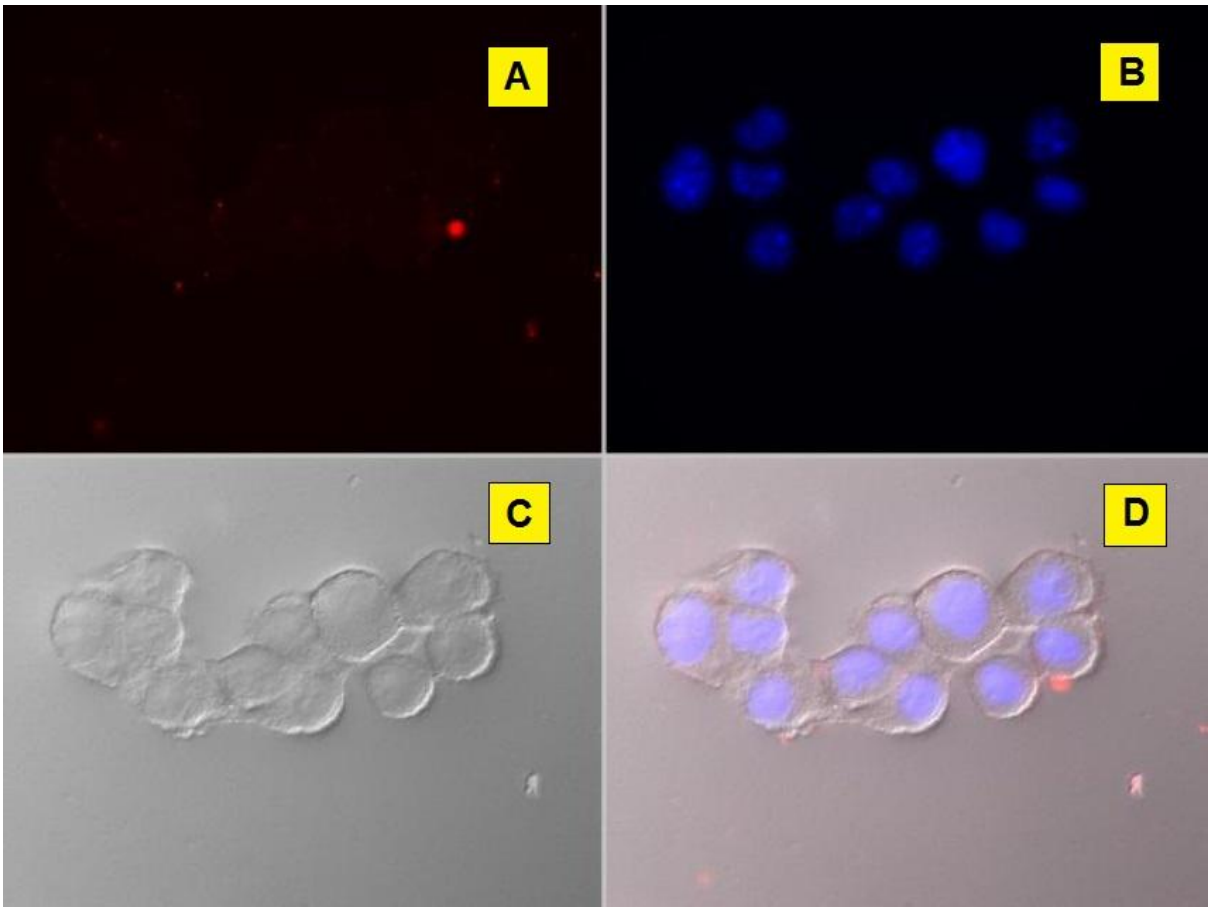

Figure 35. *"HES+PEG+2.5D a", with 300 microbodies (2.5D) per capsule, only minor binding of the capsules with the B16-F10 murine melanoma cells was detected. A) staining of the capsules, B) staining of the cell nuclear, C) dark field, D) Merge of other three channel (experiments conducted by J. Wüstehube-Lausch).*

As can be seen in Figure 35, rather weak binding between the HES-NCs and the cells was detected. The weak binding affinity was first concluded to be due to insufficient surface densities of the microbodies, and hence sample "HES+PEG+2.5D b" was prepared, with a surface microbody density of 600 per capsule. The fluorescent microscopy study of its binding with the B16-F10 murine melanoma cells is shown in Figure 36.

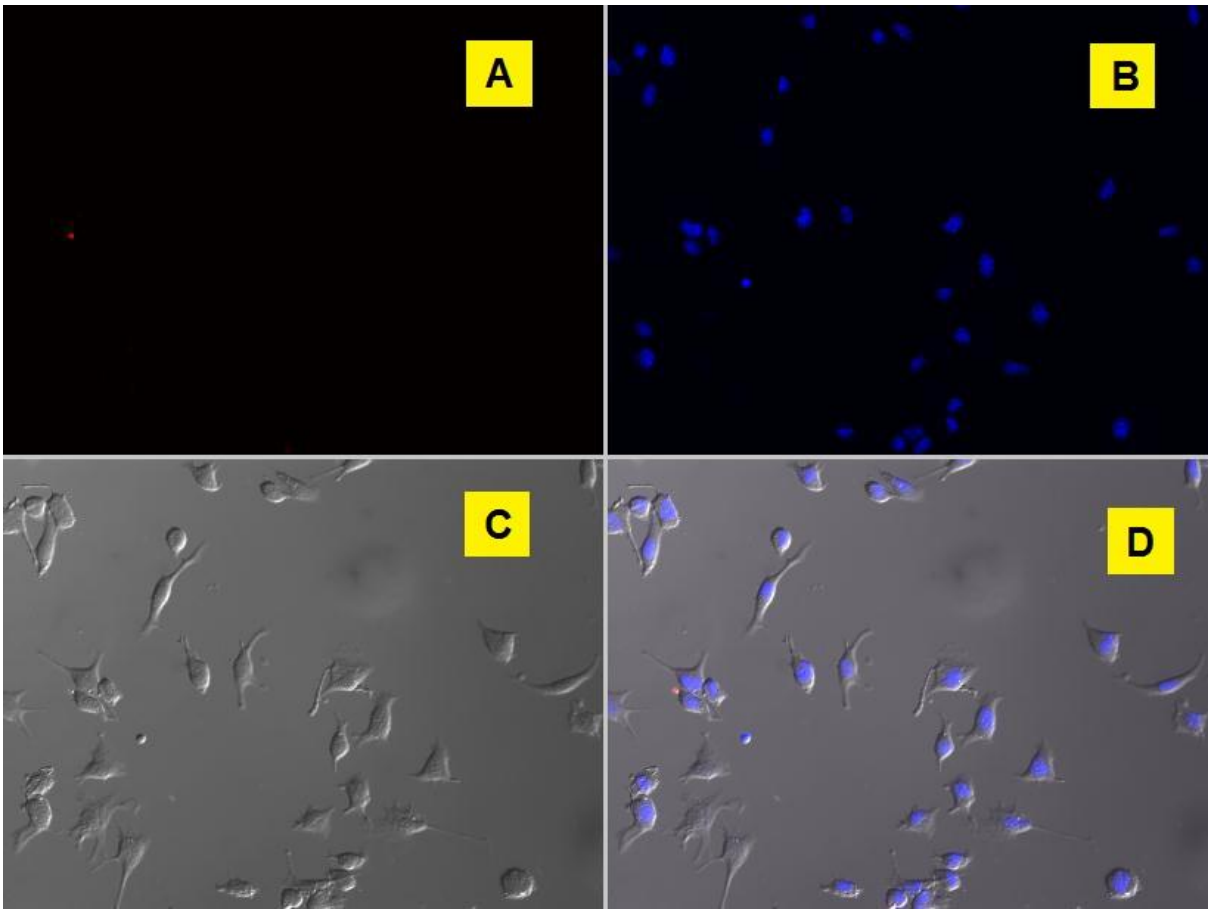

Figure 36. *"HES+PEG+2.5D b", with 600 microbodies (2.5D) per capsule, strong binding of the capsules with the B16-F10 murine melanoma cells was detected. A) stain of the capsules, B) stain of the cell nuclear, C) dark field, D) Merge of other three channel (Experiments conducted by J. Wüstehube-Lausch).*

As can be seen in Figure 36, after doubling the surface density of Microbody (2.5D), the binding between the HES-NCs and the cells was not enhanced. In the next step, sample "HES+PEG+2.5D c" and "HES+PEG+2.5D d" were prepared, with a decreased surface density of Microbody (2.5D) compared to "HES+PEG+2.5D a", with 40 and 5 molecules per capsule, respectively. The fluorescent microscopy study of the binding of these two samples with the B16-F10 murine melanoma cells has shown an increased binding affinity. Especially strong binding of the "HES+PEG+2.5D d", which has the least surface microbody density, was observed, as can be seen in Figure 37.

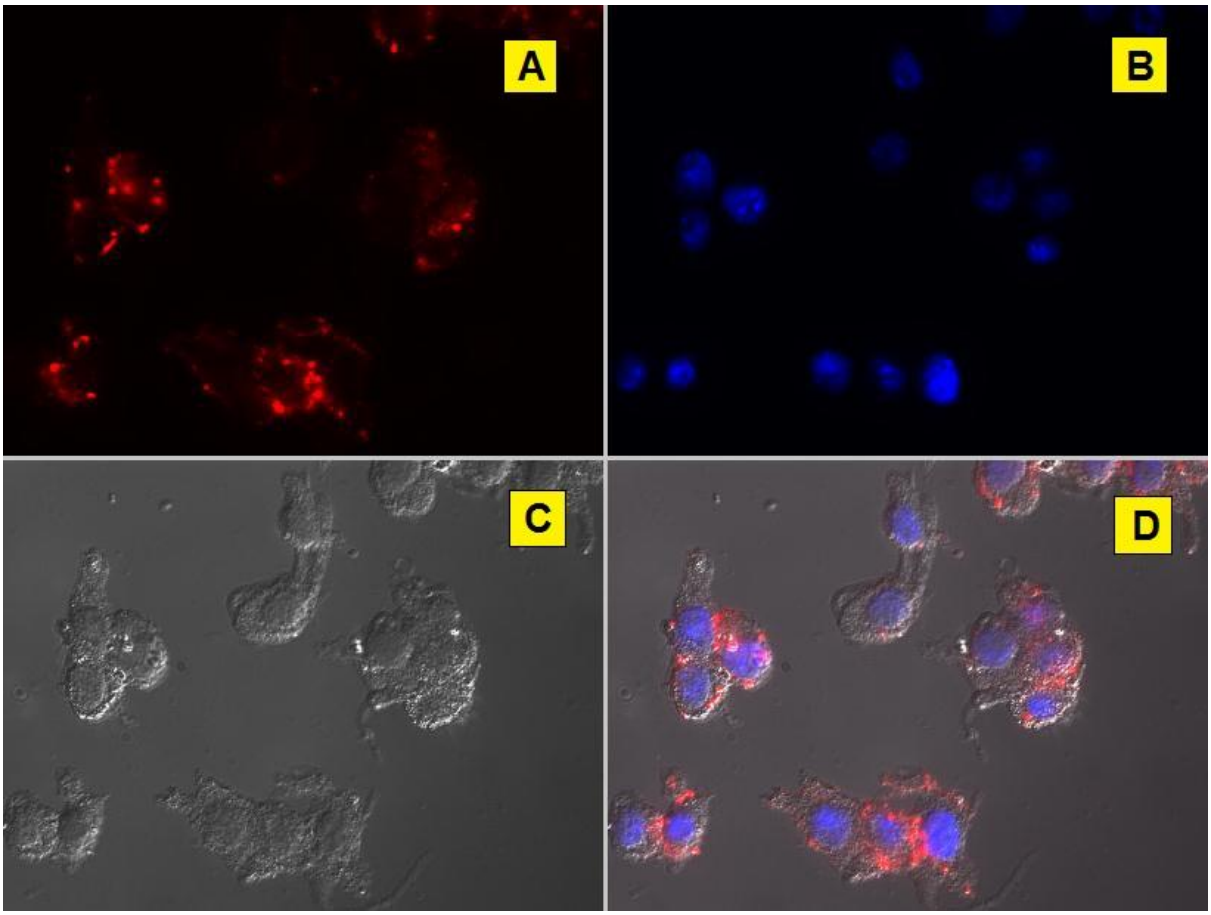

Figure 37. *"HES+PEG+2.5D d", with 5 Microbody (2.5D) per capsule, strong binding of the capsules with the B16-F10 murine melanoma cells was detected. A) stain of the capsules, B) stain of the cell nuclear, C) dark field, D) Merge of other three channel (Experiments conducted by J. Wüstehube-Lausch).*

These results demonstrates that the individual binding affinity between the microbody 2.5D and the cellular accepter on the B16-F10 murine melanoma cells is strong enough, so that a surface modification density of 5 per capsule (around 18000 nm^2/Microbody) is enough to ensure strong binding between the nanocapsule and the cells. A further increased surface modification density (1000 Microbodies per capsule, around 90 nm^2/Microbody), however, will decrease the binding, which could be due to the steric hindrance between different Microbodies on the same capsule.

This assumption has been further verified by a different Microbody, namely MC-ME-030, which binds to a different cellular acceptor (MC1R) of the B16-F10 murine melanoma cells. As can be seen in Figure 38, when 300 Microbodies was coupled to

the HES-NCs (HES+PEG+MC a), only minor binding between the nanocapsule and the cells was detected.

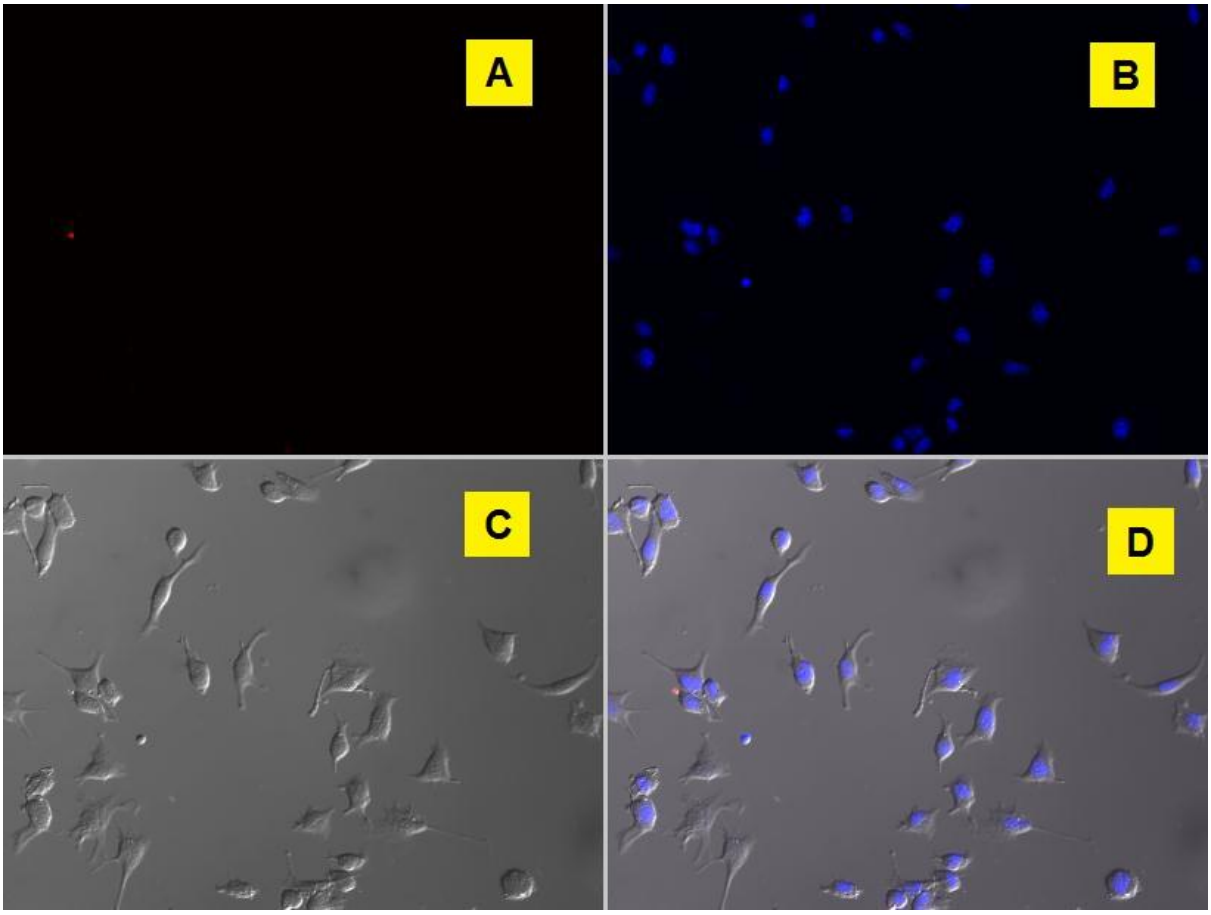

Figure 38. *"HES+PEG+MC a", with 300 Microbody (MC-ME-030) per capsule, only minor binding of the capsules with the B16-F10 murine melanoma cells was detected. A) stain of the capsules, B) stain of the cell nuclear, C) dark field, D) Merge of other three channel(Experiments conducted by J. Wüstehube-Lausch).*

However, when in average only 5 Microbodies (MC-ME-030) were coupled to each capsule, very strong binding between the functionalized HES-NCs and the B16-F10 murine melanoma cells was detected, as can be seen in Figure 39.

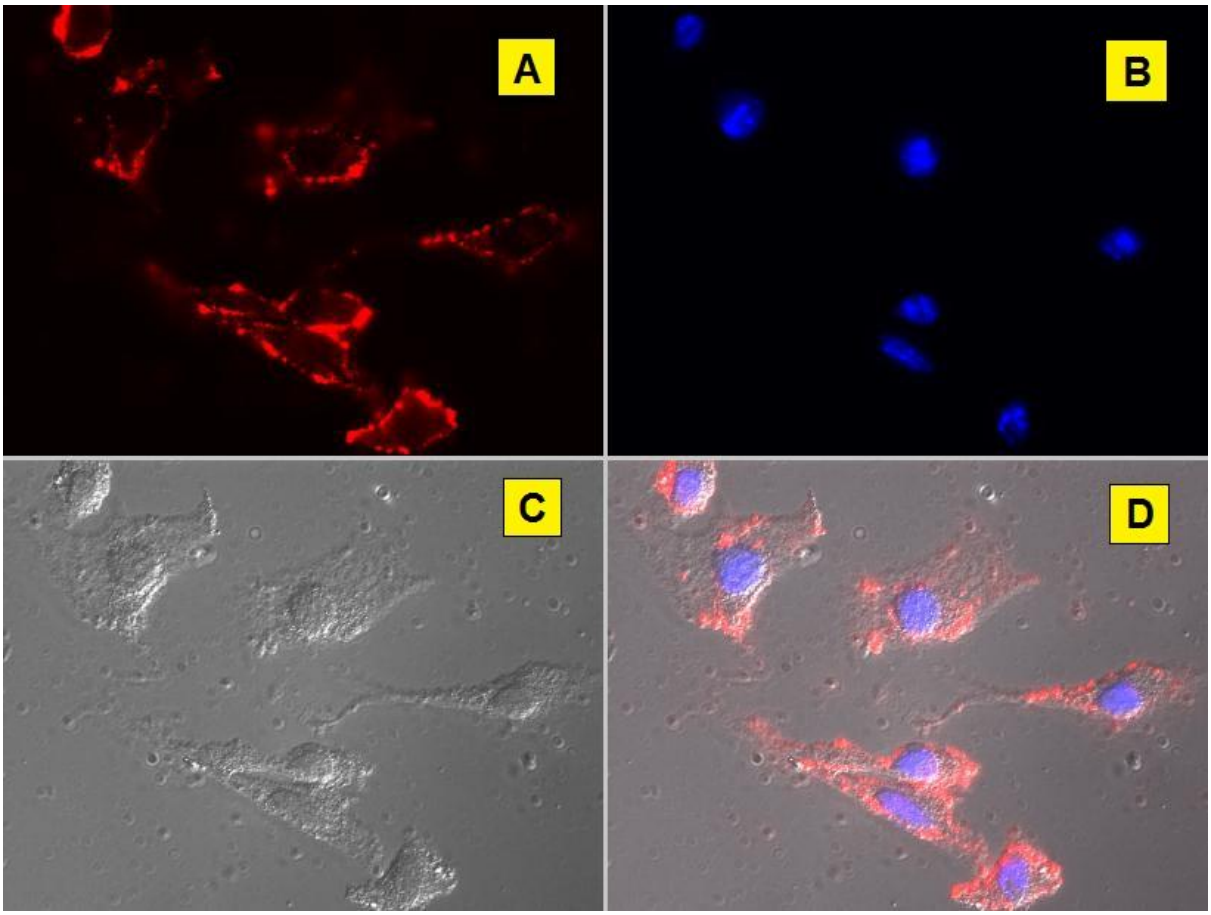

Figure 39. *"HES+PEG+MC d", with 5 Microbodies (MC-ME-030) per capsule, strong binding of the capsules with the B16-F10 murine melanoma cells was detected. A) stain of the capsules, B) stain of the cell nuclear, C) dark field, D) Merge of other three channel (Experiments conducted by J. Wüstehube-Lausch).*

Dec205 is a type I cell surface protein, while minor level of Dec205 is evidenced on some macrophage and T cells, it is expressed primarily on the surface of DCs, especially on the mDCs. By surface modification the nanocarriers by an anti Dec205 antibody, which can selectively bind to the Dec205 protein, specific binding of the nanocarrier with the DCs can be achieved. In the next section, we functionalize the surface of the HES-NCs by an anti Dec205 antibody, MOUSE ANTI HUMAN DEC205, which is abbreviated as Dec205 in the following sections.

Before coupling of the Dec205 to the capsules, the antibody was firstly functionalized with an azide group, by using a reagent (NHS-PEG4-azide) with an azide group at one end, a NHS ester group at the other and four ethylene glycol

repeating units in between. After introducing the azide group to the Dec205, its biological activity was tested, and compared to those without azide functionalization (Figure 40).

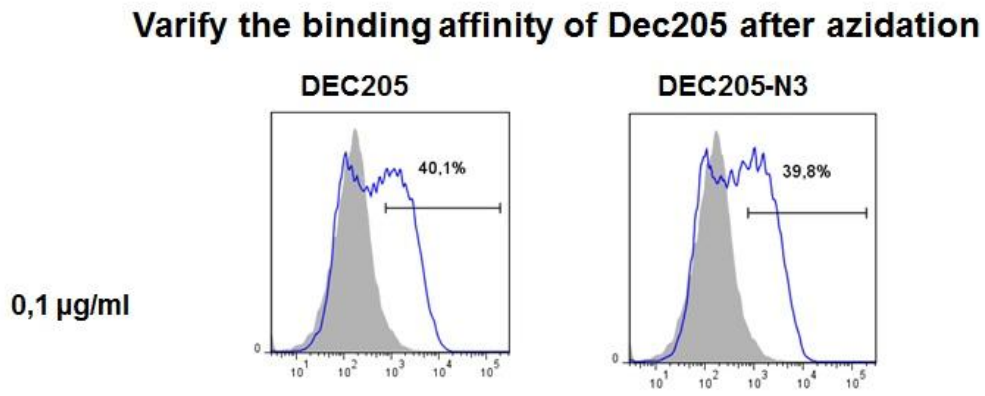

Figure 40. *Characterization of the binding affinity of Dec205 with DCs before and after azidation (Experiments conducted by Patricia Okwieka).*

As can be seen in Figure 40, in comparison to unmodified Dec205, the binding affinity of this antibody after azidation was still intact. It was then coupled to the PEGylated HES-NCs in the same matter as for coupling of the Microbodies, the number of Dec205 coupled to each capsule is controlled to be 8. The binding affinity of Dec205 functionalized HES-NCs with iDCs was then evaluated by FACS (Figure 41). Strong binding between the Dec205 coupled HES-NCs and the iDC was detected, in comparison to the unmodified HES-NCs.

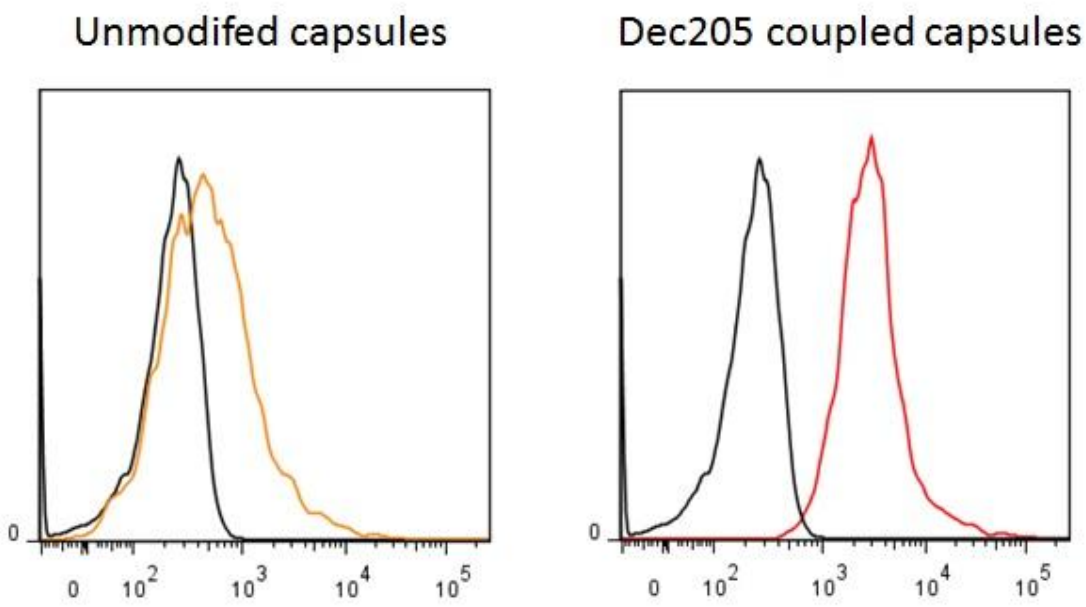

Figure 41. *FACS analysis of the binding affinity between the iDCs and the HES-NCs with or without Dec205 functionalization. Black) no capsules, orange) unmodified HES-NCs, red) Dec205 coupled HES-NCs (Experiments conducted by Patricia Okwieka).*

In the next section, a Microbody named as scFv without azide functionalization was also coupled to the PEGylated HES-NCs, by controlled reducing its disulfide bond to generate free thiol group, followed by using the Sulfosuccinimidyl 4-(N-maleimidomethyl)cyclohexane-1-carboxylate (Sulfo-SMCC) as the crosslinker, as can be seen in Scheme 6. The theoretical number of scFv coupled to each capsule is controlled to be 8.

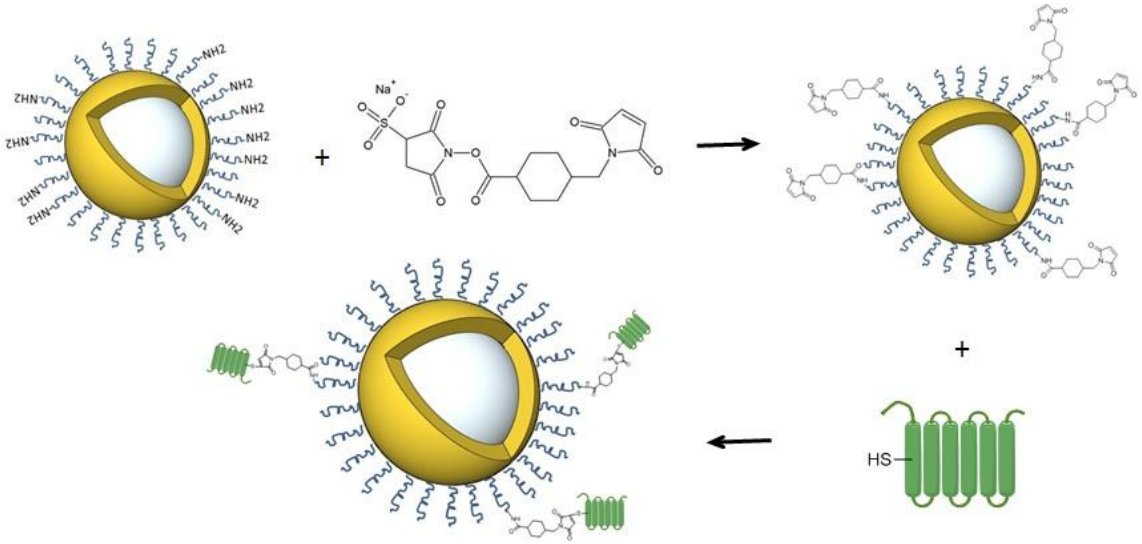

Scheme 6. Surface modification of HES-NCs by reduced scFv with thiol group.

The binding affinity of the scFv functionalized HES-NCs with Claudin18.2-HEK293 cells was evaluated by FACS, while PEGylated HES-NCs without any additional surface modification was taken as the negative control, as can be seen in Figure 42. Clear increase in the binding affinity between the scFv coupled HES-NCs and the corresponding cell line was detected.

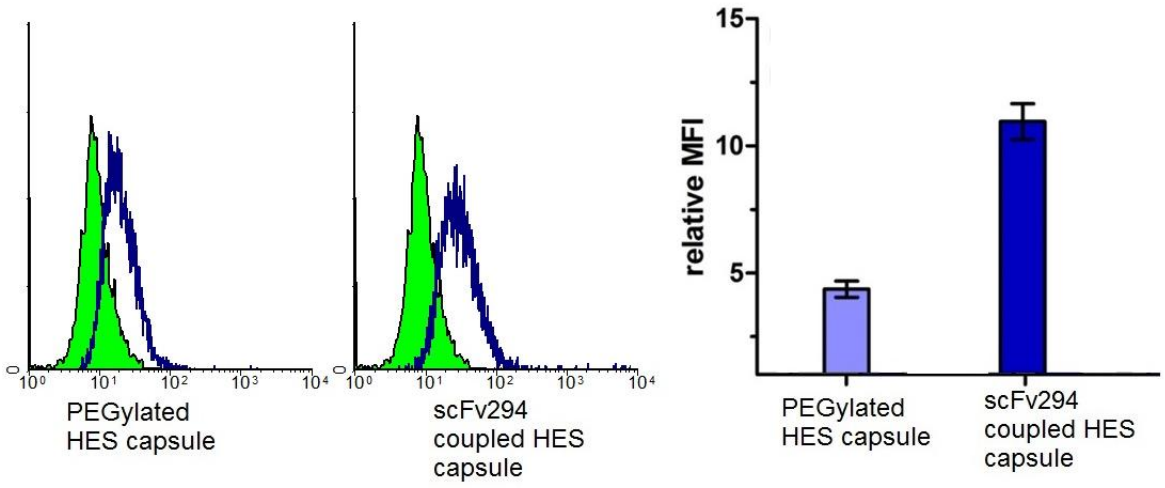

Figure 42. *Binding of scFv-conjugated HES-NCs on Claudin18.2-HEK293 cells (Experiments conducted by J. Wüstehube-Lausch).*

As the stealth property of PEGylated HES-NCs without any further surface modification has been proved by *in-vivo* plasma halftime measurement (Chapter 3, Figure 24), it is of utmost interest at this step, to investigate the influence of the additional targeting agent on the stealth property of the HES-NCs. Therefore, the plasma halftime of scFv coupled HES-NCs was measured, and compared with those of PEGylated HES-NCs, as can be seen in Figure 43.

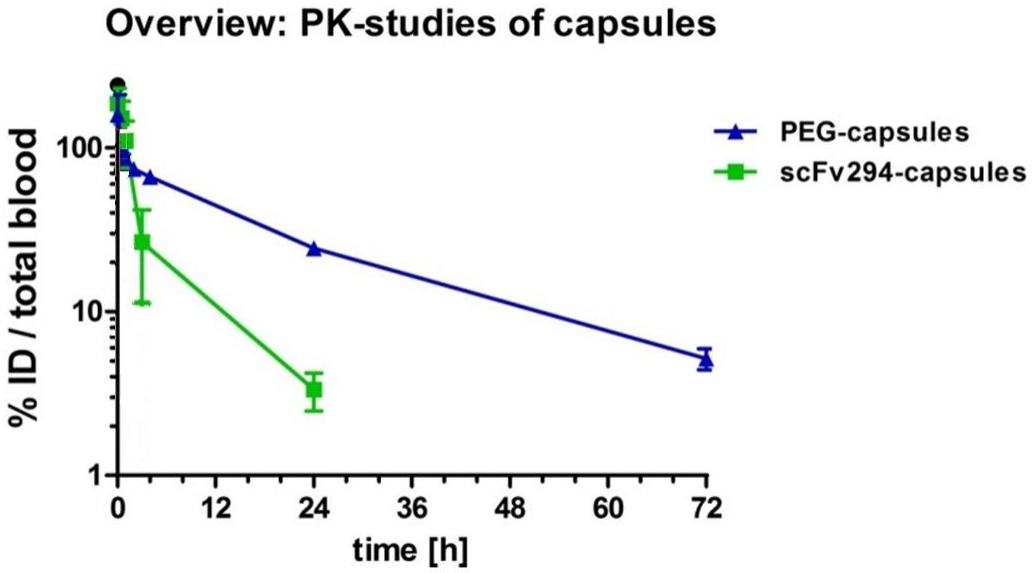

Figure 43. *Plasma half-time of scFv functionalized HES-NCs (green), in comparison to the PEGylated capsules (blue) without any further modification (Experiments conducted by Oliver Seifert).*

As can be seen in Figure 43, in comparison to PEGylated HES-NCs without any further surface modification, the PEGylated HES-NCs coupled with additional scFv microbody was removed from the blood circulation much faster. 24h after intravenous injection, there were still more than 20% of the PEGylated HES-NCs detected in the blood, while about 3% of the scFv coupled capsules could be detected. These results demonstrate that, the additional scFv Microbodies can interact with blood, enhance the opsonizaiton of the nanocarriers, and consequently hinder their stealth properties. In spite of the low amount coupled (8 Microbodies per capsule), the plasma halftime of scFv coupled HES-NCs decreased by nearly 10 times, in comparison to the PEGylated HES-NCs. Subsequently, the *in-vivo* targeting effect of the scFv coupled capsules was investigated (Figure 44).

Mouse 1 NCI-N87(GC182)	**Mouse 2** NCI-N87(GC182)	**Mouse 3** NCI-N87(GC182)	**Mouse 4** Parental NCI-N87	**Mouse 5** Parental NCI-N87	**Mouse 6** Parental NCI-N87
scFv294 conjugated capsules	scFv294 conjugated capsules	Non-conjugated capsules	scFv294 conjugated capsules	Non-conjugated capsules	No capsules

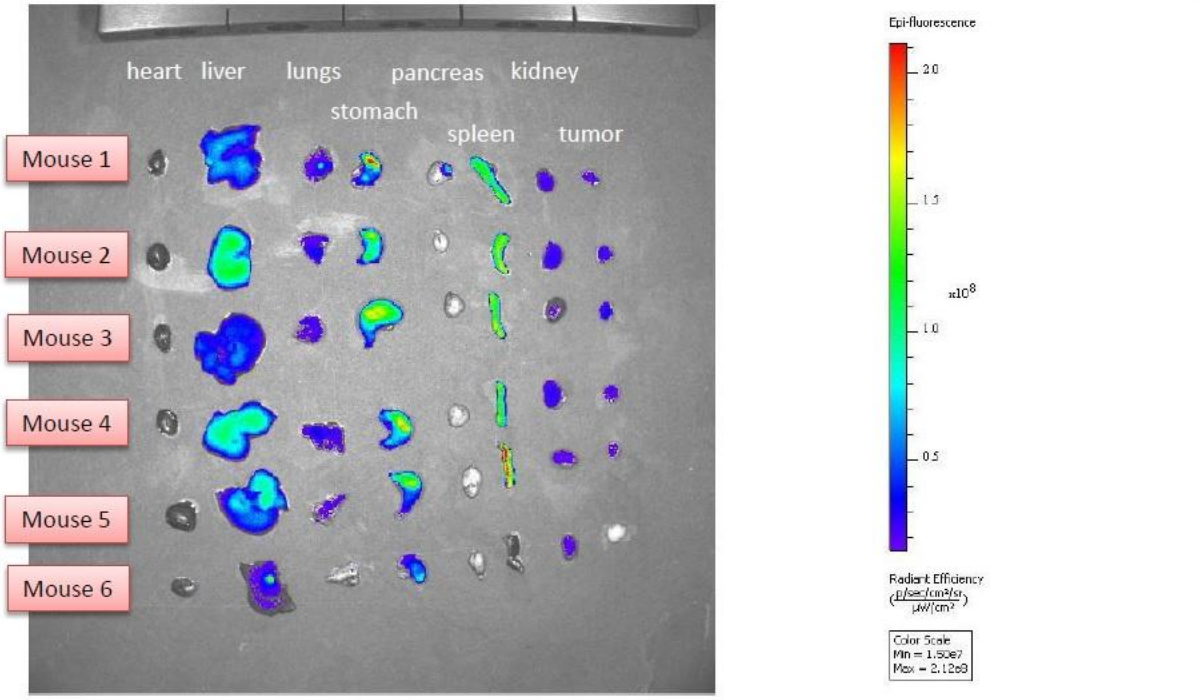

Figure 44. *In-vivo targeting efficiency of scFv functionalized HES-NCs to the tumors. Mouse 1, Mouse 2 and Mouse 3 have a scFv Microbody targeted tumor, while Mouse 4, Mouse 5 and Mouse 6 have a non-relative tumor. The strong signal in stomach was contributed to the fluorescent background of the content of the stomach, instead of the HES-NCs (Experiments conducted by Mustafa Diken).*

As can be seen in Figure 44, only weak signal was detected on the targeted tumor. In addition, not only the targeted tumor, but also the non-relevant tumor showed fluorescent intensity, which means the targeting effect on the tumor tissue was achieved by passive targeting via the EPR effect (see Chapter 4, introduction), instead of the specific binding of the HES-NCs with the tumor cells. These results demonstrate that besides the good specific cell uptake in vitro, the in vivo fate of scFv-functionalized HES nanocarriers difer strongly. Probably the additional blood-nanocarrier interactions shielded the scFv from specific interaction with the acceptors on the tumor cells, reducing the *in-vivo* specific targeting effect. In future, a targeting agent which has less interaction with blood proteins would be necessary

in order to enhance the specific targeting effect *in-vivo*. Furthermore, additional investigations need to be done, in order to quantify the influence of the additional targeting agent on the protein adsorption behavior of the PEGylated HES-NCs, and its subsequent influence on the targeting efficient.

Study of the interaction of the nanocapsules with blood plasma proteins

In order to investigate the influence of the additional targeting agent on the protein adsorption of the PEGylated HES-NCs, different techniques have been applied, including ITC, DLS, SDS-PAGE, and quantitative liquid-chromatography coupled with mass-spectrometry. Mannose-functionalized HES-NCs are studied in this case, due to its high degree of surface functionalization ($2 \cdot 10^5$ mannose/capsule), while, due to the extremely low surface functionalization density (5-10 antibody/capsule), the influence of antibody on the protein corona of the nanocapsules are hard to quantify by the above mentioned characterization methods.

First, ITC was used to determine the protein interactions from human plasma with the prepared HES-NCs. The HES-NCs were titrated with diluted human plasma to obtain the heat released from the protein adsorption at the surfaces after each titration step. The corresponding heats were corrected for the heat of dilution. The same measurement was performed with standard polystyrene (PS) nanoparticles as an reference (Figure 45), which are known to exhibit a high protein binding affinity.[234]

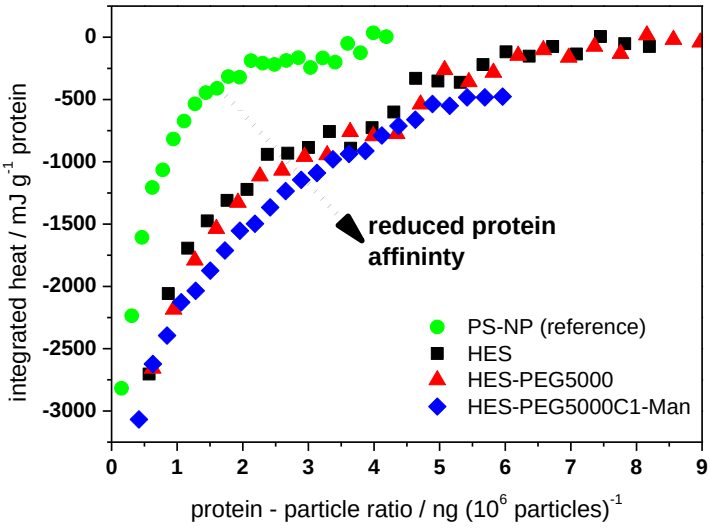

Figure 45. *ITC binding isotherms for the adsorption of plasma proteins to different nanocarriers systems: unmodified HES NCs (black squares ■), HES-PEG5000 NCs (red triangles ▲) and HES-PEG5000-C1-Man NCs (blue diamonds ♦) are compared to polystyrene nanoparticles (green circles ●) as a reference (Experiments conducted by Svenja Winzen).*

The interaction between plasma proteins and the nanocarriers were exothermic in all cases, proving protein interaction with all investigated surfaces. However, there is a significant difference between hydrophobic PS and all investigated HES-NCs. The binding affinity of the plasma proteins, which is represented by the initial slope of the binding isotherm, is strongly decreased for all HES-NCs. This matches the results reported in literature regarding the low protein affinity of HES[21-23] or saccharides in general.[29,30] More interesting, the three different HES-NCs exhibit similar protein adsorption. There is no detectable difference in the affinity caused by PEGylation or additional mannose functionalization during the ITC experiment. This is an important finding since ITC gives an insight into the protein corona surrounding the nanocarrier and it is anticipated that the attachment of targeting groups does not cause an increased unspecific protein adsorption. Furthermore, DLS was performed according to the method of Rausch et al,[235] to characterized the aggregation of particles and proteins in human plasma. As shown in Figure 46 the autocorrelation function for the HES-PEG5000-C1-Man/plasma mixtures can be perfectly described by the so

called force fit. The same is true for the HES- and HES-PEG5000-NCs mixtures with plasma (Figure 46). This means that the sum of the autocorrelation functions of both individual components is kept fixed with only the intensity fractions of plasma and capsules as free fit parameters.[235] The result indicates that no structures larger than the largest size of capsules or plasma components are formed in the mixture. However, it has to be mentioned that size distribution changes caused by a monolayer of adsorbed proteins on the capsule surface cannot be detected by this method.[236] Thus the only information obtained from DLS is that additional larger aggregates of nanocapsules caused by interaction with proteins cannot be observed. However, in combination with the ITC results, the most probable scenario would be a minor amount of proteins are still absorpted, which could only partially cover the surface of the capsules.

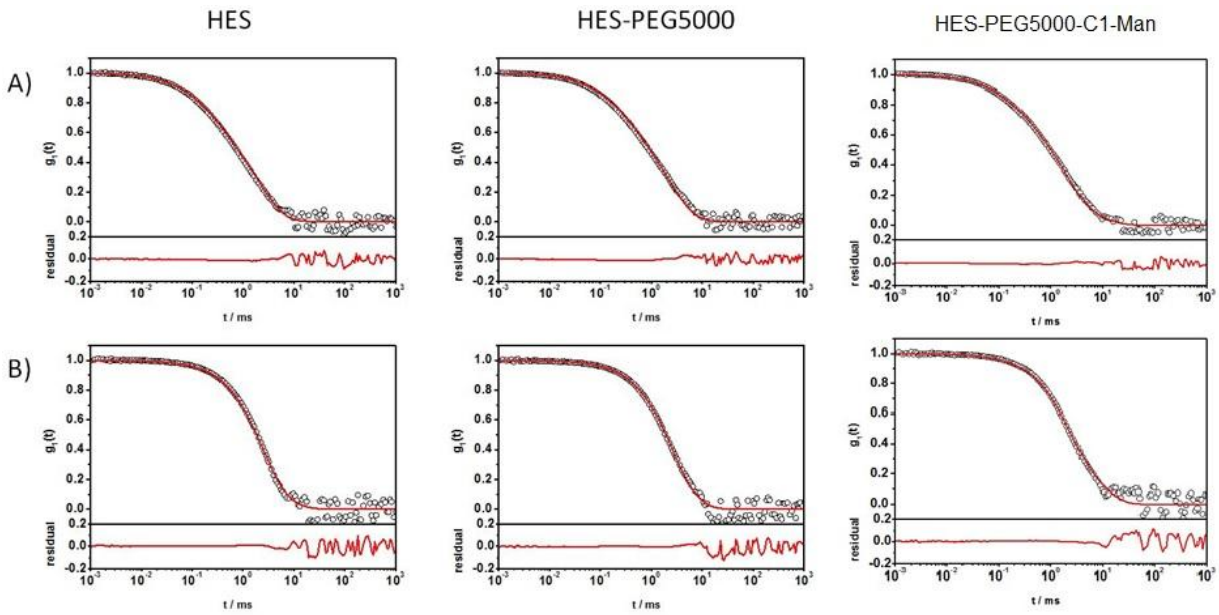

Figure 46. *Upper graphs: Autocorrelation functions (empty circles ○) of the mixture of HES NCs as well as HES-PEG5000 NCs and HES-PEG5000-C1-Man capsules, with (A) concentrated and (B) diluted human plasma. The force fit generated from the sum of the individual components is represented by the red line. Lower graphs: residuals from subtraction of the fit from the data points.*

More importantly, SDS-PAGE data (Figure 47) and proteomic mass spectrometry(Figure 48) proves, that the protein pattern which is identified on all NCs is rather similar, which is a promising prerequisite for specific targeting in plasma.

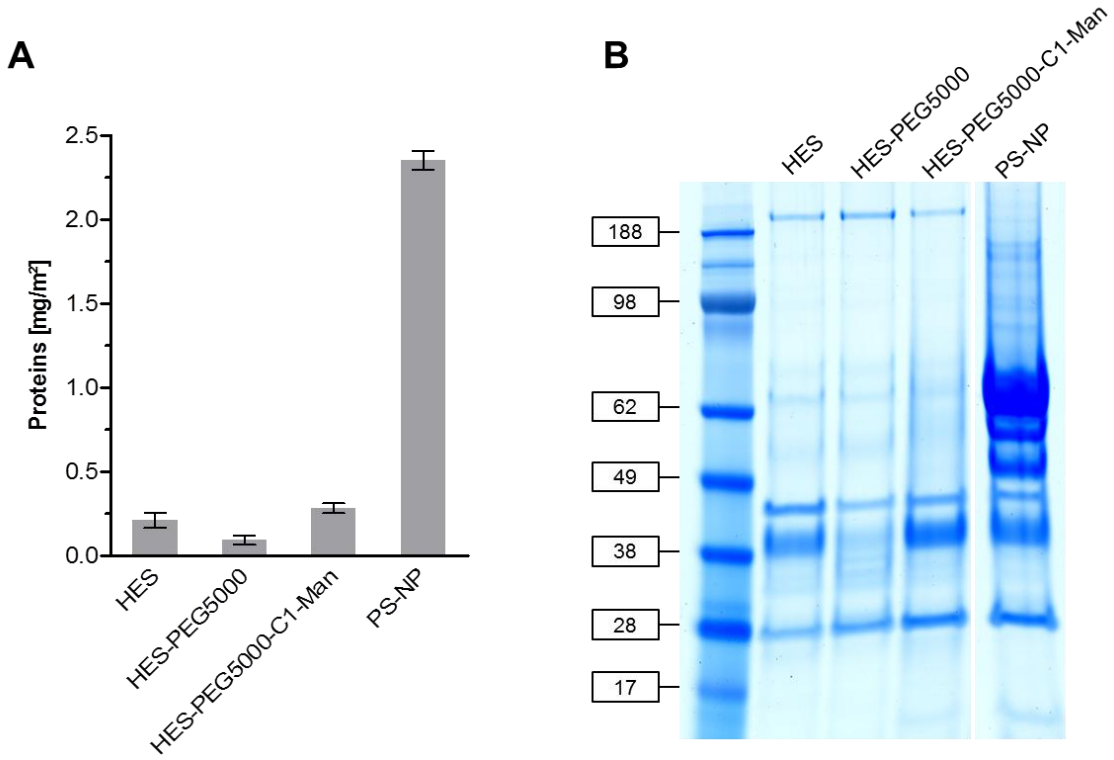

Figure 47. *A) Quantification of human plasma proteins adsorbed to the nanocarriers' surface (mg protein/m² NP). Values are expressed as mean ± SD of triplicates. B) SDS-PAGE was used to visualize the protein corona composition (*Experiments conducted by Susanne Schöttler).

A comparable composition of the protein corona was identified on the unmodified HES-NCs and HES-NCs functionalized with mannose. Only the PEGylated NCs show a slight difference with an overall lower protein adsorption (Figures 47 and 48).

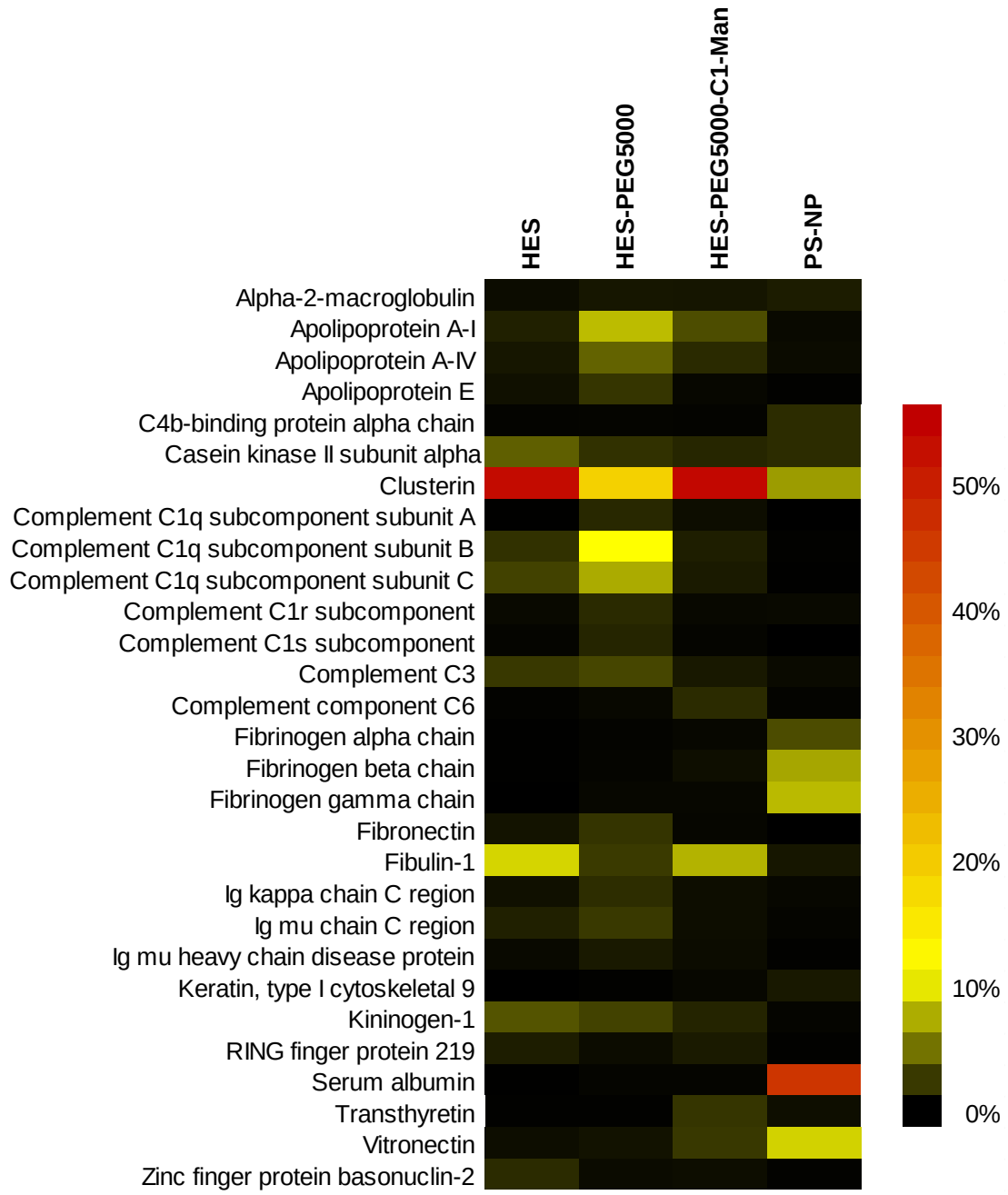

Figure 48. *Heatmap of the most abundant proteins in the protein corona of HES-NC, HES-PEG5000 NCs, HES-PEG5000-C1-Man NCs and a reference PS-NP determined by quantitative liquid-chromatography coupled with mass-spectrometry. Shown are only those proteins which constitute at least 1% of the protein corona on one of the nanocarrier. Values were calculated from the molar masses of each protein (Experiments conducted by Susanne Schöttler).*

Influence of the protein corona on the targeting efficient

An important finding is however, that in all cases protein adsorption cannot be suppressed completely. Thus, the specific binding via a c-type-lectin affinity was performed in order to elucidate the effect on subsequent protein adsorption on the presentation of the targeting mannose unit. The test was performed in buffer and after incubation with human plasma (Figure 49). Both, unmodified HES-NCs and the PEGylated HES-NCs, do not show any specific binding to the C-type lectin before and after incubation in human plasma (the negative control without NCs has the same read-out). On the other hand, the protein corona influenced the binding of c-type-lectin with mannose-functionalized NCs: with plasma proteins adsorbed, the binding of c-type-lectin is reduced, but still strong binding can be detected, compared to unmodified and PEGylated HES-NCs (Figure 49).

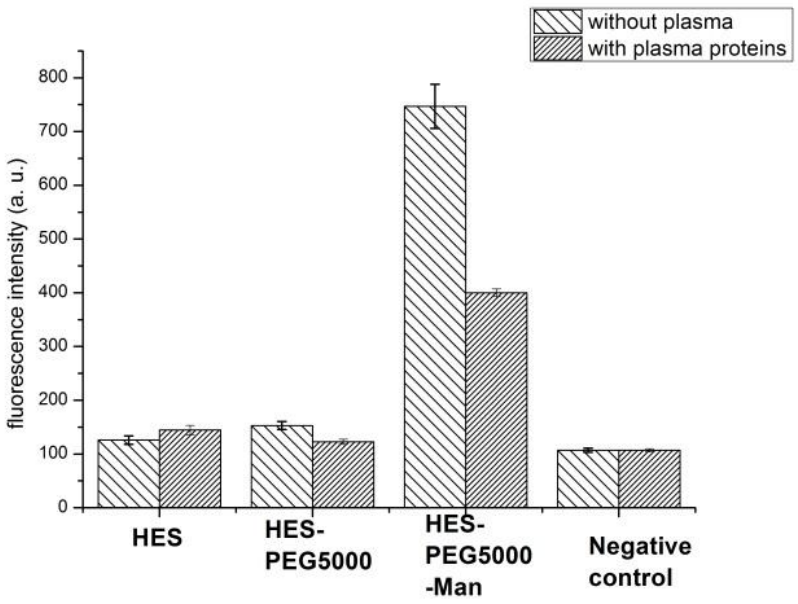

Figure 49. *Binding of unmodified (HES), PEGylated (HES-PEG5000) and mannose-functionalized (HES-PEG5000-C1-Man) HES-NCs with c-type-lectin before or after the incubation with human plasma. (no HES-NCs are added for the negative control).*

Due to their manipulatible role in the immune system, targeting the iDC is biologically more significant, however, as a phagocyte cell, the iDC is known to also take up nanoparticles unspecifically. In order to verify that after adsorption of plasma proteins, the uptake of mannose-functionalized HES-NCs into DCs is a real

receptor-mediated phenomenon, matured dendritic cells (mDC) were also investigated. mDCs have a much lower ability as a phagocyte cell and merely receptor-mediated uptake is possible.

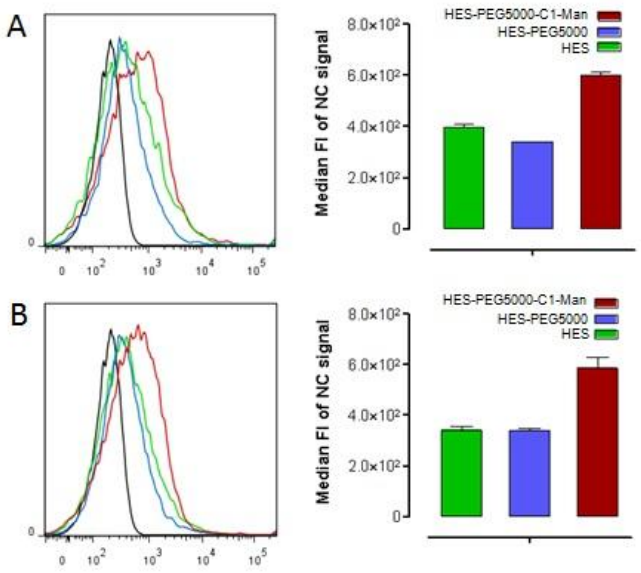

Figure 50. *In-vitro binding of HES-NCs with matured dendritic cells before (A) and after (B) incubation with human plasma. Mature dendritic cells were incubated with 150 µg mL^{-1} of HES, HES-PEG5000 and HES-PEG5000-C1-Man for 2 h at 37 °C. Cell uptake was analyzed using flow cytometry. Pre-incubation of NC with plasma (B) have little influence on cell uptake. Black line in histogram (left): untreated mDC; green line: HES; blue line: HES-PEG5000; red line: HES-PEG-C1-Man (Experiments conducted by Patricia Okwieka).*

Figure 50 clearly proves a similar uptake of HES-PEG5000-C1-Man into mDCs before (Figure 50A) and after (Figure 50B) incubation with human plasma. These results demonstrate, that PEGylated nanocarriers can be further functionalized with targeting groups, e.g. mannose, in order to specifically reach both immature and matured dendritic cells. The influence of the protein corona on the targeting efficiency is minimum. In other words, the interaction between plasma proteins and mannose is not strong enough to prevent it from being recognized by specific acceptors. This finding is in accordance with other works based on polysaccharides, inter alia HES[24], chitosan[183], hyaluronic acid[138] to functionalized the surface of nanocarriers, in order to reduce protein interactions.

Taking into consideration that, rather simple saccharide motifs, like the disaccharide moiety in bleomycin[226], have been proven to be able to selectively target cancer cells. The use of a combination of stealth nanocarriers (i.e. PEGylated materials) with such saccharide-based targeting moieties could solve the important dilemma, where the stealth effect is lost after coupling of other targeting agents.

Experimental Part

Materials

The isocyanate-PEG and isocyanate-PEG-isocyanate (PEG molecular weight of 5,000 g·mol^{-1}, 110 ethylene oxide units) was purchased from Nanocs Inc., USA. PBS buffer (pH 7.4, without Ca^{2+} and Mg^{2+}) was purchased from Gibco, Germany. Boric buffer (1M, pH 9.5) was produced by adjusting pH of boric acid (B6768 Sigma) water solution to the desired value by sodium hydroxide solution. HES (200k, 0.5 degree of substitution) was bought from Fresenius Kabi. Oil soluble surfactant poly((ethylene-*co*-butylene)-*b*-(ethylene oxide)), P(E/B-b-EO), consisting of a poly(ethylene-*co*-butylene) block (M_w =3,700 g·mol^{-1}) and a poly(ethylene oxide) block (M_w = 3,600 g·mol^{-1}) was synthesized starting from ω-hydroxypoly-(ethylene-*co*-butylene), which was dissolved in toluene after addition of ethylene oxide under anionic polymerization conditions[212]. The anionic surfactant sodium dodecylsulfate (SDS) was purchased from Fluka. C-type-lectin (Galanthus nivalis snowdrop lectin fluorescein labeled 2 mg) was bought from BIOZOL Diagnostica Vertrieb GmbH. The fluorescent dye Cy5-oligo was purchased from BioChemica, Aldrich. DBCO-PEG4-NHS was bought from Jana Bioscience. Dimethylsulfoxide (<50 ppm water content) was purchased from Acros Organics. Demineralized MilliQ water was used for the synthesis of nanocapsules. Mannose-azide. Polystyrene particles was prepared according to the publication.[195] The Microbody 2.5D, MC-ME-030, and scFv was obtained from BioNTech. The MOUSE ANTI HUMAN CD205 (Dec205) antibody was bought from Bio-Rad AbD Serotec GmbH, with the catalog number of MCA4755. All the other chemicals were purchased from Sigma Aldrich, and used as received.

Blood samples were taken at the Transfusion Centre of the University Medical Center of the Johannes Gutenberg-University Mainz from 10 healthy donors after obtaining informed consent. The study was approved by the local ethics committee. Li-Heparin was added to prevent blood clotting. The blood was then centrifuged to pellet red and white blood cells and the plasma supernatant was pooled. Aliquots were stored at -80 °C. After thawing, the plasma was centrifuged at 20,000 g for 1 h

at 4 °C to remove any residual precipitates. A protein concentration of 66 $g \cdot L^{-1}$ was determined for the plasma.

Methods.

NMR

^{1}H NMR and ^{13}C spectrums are measured at 300 MHz on a Bruker Avance 300 Spectrometer.

Fluorescence

The fluorescamine (FA) assay[203] is used to quantify the available primary amine groups at the surface of the nanocapsules, and the amine functionalized mannose in the solution. A stock solution of FA is prepared by mixing 2 mg of FA and 1.5 mL of anhydrous acetone. A standard working function is established from an aqueous hexylamine solution as reference. For a typical quantification step, 25 µL of the nanocapsule dispersion (or amine functionalized mannose solution) in water are added into 725 µL of boric buffer (pH 9.5), followed by the addition of 200 µL of the FA stock solution. The mixture is vortexed (Heidolph REAX2000 at maximum speed) for 30 s, and the fluorescence intensity is measured by a Tecan plate reader at 25 °C by excitation at 410 nm and detecting the emission at 470 nm. All fluorescence measurements are repeated three times.

Electron Microscopy.

The same diluted dispersion as for DLS is used to prepare electron microscopy samples. Scanning electron microscopy (SEM) measurements are carried out by using a LEO (Zeiss) 1530 Gemini device (Oberkochen, Germany). then 15 µL of the dispersion is placed on the silica wafer and dried at room temperature overnight. Transmission electron microscopy (TEM) measurements are carried out by using Jeol 1400 device at 120 kV accelerating voltage. The samples are diluted in the same way as for SEM sample preparation. Then 2 µL of the diluted sample is placed on a copper grid, which is covered by a 5 nm thick carbon film.

Functionalization of the surface of HES-NCs with monoisocyanate-PEG or isocyanate-PEG-isocyanate

For a typical coupling reaction, 2 mL of the nanocapsule dispersion is centrifuged at 4000 rpm for 30 min to remove the excess of surfactant. The upper phase is discarded, while the precipitate is redispersed in 2.5 g of anhydrous cyclohexane by pipetting up and down. Either 16 mg of monoisocyanate-PEG (MeO-PEG110-NCO with Mn=5000 g·mol−1) or isocyanate-PEG-isocyanate (OCN-PEG110-NCO with Mn=5000 g·mol−1) was dissolved in 0.63 g (800 µL) of anhydrous acetone and added dropwise into the capsule dispersion, which is magnetically stirred at 500 rpm. The reaction is allowed to proceed for 5 h, and centrifuged at 4000 rpm (Eppendorff centrifuge 5417C) afterwards to remove non-coupled PEG. The precipitate is redispersed in 400 µL of cyclohexane and used for further steps.

Redispersion of capsules in water

A 0.1wt% SDS solution is prepared, and filtered (sterile, with 0.2 µm pore size). 5 mL of this SDS solution is gently shaken in a sonication bath (Bandelin Sonorex, type RK 52H), while nanocapsule (from 2 mL of the as prepared dispersion) redispersed in 400 µL of cyclohexane is added slowly. Then the whole dispersion is magnetically stirred at 1000 rpm at room temperature overnight, in an open vial, to allow evaporation of cyclohexane. The obtained dispersion is ultrafiltrated by a Amicon Centrifugal Filter (Ultra-0.5, Ultracel-100 Membrane, 100 kDa), in order to remove the excess of SDS and used for further steps.

Synthesis of mannose-azide

Synthesis of α-D-Mannopyranosyl azide *(Experiments conducted by Jens Langhanki).*

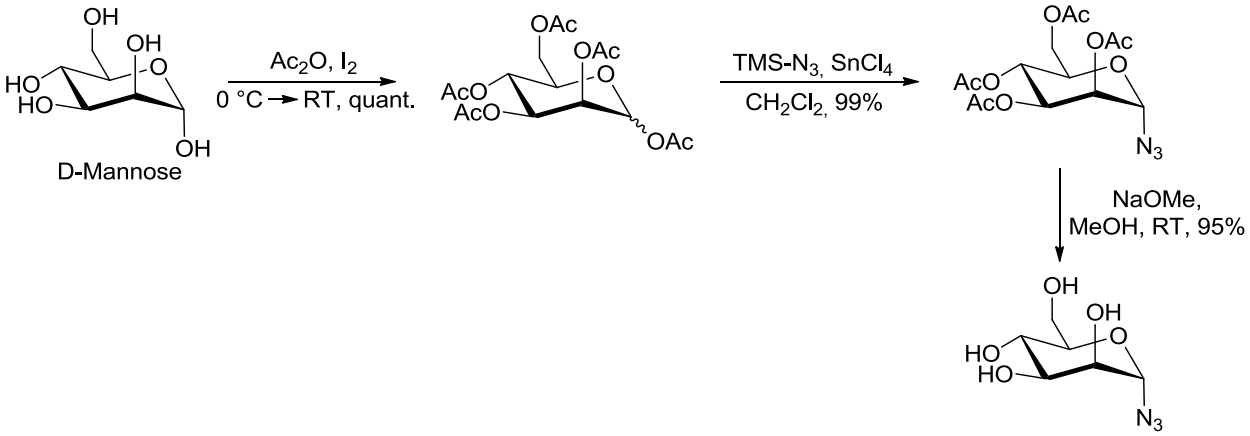

Scheme 7*. Synthesis of α- D-Mannopyranosyl azide.*

General Procedures: All reagents were reagent grade and used without further purification unless otherwise noted. All reactions involving air or moisture sensitive reagents or intermediates were performed under an inert atmosphere of argon in glassware that was oven dried. Reaction temperatures referred to the temperature of the particular cooling/heating bath. Chromatography was performed using flash chromatography of the indicated solvent system on 35-70 µm silica gel (*Acros Organics*) unless otherwise noted. ^{1}H NMR and ^{13}C NMR spectra were recorded on a *Bruker Avance-II 400* MHz. Chemical shifts were referenced to the deuterated solvent (e.g., for $CDCl_3$, δ= 7.26 ppm and 77.16 ppm for ^{1}H and ^{13}C NMR, respectively) and reported in parts per million (ppm, δ) relative to tetramethylsilane (TMS, δ = 0.00 ppm).[237] Coupling constants (*J*) were reported in Hz and the splitting abbreviations used were: s, singlet; d, doublet; t, triplet; m, multiplet;br, broad. Reactions were monitored by thin-layer chromatography (TLC) carried out on

0.25 mm E. Merck silica gel plates ($60F_{254}$) using an 1M ethanolic solution of sulfuric acid with 0.2% 3-methoxyphenol and heat as developing agents. Specific reactions were monitored by LC-MS on a 1200 HPLC-unit from *Agilent Technologies* with binary pump and integrated diode array detector coupled to a LC/MSD-Trap-mass-spectrometer from *Bruker*. Ionization was achieved by an electron-spray-ionization source (ESI) or an atmospheric-pressure-chemical-ionization source (APCI). High-resolution masses were recorded on a *Waters QTof-Ultima 3*-Instrument with *Lockspray*-Interface and a suitable external calibrant. Infrared spectra were recorded as FT-IR spectra using a diamond ATR unit and are reported in terms of frequency of absorption (ν, cm^{-1}). Dichloromethane was distilled from calcium hydride.

1,2,3,4,6-Penta-*O*-acetyl-D-mannopyranose. Iodine (560 mg, 2.2 mmol, 0.04 eq.) and acetic anhydride (50 mL) were mixed under Ar-atmosphere. D-Mannose (10 g, 55.5 mmol, 1 eq.) was added portion by portion at 0 °C. After stirring for 30 min at 0 °C and additionally for 18 hours at room temperature TLC (cyclohexane/toluene/ethylacetate 3:3:1) showed complete consumption of the starting material. The reaction mixture was diluted with CH_2Cl_2 (50 mL) and was washed twice with cold saturated aqueous Na_2SO_3 solution (2x 80 mL), then with a saturated aqueous solution of $NaHCO_3$ (4x 50 mL). The separated organic layer was dried over anhydrous Na_2SO_4. The solvent was removed *in vacuo* to afford the desired peracetylated D-mannose (21.5 g, 55.1 mmol, 99%, mixture of both anomers α/ 12:88) as a yellowish high viscous oil.

R_f 0.30 (silica gel, cyclohexane/toluene/ethyl acetate, 3:3:1);

Signals assignable to ⟨-anomer: ^{1}H NMR, COSY (600 MHz, $CDCl_3$) δ (ppm) = 6.09 (d, ^3J = 1.9 Hz, 1H, H-1), 5.34–5.36 (m, 2H, H-3, H-4), 5.25–5.27 (m, 1H, H-2), 4.28

(dd, ^{2}J = 12.4 Hz, ^{3}J = 4.9 Hz, 1H, H-6a), 4.10 (dd, ^{2}J = 12.4 Hz, ^{3}J = 2.5 Hz, 1H, H-6b), 4.03-4.07 (m, 1H, H-5), 2.18, 2.17, 2.10, 2.05, 2.01 (5x s, 15H, COCH_3); ^{13}C NMR, HSQC, HMBC (151 MHz, $CDCl_3$) δ (ppm) = 170.8, 170.2, 169.9, 169.7, 168.2 (5x $COCH_3$), 90.7 (C-1), 70.7 (C-5), 68.8 (C-3), 68.4 (C-2), 65.6 (C-4), 62.2 (C-6), 21.0, 20.9, 20.9, 20.8, 20.8 (5x $COCH_3$).

2,3,4,6-Tetra-*O*-acetyl-⟨-D-mannopyranosyl azide. 1,2,3,4,6-Penta-*O*-acetyl-D-mannopyranose (13.6 g, 34.9 mmol, 1 eq.) was dissolved in anhydrous CH_2Cl_2 (140 mL) under argon. Trimethylsilyl azide (16.1 g, 18.5 mL, 139 mmol, 4 eq.) and tin(IV) chloride (2.37 g, 1.06 mL, 9.1 mmol, 0.26 eq.) was added. After stirring for four hours at room temperature TLC (cyclohexane/toluene/ethylacetate 3:3:1) showed complete consumption of the starting material. The reaction mixture was washed successively with saturated aqueous $NaHCO_3$ solution (100mL), water (100 mL) and brine (100 mL). The organic layer was dried over anhydrous Na_2SO_4. The solvent was removed *in vacuo* and the residue was purified by flash column chromatography (cyclohexane/ ehtylacetate, 3:1) to afford the title compound (12.9 g, 34.4 mmol, 99%) as a clear, colorless oil.

R_f 0.49 (silica gel, cyclohexane/toluene/ethyl acetate, 3:3:1);

^{1}H NMR, COSY (400 MHz, $CDCl_3$) δ (ppm) = 5.38 (d, ^{3}J = 1.9 Hz, 1H, H-1), 5.14 (dd, ^{3}J = 3.0 Hz, ^{3}J = 1.9 Hz, 1H, H-2), 5.30–5.21 (m, 2H, H-3, H-4), 4.32-4.27 (m, 1H, H-6a), 4.17–4.11 (m, 2H, H-5, H-6b), 2.16, 2.10, 2.04, 1.98 (4x s, 12H, COCH_3); ^{13}C NMR, HSQC, HMBC (100.6 MHz, $CDCl_3$) δ (ppm) = 170.7, 170.0, 169.9, 169.7 (4x $COCH_3$), 87.6 (C-1), 70.7 (C-5), 69.3 (C-2), 68.3 (C-3), 65.7 (C-4), 62.2 (C-6), 21.0, 20.8, 20.8, 20.7 (4x $COCH_3$).

The spectral data are in accordance with literature. (7)

α-D-Mannopyranosyl azide. 2,3,4,6-Tetra-*O*-acetyl-α-D-mannopyranosyl azide (10 g, 26.8 mmol) was dissolved in methanol (100 mL) and sodium methoxide was added until pH 9–10 (approx. 60 mg). The reaction mixture was stirred at room temperature for 16 hours. Subsequently the solution was neutralized by Amberlite 120 H^+ resin until pH 7. The mixture was filtered over Celite witch was washed thoroughly with methanol. The solvent was removed *in vacuo* to afford the desired α-D-Mannopyranosyl azide (5.23 g, 25.5 mmol, 95%) as a colorless syrup.

^{1}H NMR, COSY (400 MHz, $CDCl_3$) δ (ppm) = 5.43 (d, ^3J = 1.9 Hz, 1H, H-1), 3.91–3.87 (m, 1H, H-6a), 3.85 (dd, ^3J = 3.3 Hz, ^3J = 1.9 Hz, 1H, H-2), 3.79–3.69 (m, 3H, H-3, H-5, H-6b), 3.65-3.59 (m, 1H, H-4); ^{13}C NMR, HSQC, HMBC (100.6 MHz, $CDCl_3$) δ (ppm) = 89.7 (C-1), 74.6 (C-5), 69.8, 69.7 (C-2, C-3), 66.3 (C-4), 60.7 (C-6).

Coupling of mannose-azide to isocyanate-PEG-isocyanate functionalized capsule

To 5 mL of the capsule dispersion with a solid content of 0.1 wt% is added 500 µL of 0.8M boric acid solution. The pH of the solution is adjusted to 8.3 and 0.12 mg of DBCO-PEG4-NHS is added, which is prepared as a stock solution of 1mg in 1mL of anhydrous DMSO. The reaction is allowed to proceed for 4h, the uncoupled DBCO is removed by ultrafiltration. And the coupled DBCO is quantified by a fluoregenetic reaction with anthracene azide[238]. Azide mannose is added with a 1:1 mol ratio to coupled DBCO.

Synthesis of 2-Animoethyl α-D-mannopyranoside

2-Animoethyl α- *D*-mannopyranoside was prepared according to [239] ,

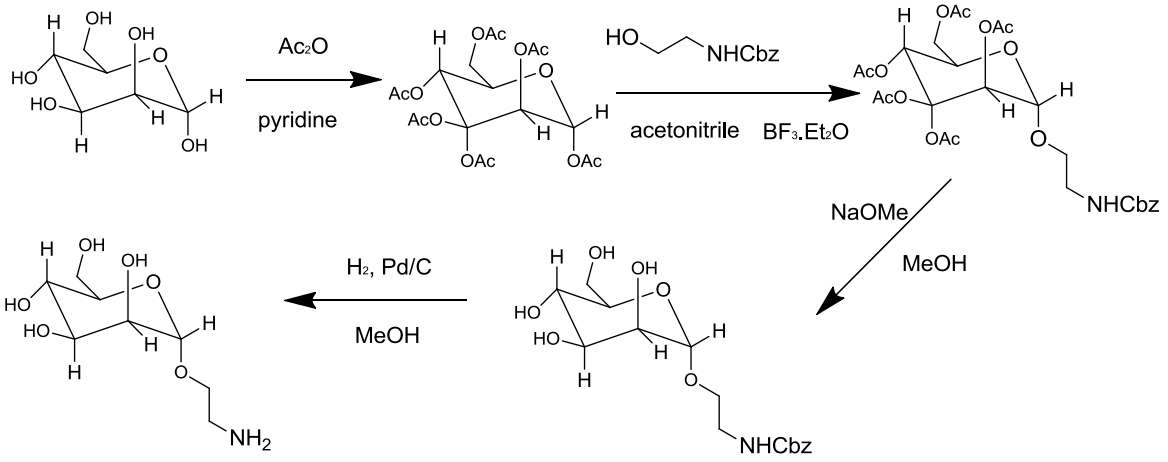

Scheme 8. *Synthesis of aminoethyl mannoside.*

5.0 g of *D*-mannose is dissolved in 35 mL of pyridine. 14.0 g of acetic anhydride is added in one portion. The reaction mixture is stirred at room temperature for 16h. Afterwards the solvent is removed at 50°C under vaccum, the residual is dissolved in ethyl acetic, washed successively by MilliQ water and brine, and dried by rotation evaporation. 10.2 g of peracetylated mannose is produced as a viscous oil, ^{1}H NMR (300 MHz, CDCl3, mixture of both anomers): signals of β-anomer : 1.98 (s, 3H, COCH3), 2.07 (s, 3H, COCH3), 2.08 (s, 3H, COCH3), 2.15 (s, 3H, COCH3), 2.19 (s,3H, COCH3), 3.99–4.05 (m, 1H, 5-H), 4.07 (dd, J = 2.4, 12.4 Hz, 1H, 6-Ha), 4.26 (dd, J =4.9, 12.4 Hz, 1H, 6-Hb), 5.23 (dd, J = 2.0, 3.1 Hz, 1H, 3-H), 5.31–5.34 (m, 2H, 3-H, 4-H),6.06 (d, J = 2.0 Hz, 1H, 1-H); signals of α-anomer: 1.98 (s, 3H, COCH3), 2.03 (s,3H, COCH3), 2.07 (s, 3H, COCH3), 2.15 (s, 3H, COCH3), 2.16 (s, 3H, COCH3), 3.79 (ddd, J= 2.4, 5.3, 9.9 Hz, 1H, 5-H), 4.11 (dd, J = 2.4, 12.4 Hz, 1H, 6-Ha), 4.28 (dd, J = 5.3, 12.4 Hz,1H, 6-Hb), 5.11 (dd, J = 3.3, 10.0 Hz, 1H, 3-H), 5.27 (t, J = 10.0 Hz, 1H, 4-H), 5.46 (dd, J =1.2, 3.3 Hz, 1H, 2-H), 5.84 (d, J = 1.2 Hz, 1H, 1-H); ^{13}C NMR (101 MHz, CDCl3, mixture of both anomers): signals of β-anomer: 20.73, 20.75, 20.80, 20.86, 20.95 (5 q, 5COCH3), 62.2 (t, C-6), 65.6 (d, C-4), 68.4 (d, C-2), 68.8 (d, C-3), 70.7 (d, C-5), 90.7 (d, C-1),168.2, 169.6, 169.8, 170.1, 170.7 (5 s,

5 COCH3); signals of α-anomer: 20.63,20.76, 20.81, 20.84, 20.86 (5 q, 5 COCH3), 62.1 (t, C-6), 65.4 (d, C-4), 68.3 (d, C-2), 70.7 (d,C-3), 73.4 (d, C-5), 90.5 (d, C-1), 168.5, 169.7, 169.9, 170.3, 170.8 (5 s, 5 COCH3).

2.52 g of Mannose pentaacetate is dissolved in 25 mL of anhydrous acetonitrile in a 50 mL schlenk tube, which is sealed by a rubber stopper and flushed with argon. 1.526 g of N-Z-ethanolamine (1.2 equi) is dissolved in 2 mL of anhydrous acetonitrile, and added dropwise into the schlenk tube. The system is placed in ice bath, and 4.61 g of BF3•Et2O (5 equivalent) is added dropwise. The solution is stirred in ice bath for the other 30 min, and overnight at room temperature. 5 equivalent of TEA was added to quench the reaction. Solvent is removed by vacuum, and the product purified by column chromatography on silica, with 1:1 mixture of ethyl acetic and petroleum ether (low boiling point) as elute. The second compound come out of the column is the product. ^{1}H NMR (300 MHz, CDCl3): 2.00 (s, 3H, COC*H*3),2.04 (s, 3H, COC*H*3), 2.09 (s, 3H, COC*H*3), 2.16 (s, 3H, COC*H*3), 3.36–3.53 (m, 2H,C*H*2NH), 3.58 (ddd, *J* = 3.6, 6.8, 10.2 Hz, 1H, C*H*aHbCH2NH), 3.78 (ddd, *J* = 3.9, 6.210.2 Hz, 1H, CHa*H*bCH2NH), 3.97 (ddd, *J* = 2.3, 5.7 9.5 Hz, 1H, 5-H), 4.08 (dd, *J* = 2.3,12.2 H 1H, 6-Ha), 4.26 (dd, *J* = 5.7, 12.2 Hz, 1H, 6-Hb), 4.82 (d, *J* = 1.7 Hz, 1H, 1-H), 5.12(s, 2H, C*H*2Ph), 5.20 (bt, *J* = 5.8 Hz, 1H, N*H*), 5.25 (dd, *J* = 1.7, 3.2 Hz, 1H, 2-H), 5.26 (dd, *J*S12= 9.5, 10.1 H), 5.31 (dd, *J* = 3.2, 10.0 Hz, 1H, 3-H), 7.29–7.39 (m, 5H, C6*H*5); ^{13}C NMR(101 MHz, CDCl3): 20.7, 20.8, 20.9 (3 q, 4 COcc*C*H3), 40.7 (*C*H2NH), 62.5 (t, C-6), 66.1 (d, C-4), 66.9 (t, *C*H2Ph), 67.8 (t, *C*H2CH2NH), 68.8 (d, C-5), 69.0 (d, C-3), 69.4 (d,C-2), 97.8 (d, C-1), 128.2, 128.6 (2 d, *o*-, *m*-, *p*-C from C6H5), 136.4 (s, *i*-C from C6H5),156.4 (s, N*C*OO), 169.8, 170.0, 170.1, 170.7 (4 s, 4 *C*OCH3).

975 mg of the product from last step is dissolved in 30 mL MeOH, and 34 mg of NaOMe is added (113 mg 30% solution in MeOH). The reaction is stirred overnight, and the ions are removed by Abmerlite IR120, H+ form. The resin is removed by filtration, and solvent removed by rotational evaporation. ^{1}H NMR (300 MHz, MeOD): 3.27–3.39 (m, 2H,C*H*2NH), 3.47–3.55 (m, 2H, 5-H, C*H*aHbCH2NH), 3.60 (t, *J* = 9.5 Hz, 1H, 4-H), 3.68 (dd, *J* =5.8, 11.7 Hz, 1H, 6-Ha), 3.69 (dd, *J* = 3.4, 9.3 Hz, 1H, 3-H), 3.74 (ddd, *J* = 4.9, 6.4, 10.2 Hz,1H, CHa*H*bCH2NH), 3.80 (dd, *J* = 1.7, 3.4 Hz,

1H, 2-H), 3.81 (dd, *J* = 2.3, 11.7 Hz, 1H, 6-Hb), 4.75 (d, *J* = 1.6 Hz, 1H, 1-H), 5.06 (s, 2H, C*H*2Ph) , 7.24–7.36 (m, 5H, C6*H*5); ^{13}C NMR(101 MHz, MeOD): 41.7 (t, CH2*C*H2NH), 62.8 (t, C-6), 67.5 (t, *C*H2Ph,*C*H2CH2NH), 68.5 (d, C-4), 72.0 (d, C-2), 72.5 (d, C-3), 74.7 (d, C-5), 101.6 (d, C-1), 128.8,129.0, 129.5 (3 s, *o*-, *m*-, *p*-C from C6H5), 138.3 (s, *i*-C from C6H5), 158.9 (s, N*C*OO).

The product from the third step is further hydrogenated by dissolving in MeOH on Pd deposited active carbon. The reduction is carried out overnight. The catalyst is removed by Celite filtration, and the solvent removed by rotational evaporation to get the final product, 356 mg, as white powder. ^{1}H NMR (300 MHz, MeOD): 2.82–2.86 (m, 2H,C*H*2NH2), 3.48 (ddd, *J* = 4.7, 5.9, 10.2 Hz, 1H, C*H*aHbCH2NH2), 3.56 (ddd, *J* = 2.1, 5.8,9.7 Hz, 1H, 5-H), 3.63 (t, *J* = 9.4 Hz, 1H, 4-H), 3.73 (dd, *J* = 5.8, 11.8 Hz, 1H, 6-Ha), 3.74(dd, *J* = 3.4, 9.1 Hz, 1H, 3-H), 3.79 (ddd, *J* = 4.7, 5.9, 10.2 Hz, 1H, CHa*H*bCH2NH2), 3.86(dd, *J* = 1.7, 3.4 Hz, 1H, 2-H), 3.86 (dd, *J* = 2.1, 11.8 Hz, 1H, 6-Hb), 4.80 (d, *J* = 1.7 Hz, 1H,1-H); ^{13}C NMR (101 MHz, MeOD): 101.7 (d, C-1), 74.6 (d, C-5), 72.5 (d, C-4),72.0 (d, C-2), 70.0 (t, *C*H2CH2NH2), 68.6 (d, C-3), 62.8 (t, C-6), 42.0 (t, *C*H2NH2).

Coupling of mannose-amine to isocyanate-PEG-isocyanate functionalized capsule

The isocyanate-PEG-isocyanate functionalized HES capsule in cyclohexane phase is redispersed in 5 g 0.1wt% SDS solution, which contains additionally 20mg of amine functionalized mannose. Other conditions are the same as for redispersion of PEG functionalized capsules in water.

Coupling of Microbody 2.5D and MC-ME-030 to the surface of the PEGylated Nanocapsules

To 5 mL of the capsule dispersion with a solid content of 0.1 wt% is added 500 µL of 0.8M boric acid solution. The pH of the solution is adjusted to 8.3 and different amounts of DBCO-PEG4-NHS is added, which is prepared as a stock solution of 1mg in 1mL of anhydrous DMSO. The reaction is allowed to proceed for 4h, the

uncoupled DBCO is removed by ultrafiltration. And the coupled DBCO is quantified by a fluoregenetic reaction with anthracene azide[238]. Azide functionalized Microbodies are added with a 1:1 mol ratio to coupled DBCO.

Coupling of Microbody scFv to the surface of the PEGylated Nanocapsules

The scFv-Fragment is reduced by Tris(2-carboxyethyl)phosphine (TCEP) (1:62.5 (8mM); 2h;RT), to create thiol groups on the scFv-Fragment, followed by dialyzing in Nellis-buffer (degased by flushing with N2; 100 mM Phosphate buffer (76,3 mM NaH_2PO_4 & 23,7 mM Na_2HPO_4, 300 mM NaCl, 4 mM Ethylenediaminetetraacetic acid (EDTA)); pH 6.7; overnight).

HES-NCs are incubated with Sulfosuccinimidyl 4-(N-maleimidomethyl)cyclohexane-1-carboxylate (Sulfo-SMCC, 3 mM) in PBS (pH 7.4) for 1h at room temperature. The free Sulfo-SMCC is removed by ultrafiltration (ultrafilter 100K MWCO, 5000 rpm, 20 min), followed by the addition of the reduced scFv-Fragment. The number of scFv-Fragment added per capsule is calculated to be 8. After overnight incubation, the dispersion is further purified by ultrafiltration, and send for biological test.

Coupling of Dec205 to the surface of the PEGylated Nanocapsules

0.4 mg of Dec205 is dissolved in 400 µL of PBS buffer, and the pH is adjusted to 7.60±0.05, the stock solution of $1.16 * 10^{-3}$ mg of NHS-PEG4-Azide in anhydrous DMSO is added, which is 3.7 mol equivalent to the Dec205. The reaction is allowed to proceed for 1h, while the excess of NHS-PEG4-Azide is removed by dialyzing.

The coupling of the azide Dec205 to the PEGylated HES-NCs is carried out following the same procedure as for coupling of Microbodies to the capsules.

Incubation of capsules with human plasma

To 100 µL dispersion of each capsule dispersion with a solid content of 1.0wt%, 16.7 µL of human plasma with a protein concentration of 15 $g \cdot L^{-1}$ were added at room

temperature. The system is incubated at room temperature over night, and purified in the next morning by centrifugation at 6000 rpm for 20 min. The upper phase is discarded, and the precipitate is redispersed in MilliQ water for further analysis. The capsule to protein ratio is the same as for ITC and DLS measurement.

Isothermal Titration Calorimetry (ITC) *(Experiments conducted by Svenja Winzen).*

The isothermal titration calorimetry measurements were performed using a NanoITC Low Volume (TA Instruments, Eschborn, Germany) with an effective cell volume of 170 µL. In an experiment 50 µL of human plasma with a protein concentration of 15 $g \cdot L^{-1}$ were titrated to 300 µL of each HES-capsule suspension (HES 1.30 $g \cdot L^{-1}$, HES-PEG5000 1.25 $g \cdot L^{-1}$, HES-PEG5000-C1-Man 1.15 $g \cdot L^{-1}$). The same titration was performed with a suspension of polystyrene nanoparticles at a concentration of 0.92 g/L for comparison. The experimental temperature was kept constant at 25 °C. Additionally, the same amount of plasma was titrated into pure water to determine the heat of dilution for reference. The number and injected volume of the titration steps were the same for all measurements (25 x 2 µL). The spacing between injections was set to 300 s. The integrated reference heats were then subtracted from the integrated heats of the adsorption experiments. All titrations were measured in triplicates to ensure proper reproducibility.

Dynamic Light Scattering (DLS) of capsule / plasma mixtures

All dynamic light scattering experiments were performed on a commercially available instrument from ALV GmbH (Langen, Germany) consisting of a goniometer and an ALV-5000 multiple tau full-digital correlators with 320 channels. A helium-neon laser from JDS Uniphase (Milpitas, USA) with an operating intensity of 25 mW and a laser wavelength of $\lambda = 632.8$ nm was used as a light source. All solutions for the light scattering experiments were prepared in dust-free quartz cuvettes from Hellma (Müllheim, Germany) with an inner diameter of 18 mm, which were cleaned before with distilled acetone. For the measurements of nanocapsule-plasma mixtures 2 mL of concentrated (60 $g \cdot L^{-1}$) or with 0.15 M NaCl solution diluted (0.075 $g \cdot L^{-1}$) human plasma were filtered into the cuvette through a Millex-GS filter (Merck Millipore, Darmstadt, Germany) with a pore size of 0.2 µm. To this solution 10 µL of a 7.3 $g \cdot L^{-1}$ capsule dispersion were added. The mixtures were then incubated at 37 °C for 30 min followed by the DLS measurements at the same temperature.

C-type lectin interaction

The binding of different capsules with a mannose specific c-type-lectin, Galanthus nivalis snowdrop lectin, was studies by incubating different capsules with a fluorescein labeled c-type-lectin. To 500 µL of capsule dispersion (0.1 wt %) in HEPES buffer (0.1 M, pH 7.5) was added 10 µg of c-type-lectin in MilliQ water. The system is shaken at room temperature for 2h, and then overnight at 4 °C. The dispersion is centrifuged at 3150 rzb for 10 min, the precipitate is isolated, and redispersed in 500 µL of HEPES buffer (0.1 M, pH 7.5). The fluorescence of the final dispersion is measured by a Tecan plate reader at 25 °C by excitation at 495 nm and detecting the emission at 519 nm. All fluorescence measurements are repeated three times.

in-vitro test *(experiments conducted by Patricia Okwieka).*

Generation of immature or mature dendritic cells (iDC or mDC)

Buffy coats from healthy human donors were used to isolate peripheral blood mononuclear cells (PBMC) by standard Ficoll density centrifugation. Donor blood was obtained according to the declaration of Helsinki. Dendritic cells were generated from monocytes using plastic adherence. PBMC were seeded at a density of 1,5 x 10^7 cells per well of a 6-well plate. Cells were allowed to adhere in a humidified environment at 37 °C with 5% CO_2 for 1 h in 3 mL of DC-medium (RMPI with 2% heat-inactivated pooled human serum (HS), 100 U/mL streptomycin (Sigma). By multiple washing with phosphate buffered saline (PBS, Invitrogen) non-adhering cells were removed. Monocytes were kept in DC-medium containing 800 U/mL granulocyte/ macrophage-colony stimulating factor (GM-CSF, Genzyme) and 500 U/ mL interleukin (IL)-4 (PromoKine) at 37 °C/ 5% CO_2 for two days. Afterwards old medium was removed and fresh medium supplemented with with 1600 U/ mL GM-CSF and 1000 U/ mL IL-4 was added on days 3 and 5. On day 6 immature dendritic cells (iDC) were harvested or maturation of iDC was induced to generate mature DC (mDC). By incubation with PBS/ EDTA (2 mM) for 10 min at 37 °C and subsequent washing with cold PBS iDC were obtained. Maturation of iDC was induced by incubation of cells with DC medium supplemented with 500 U/ mL IL-4, 1600 U/ mL GM-CSF , 10ng/mL IL-1β, 10 ng/ mL TNF-α, 1000 U/ mL IL-6 and 1 µg/mL PGE_2 for 2 days. Mature dendritic cells were harvested using cold PBS. For NC loading of DC, cryopreserved i or mDC were used.

Loading of DC with nanocapsules

1 x 10^5 DC were incubated with NC at 37 °C/ 5% CO_2 in DC medium supplemented with 1600 U/ mL GM-CSF and 500 U/ mL IL-4. Two different nanocapsule concentrations (50 or 150 µg/ mL) and incubation periods (2 or 16 h) were analyzed. Afterwards cells were collected using multiple washing steps with cold PBS. The nanocapsule containing supernatant was removed by centrifugation for 5 min at 470 g.

Flow cytometry analysis of NC-loaded DC

Pelleted DC were stained with CD11c-FITC (Miltenyi), CD45-APC-Cy7 (BD) and CD45-V450 (BD). Cells were allowed to incubate with the various antibodies for 15 min at 4 °C. After a washing step with PBS/ 0.1% BSA, the cells were centrifuged and resuspended in 0.3 mL PBS/ 0.1% BSA. NC uptake by DC was detected using a LSR-Fortessa or FACS Canto II analyzer, both equipped with FACSDiva™ software (Becton Dickinson). Fluorescence of the NC dyes sulforhodamine (SR101) or Cy5-oligo was detected using a 586/15 nm bandpass filter with excitation by a 100 mW/ 561 nm laser or a 660/20 nm bandpass filter with excitation by a 40 mW 633 nm laser, respectively. Conjugates like FITC were excited using a 100 mW 488 nm laser (filter 530/30 nm) and a 100 mW 405 nm laser (filter 450/50). Cells were analyzed using FlowJo 7.6.5 (Tree Star Inc.).

Fluorescent Microscopy analysis of the binding of the capsules with cells

3 * 10^5 B16F10 cells were splitted in a well of a 6-well-plate, and incubated at 37 °C overnight, under 5% CO_2. The cells were washed by PBS buffer for once before they were incubated with the HES-NCs, followed by the addition of 60 µL of nanocapsule dispersion (1 wt%), and incubated on ice for 3h. The cells are fixed by using 2% formaldehyde (15min, RT), and subsequently washed by PBS for three times. The cells are then embedded with DAPI 1:5000 in Fluorescent Mounting Medium, and analyzed for the binding of the nanocapsules by using Zeiss-Microscope (Axio, Imager.M2).

In-vivo test

Pharmakokinetic studies for plasma half-life studies *(experiments conducted by Oliver Seifert).*

Female SWISS (Janvier, CD1, 8 weeks old animals per construct) received an intravenous (i.v.) injection of 300 µg of the capsule in a total volume of 100 µL (in PBS). Blood samples (50 µL) were taken in the time intervals of 2 min, 30 min, 1 h, 2

h, 4 h, 6 h, 1 day and 3 days, incubated with heparin and stored at 4°C. Using Li-COR, fluorescence intensity of the blood samples was measured to analyze the concentration of the functionalized capsules. Comprising standard curve and weight of animals, the percentage of injected doses was calculated. $T_{1/2}\beta$ and area under the curve (AUC) were calculated with Excel.

In vivo / Ex vivo Fluorescence Imaging for the bio-distribution of the capsules *(experiments conducted by Mustafa Diken).*

Six to eight-week old female BALB/c mice were obtained from Charles River. All mice were kept and handled in accordance with federal and state policies on animal research.

In vivo/ ex vivo fluorescence imaging of fluorescently labeled unmodified or PEGylated HES-NCs was performed using the IVIS Spectrum Imaging system (Perkin Elmer). Upon intravenous injection of nanocapsules (1mg), BALB/c mice (n = 3) were anesthetized with isofluorane at different time points (30min, 1h, 2h, 4h, 6 h, 8 h, 24 h) and placed in the light-tight chamber of IVIS Spectrum. Fluorescence emission was visualized by using the light source and filters with excitation at 745 nm and emission at 800 nm for an exposure time of 3 s. 24 h after injection, mice were sacrificed and fluorescence signal from isolated organs such as brain, lungs, heart, kidneys, liver and spleen were collected *ex vivo* using the same filter set and exposure time. Fluorescence images were presented as superimposed to black & white photos of mice/organs and the fluorescence intensity was depicted with a pseudocolor scale.

Protein corona analysis *(experiments conducted by Susanne Schöttler).*

SDS polyacrylamide gel electrophoresis (SDS-PAGE).

For SDS PAGE 16.25 µL of the protein sample was mixed with 6.25 µL NuPAGE LDS Sample Buffer and 2.5 µL NuPAGE Sample Reducing Agent and applied onto a NuPAGE 10% Bis-Tris Protein Gel (all Novex, Thermo Fisher Scientific). The electrophoresis was carried out in NuPAGE MES SDS Running Buffer at 150 V for 1.5 h with SeeBlue Plus2 Pre-Stained Standard (Invitrogen) as a molecular marker. The gel was stained using SimplyBlue SafeStain (Novex, Thermo Fisher Scientific).

Protein in-solution digestion.

Proteins were digested following the protocol of Tenzer et al.[220] with following modifications: 25 µg of each protein sample was precipitated and trypsin was used with a 1:50 ratio (enzyme:protein). For LC-MS analysis the samples were diluted 10-fold with aqueous 0.1% formic acid and spiked with 50 fmol/µL Hi3 EColi Standard (Waters Corporation) for absolute quantification.

Liquid-chromatography mass-spectrometry (LC-MS) analysis.

Quantitative analysis of protein samples was performed using a nanoACQUITY UPLC system coupled with a Synapt G2-Si mass spectrometer (Waters Corporation). Tryptic peptides were separated on the nanoACQUITY system equipped with a C18 analytical reversed-phase column (1.7 µm, 75 µm x 150 mm, Waters Corporation) and a C18 nanoACQUITY Trap Column (5 µm, 180 µm x 20 mm, Waters Corporation). Samples were processed with mobile phase A consisting of 0.1% (v/v) formic acid in water and mobile phase B consisting of acetonitrile with 0.1% (v/v) formic acid. The separation was performed at a sample flow rate of 0.3 µL/min, using a gradient of 2-37% mobile phase B over 70 min. As a reference compound 150 fmol/µL Glu-Fibrinopeptide was infused at a flow rate of 0.5 µL/min.

Data-independent acquisition (MSE) experiments were performed on the Synapt G2-Si operated in resolution mode. Electrospray Ionization was performed in positive ion

mode using a NanoLockSpray source. Data was acquired over a range of *m*/*z* 50-2000 Da with a scan time of 1 s, ramped trap collision energy from 20 to 40 V with a total acquisition time of 90 min. All samples were analyzed in two technical replicates. Data acquisition and processing was carried out using MassLynx 4.1 and TansOmics Informatics software was used to process data and identify peptides. Data were post acquisition lock mass corrected. Noise reduction thresholds for low energy, high energy and peptide intensity were fixed at 120, 25, and 750 counts, respectively. During database searches, the protein false discovery rate was set at 4%. The generated peptide masses were searched against a reviewed human protein sequence database downloaded from Uniprot. The following criteria were used for the search: one missed cleavage, maximum protein mass 600 kDa, fixed carbamidomethyl modification for cysteine and variable oxidation for methionine. For identification a peptide was required to have at least three assigned fragments and a protein was required to have at least two assigned peptides and five assigned fragments. Quantitative data were generated based on the TOP3/Hi3 approach[240], providing the amount of each protein in fmol.

5. Bioorthogonal synthesis of HES-NCs by catalyst free click chemistry

Kang B. et al. Manuscript in preparation.

Introduction

Nanomedicine is a promising platform for the treatment of cancer, and has drawn intensive researching intensity in the past decades, due to its outstanding properties including specific binding with targeted cell lines and reducing the systematic toxicity of the traditional chemotherapy. While the targeting effect of different ligands coupled with a variety of different nanocarriers have been investigated thoroughly and numerous *in vitro* and some *in vivo* successes have been achieved, most of these nanocarriers are based on inorganic nanoparticles or artificial polymers, which are not biodegradable, hence makes the safe removal of the nanocarrier after injection difficult. Furthermore, it is often the case, that for each therapeutic agent, an individualized nanocarrier is designed. An once well-established nanocarrier, which can serve as can drug delivery platform for a large variety of different drug/potential therapeutic agent, is still sparse. The HES-NCs previously prepared in our group via polyaddition between TDI and HES also have limited feasibility, despite the long plasma half-life times[168], depressed unspecific binding with different cells[86] and specific targeting due to the attachment of ligands[213], when used to encapsulate and protect pharmaceutical agents, which often contain nucleophiles like amines, thiols, or alcohols, and consequently will participate in the polycondensation reaction with the diisocyanate electrophile. New strategies have to be developed, which use bio-orthogonal reactions to generate the nanocarriers allowing the encapsulation of more complex pharmaceutical agents.

Among the different click reactions,[241] the azide-alkyne Huisgen cycloaddition is probably the most promising, due to the stability of the resulting 1,2,3-triazoles, and the tolerance of this reaction to a vast variety of reaction conditions and functional groups, i.e. orthogonality against other reactions.[242] Recently we were able to prepare nanocapsules in a water-in-oil miniemulsion via click reaction.[243] In this work, an electron- deficient propiolic acid diester, namely hexanediol dipropiolate (HDDP), was used as a crosslinker for HES. For the generation of nanocarriers by click

chemistry, HES was modified with multiple azide groups, allowing metal-free click polyaddition. In a previous publication, our group studied the kinetics of a heterogeneous click polyaddition by NMR spectroscopy[154]. Herein we describe the synthesis of an azido-derivative that can be used to modify polysaccharides, like HES, with a tailorable amount of azide groups by isocyanate chemistry. This chemistry further allows us to tailor the hydrophilicity and the molecular interactions by hydrogen bonding between the polysaccharides and the subsequent shell of the nanocontainer. These HES nanocontainers shall be biocompatible and biodegradable generated by bioorthogonal and copper-free click chemistry to enable the encapsulation of basically any cargo.

In this chapter, different methods for the functionalization of HES with azide groups are designed and their feasibilities are investigated. In the end, a novel general azidation agent, i.e. 1-(2-(2-(2-(2-azidoethoxy)ethoxy)ethoxy)ethyl)-3-((2-(isocyanatomethoxy)ethoxy)methyl)urea was developed, which has the following advantages:

i) It functionalizes the HES at room temperature without any catalyst, which helps to keep the backbone of polysaccharide intact and minimize the cytotoxicity.

ii) The modified HES has a tunable degree of substitution with full range water solubility.

iii) By using this general azidation agent, not only HES, but also other sugars and peptides, can be functionalized with azide groups. In addition, it could also be used to functionalize the end group of other polymers which is sometimes too unstable to be functionalized otherwise, e.g. hydroxyl group ended polyester.

iv) During coupling of the azide groups to the HES, this general azidation agent can create additional urea and/or urethane groups in the functionalized molecule, which will introduce hydrogen bond interaction in the polymeric shells of the nanocapsules, and may further enhance the stability and suppress the permeability of the nano-scaled shell.

The azide functionalized HES prepared is then used to synthesize nanocapsules in a water-in-oil miniemulsion system, by using HDDP as catalyst free click crosslinking agent.

5.1 Results and discussion

Synthesis of azide HES

The number of azide groups coupled to the HES molecule is expressed in the term of the degree of functionalization, which is the mean number of azide groups per glucose unit, and ranges between 0 and 3. In summary, three different strategies have been developed, which are named as Method 1, Method 2 and Method 3 a/b in the following section.

Method 1

In method 1, the well reported two step strategy for the substitution of alcohols to azide groups, i.e. tosylation followed by azidation (Scheme 9), has been adopted for HES.

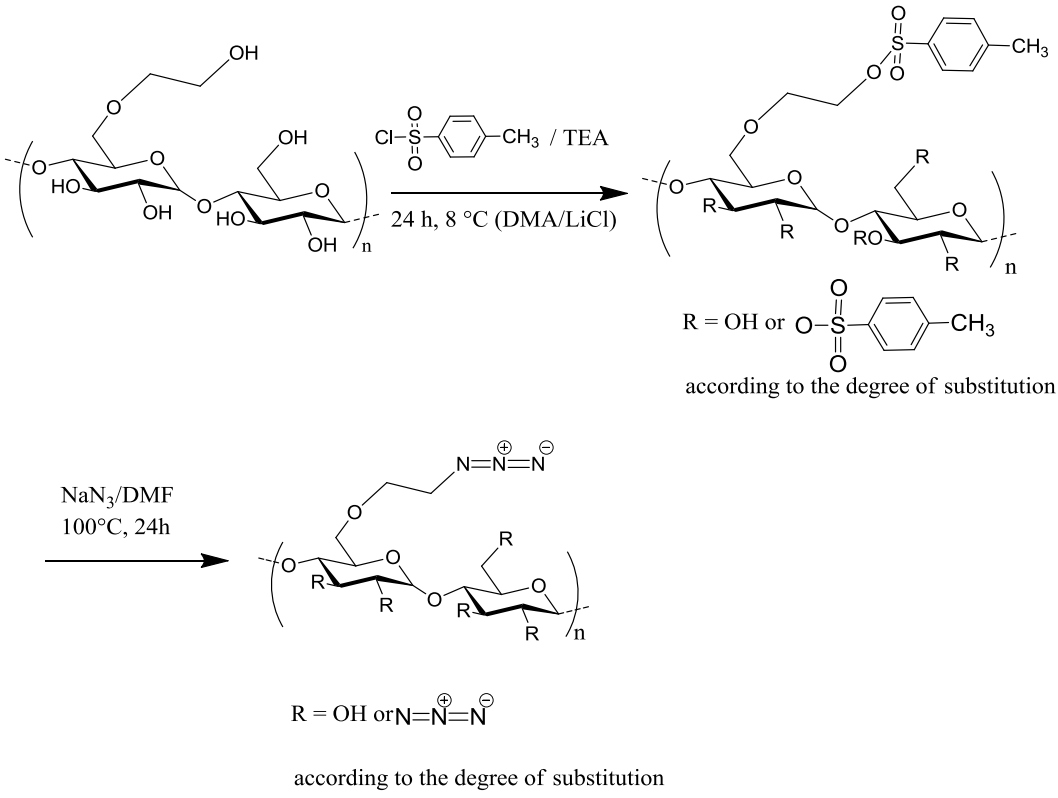

Scheme 9. *Tosylation of HES and subsequent azidation of tosylated HES.*

Elemental analysis after the second step revealed a degree of substitution of 0.05, i.e. in average one azide group to every 20 glucose units was coupled. Due to the hydrophobicity of the azide group, the solubility of this modified HES in water is below 1 wt% and no stable nanocapsules were obtained, which is expected, when

we consider for the nanocapsules prepared from TDI, 10 wt% of HES in water solution was used and a 1:1 mole ratio between the hydroxyl group and the isocyanate group was applied, which stands for a degree of substitution of 2.5, in order to obtain the stable capsule. The azide functionalized HES in Method 1 has neither the desired degree of substitution nor enough water solubility.

There are several other setbacks for this method. Firstly, the sugar backbone is not stable at elevated temperatures in DMF solution at the presence of sodium azide, after the second step, the NMR spectrum changes significantly compared to the original HES, indicating destroyed sugar chain. Secondly, the chemical environments for different groups in this azide HES are close, which result in the heavily overlapping between the peaks in NMR measurement, and hence make the quantification of the degree of functionalization by NMR spectroscopy impossible. The only quantification method is elemental analysis. In order to circumvent all of these setbacks, new azidation strategy has to be developed.

Method 2

A new azidation strategy was developed to overcome the problems (degradation, low water-solubility) which were identified for the azidation-protocol of HES method 1.

11-Azido-3,6,9-trioxaundecan-1-amine is added slowly by a syringe pump into an excess of hexamethylene diisocyanate. Under these conditions, the amine will preferably react with one isocyanate from the di-isocyanate, after the removal of excess diisocyanate in vacuum, 1-(2-(2-(2-(2-azidoethoxy)ethoxy)ethoxy)ethyl)-3-(6-isocyanatohexyl)urea (azidation agent 1) will be obtained, containing an azide group (to click) at one end, an isocyanate (to react with HES and to introduce H-bonds as a urethane) at the other, and a urea group (H-bonds) in between (Scheme 10).

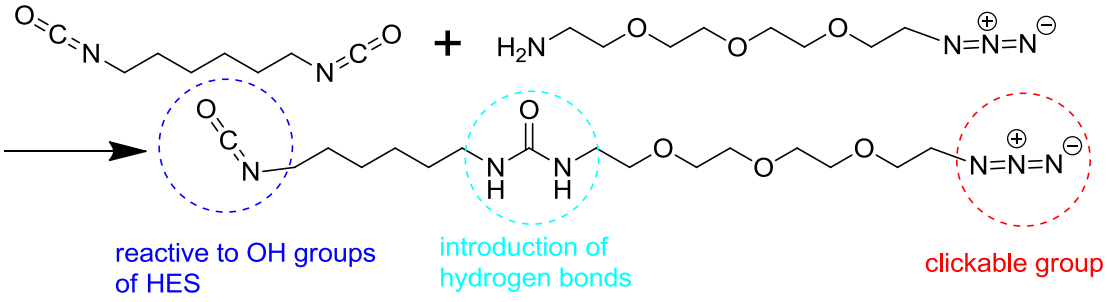

Scheme 10. *Schematic representation of the preparation of new azidation agent 1.*

Reaction of azidation agent 1 with HES was conducted in anhydrous DMF at 25 °C. Since the reaction is carried out at room temperature, the backbone of the polysaccharide is protected from degradation, and the reaction works in a quantitative way for a wide range of degree of functionalization (Scheme 11).

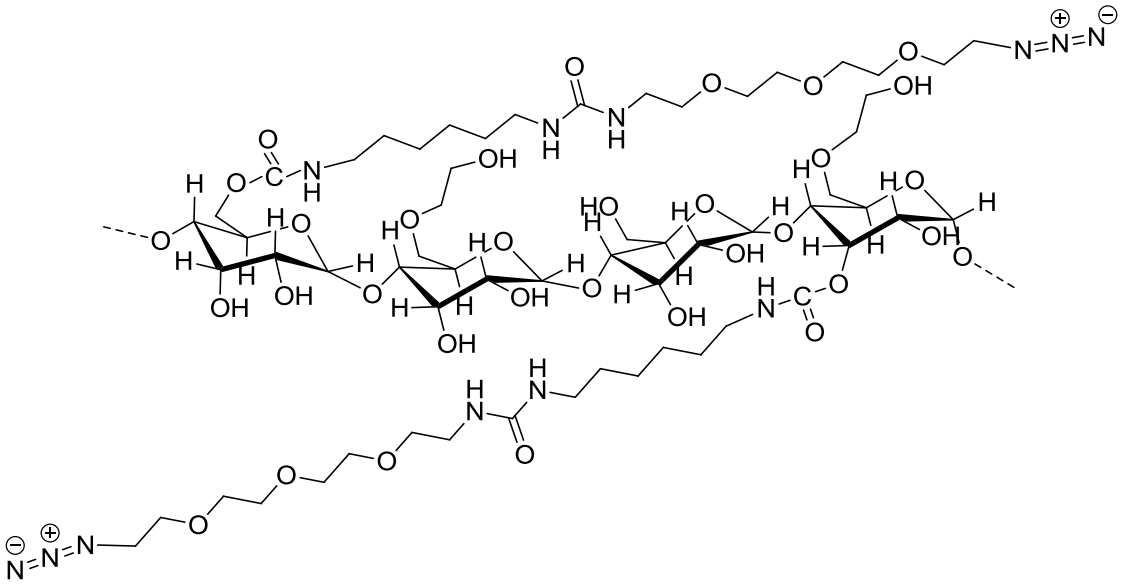

Scheme 11. *Structure of azidated HES via the diisocyanate route.*

The azidated HES obtained, named as azide HES 1, was not soluble in any organic solvent or water, and has been sent for solid state NMR for characterization. The successful coupling of azidation agent 1 to the OH-groups of HES was proven by solid state NMR (Figure 51). The urea and urethane groups in this azide HES will form additional hydrogen bond between each other in the shells of the capsules, which could also help to form a dense shell when it is used to prepare capsules. The presence of NH-CH_2 at 42 ppm and NH-CO-NH at 160 ppm individually confirmed the urethane linkage between azidation agent 1 and HES, and the urea linkage within azidation agent 1.

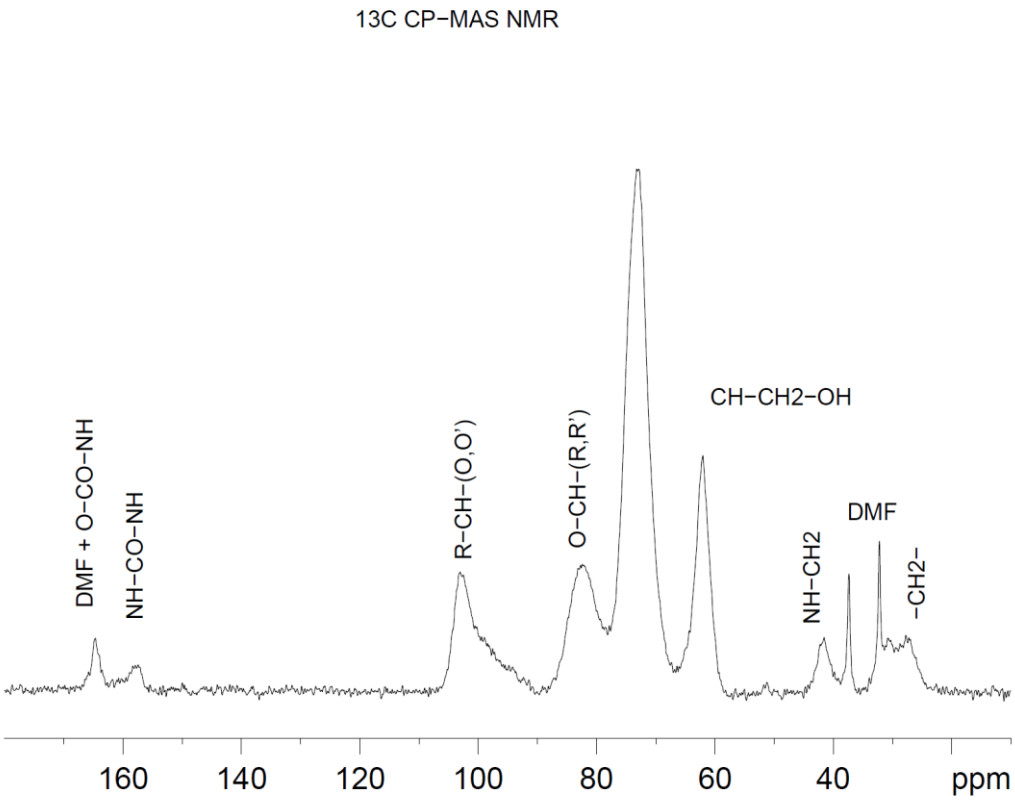

Figure 51. *Solid state ^{13}C NMR spectrum as a proof of attaching the azidation agent 1 to HES.*

Despite the successful attachment of azide groups to HES, the solubility in water of the modified HES is still below 1%, probably due to the additional alkyl chains in the diisocyanate.

It will be necessary to have fully water-soluble “azide-HES” with variable degree of azidation to investigate the synthesis and to obtain a stable and dense shell for the capsules. In order to further improve the water-solubility, **Method 3** was developed.

Method 3

This method uses a diisocyanate with a hydrophilic linker, which will increase the water-solubility of the modified HES. For this purpose, two methods has been developed, in **Method 3a**, a water soluble dicarboxylic acid was used, while in **Method 3b**, a water soluble diamine. The diisocyanate obtained from the first method is termed as diisocyanate 2, while the latter is termed as diisocyanate 3.

Method 3a

A diisocyanate, 1,2-bis(isocyanatomethoxy)ethane, was synthesized from 2,5-dioxa-1,6-hexanedicarboxylic acid as the precursor, through the Curtius rearrangement (Scheme 12). It is termed as diisocyanate 2 in the following sections.

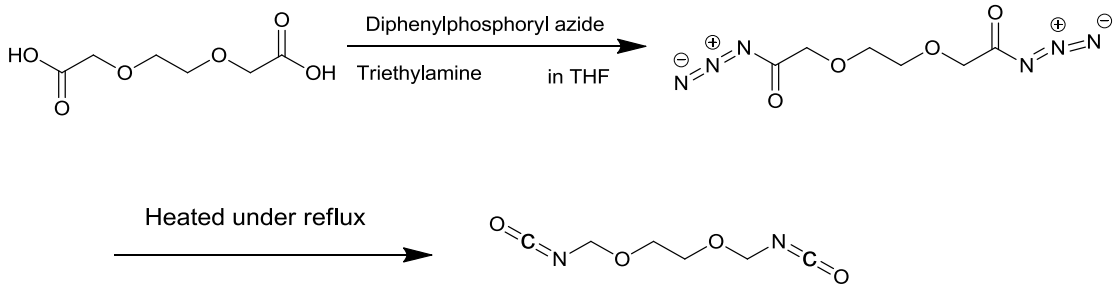

Scheme 12. *Synthesis of diisocyanate 2 with water soluble backbone.*

The formation of diisocyanate has been proved by IR spectrum (Figure 52). The transfer from the reagent to the product is proven by the absence of chemical shift at 171 ppm, which corresponds to the carboxylic group, and the new peak at 122 ppm, which corresponding to the diisocyanate group.

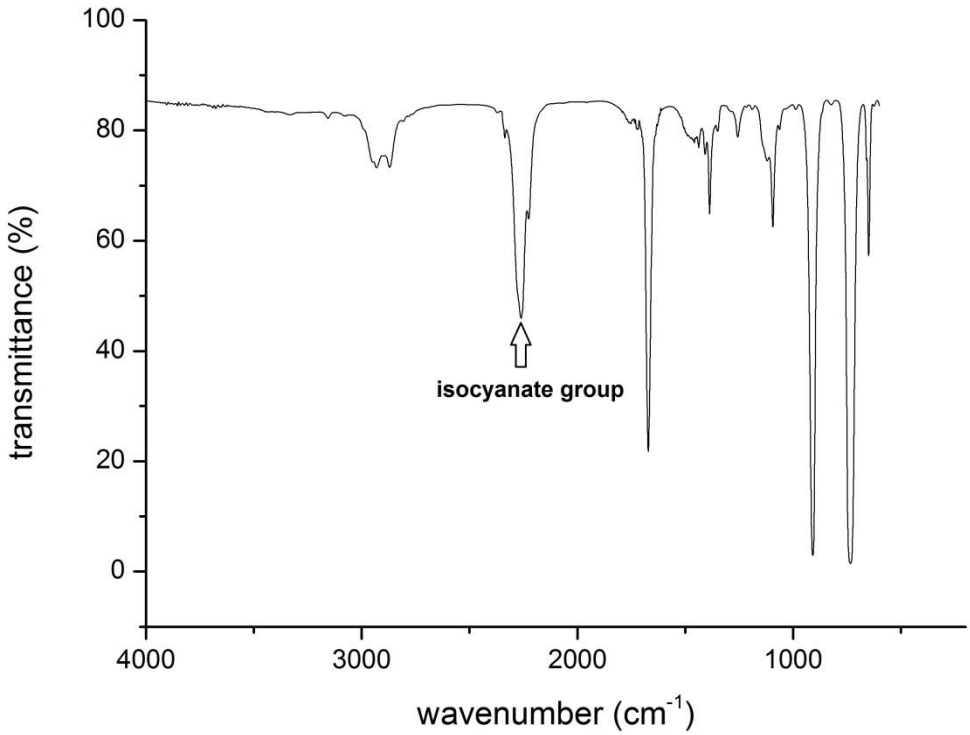

Figure 52. *IR of di-isocyante2 shortly after synthesis. The presence of isocyanate group is proved.*

The same reaction is used to couple this hydrophilic diisocyanate with the amine functionalized azide, and a new azidation agent, 1-(2-(2-(2-(2-azidoethoxy)ethoxy)ethoxy)ethyl)-3-((2-(isocyanatomethoxy)ethoxy)methyl)urea, termed as Azidation agent 2, was obtained, with improved water solubility. The reaction between this water soluble azidation agent and HES was carried out in anhydrous DMF at 25 °C. The obtained azide HES, named as azide HES 2, has the structure as shown in Scheme 13.

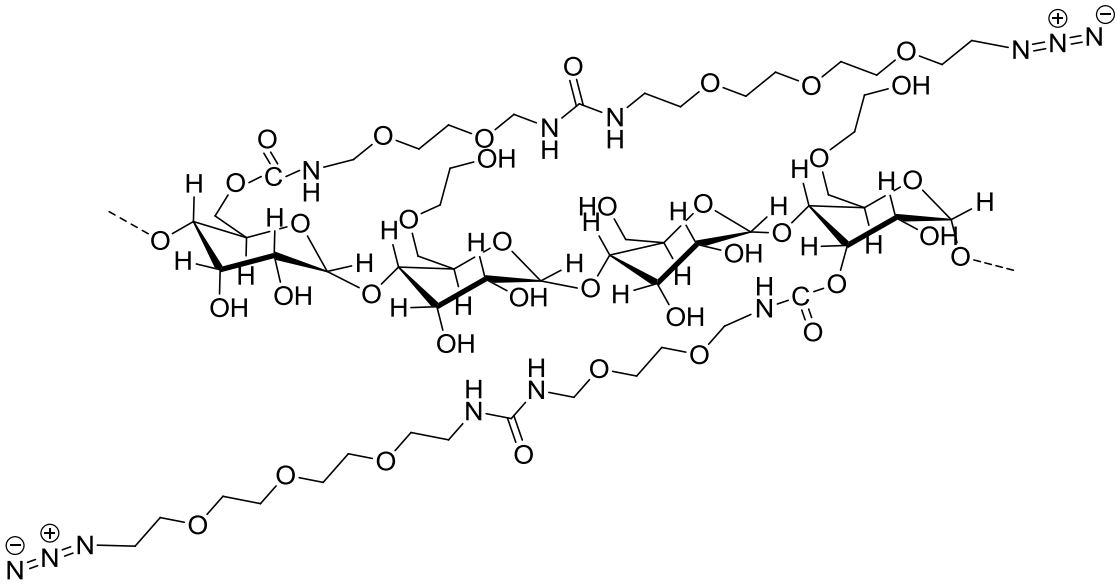

Scheme 13. *Structure of water soluble azide HES 2.*

However, IR analysis of the azide HES 2 did not shown peak corresponding to azide groups at 2000 cm^{-1}, as can be seen in Figure 53.

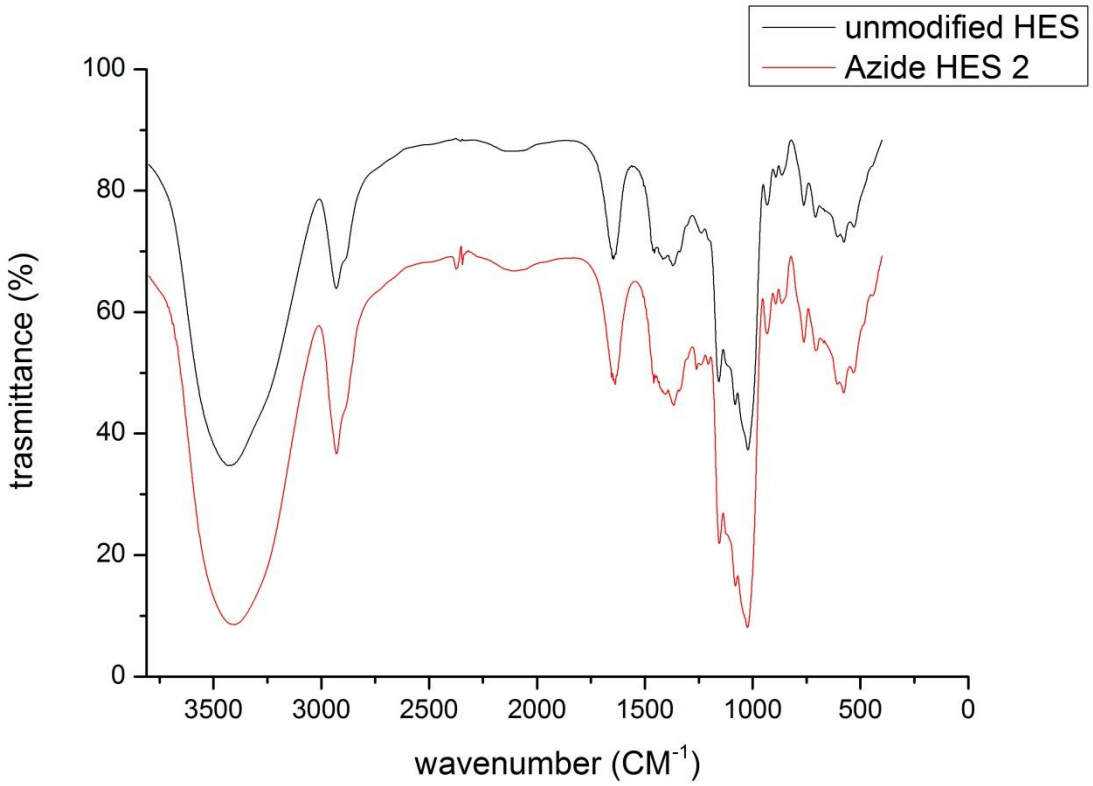

Figure 53. *IR spectrum for azide functionalized HES by* Azidation agent 2*, with no detectable peak at 2000 cm^{-1}, which is corresponding to the azide, in comparison to the IR spectrum of unmodified HES.*

In order to identify the problem, a kinetic study of the synthesis of diisocyanate 2 was carried out, by taking the reaction mixture out after certain time, and sending it to ^{1}H NMR spectroscopy. The spectrum can be seen in Figure 54.

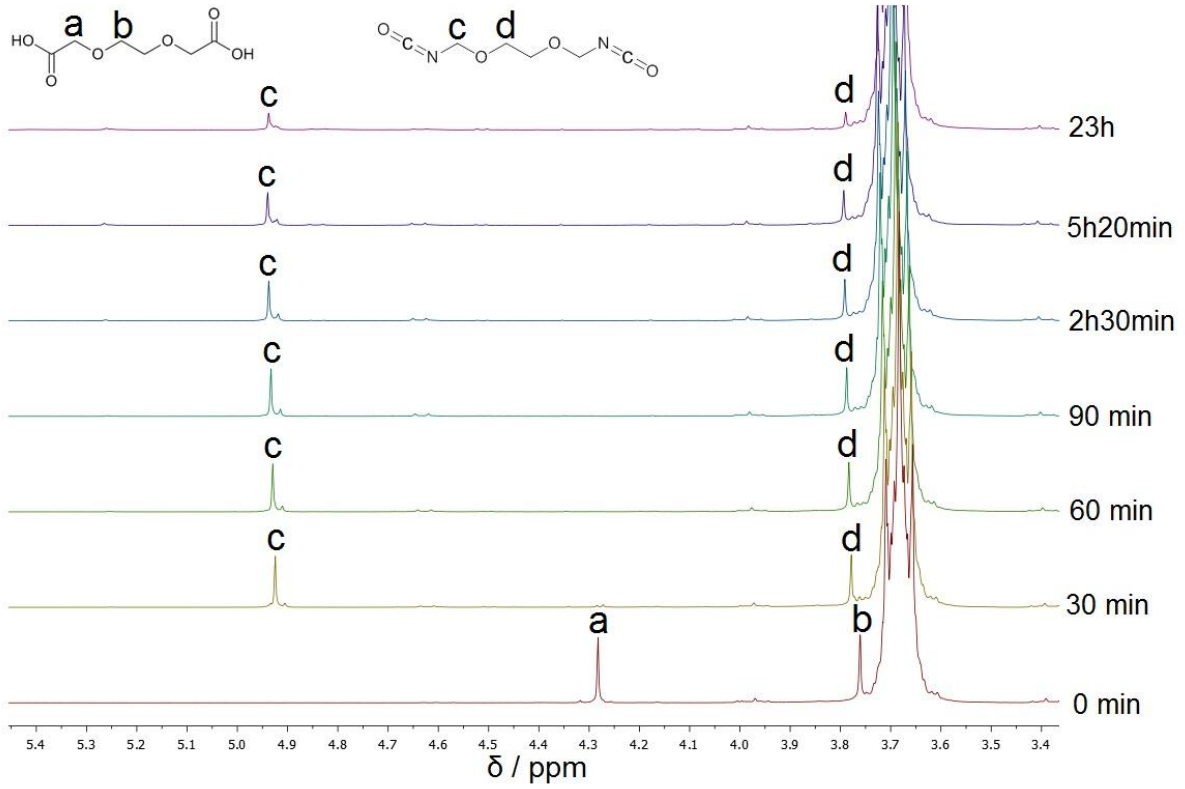

Figure 54. *Kinetic study of diisocyanate 2 synthesis by ^{1}H NMR spectroscopy in $CDCl_3$ (250 MHz, 298K).*

The two peaks with a chemical shift at 3.75 ppm and 4.29 ppm are corresponding to the two carbons of the dicarboxylic acid, as initial reagent. A change of chemical shift for the protons, which belong to the carbon adjacent to the isocyanate group, from 4.29 ppm to 4.92 ppm, is the evidence that the carboxylic groups have transformed to isocyanate groups. This reaction is already completed within 30 min, further quantification showed a decreased amount of the signal from the backbone as time goes on, compared to the internal reference. Due to the fact that there is only one carbon atom between the isocyanate and oxygen atom, the diisocyanate degenerates with a half-life time of 16 h, as can be seen in Figure 55.

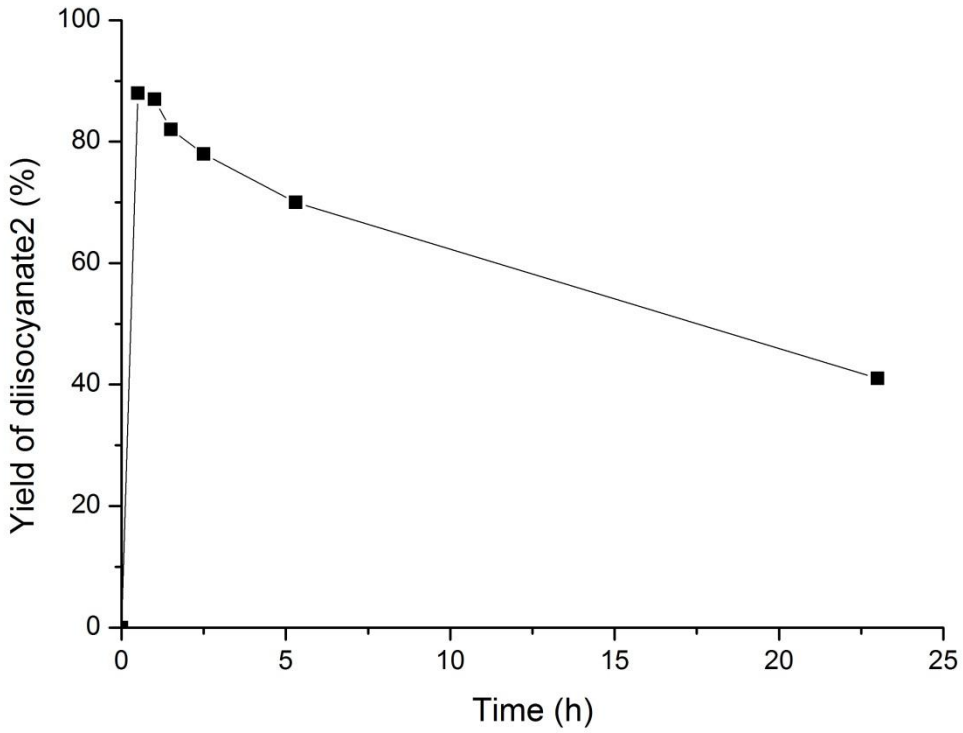

Figure 55. *Kinetic and stability of diisocyanate 2.*

Taking into consideration of the fact, that the reaction between the diisocyanate 2 and the 11-Azido-3,6,9-trioxaundecan-1-amine already needs two hours, the half reaction time of isocyanate and hydroxyl groups are in the range of 5h, and the solvent removal steps which is necessary between these two steps, the final azide linker which could be successfully coupled onto the sugar is neglectable. To ensure the efficient coupling of the azide linker, a more stable isocyanate is desired. In comparison to the structure of diisocyanate2, we want to prepare 1,2-bis(2-isocyanatoethoxy)ethane as diisocyanate3, which has an extra carbon atom between the isocyanate groups and the oxygen atom, as can be seen in Scheme 14.

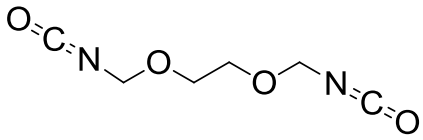

1,2-bis(isocyanatomethoxy)ethane, diisocyanate 2

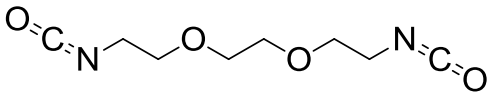

1,2-bis(2-isocyanatoethoxy)ethane, diisocyanate 3

Scheme 14. *Comparison between the chemical structure of diisocyanate 2 and diisocyanate 3.*

Method 3b

2,2′-(ethylene dioxy)bis(ethylamine) is taken as the precursor for the diisocyanate 3 (1,2-Bis(2-isocyanatoethoxy)ethane). Reaction of 2,2′-(ethylenedioxy)bis(ethylamine) with triphosgene in anhydrous DCM, followed by reflux at 60 °C results in the formation of diisocyanate 3, as can be seen in Scheme 15. The solvent is evaporated at reduced pressure, and the product extracted from solid residual by diethyl ether. The extracted volume is dried by anhydrous sodium sulfate, and the solvent removed in vacuum.

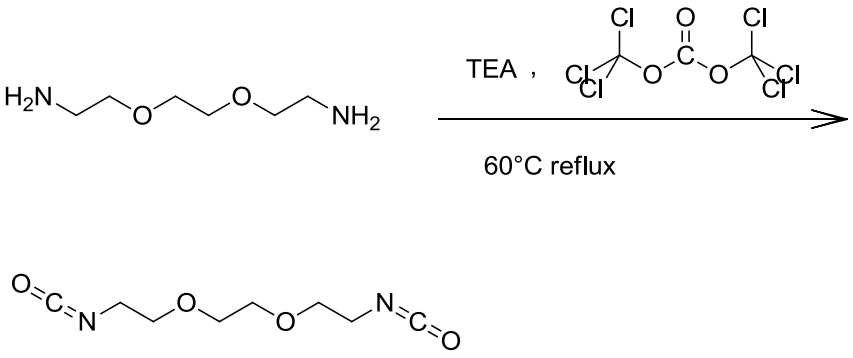

Scheme 15. *Schematic representation of the reaction route for the synthesis of diisocyanate 3.*

The ^{1}H NMR spectrum of the obtained product verified the formation of diisocyanate, as can be seen in Figure 56 and Figure 57. The isolated yield is 92%.

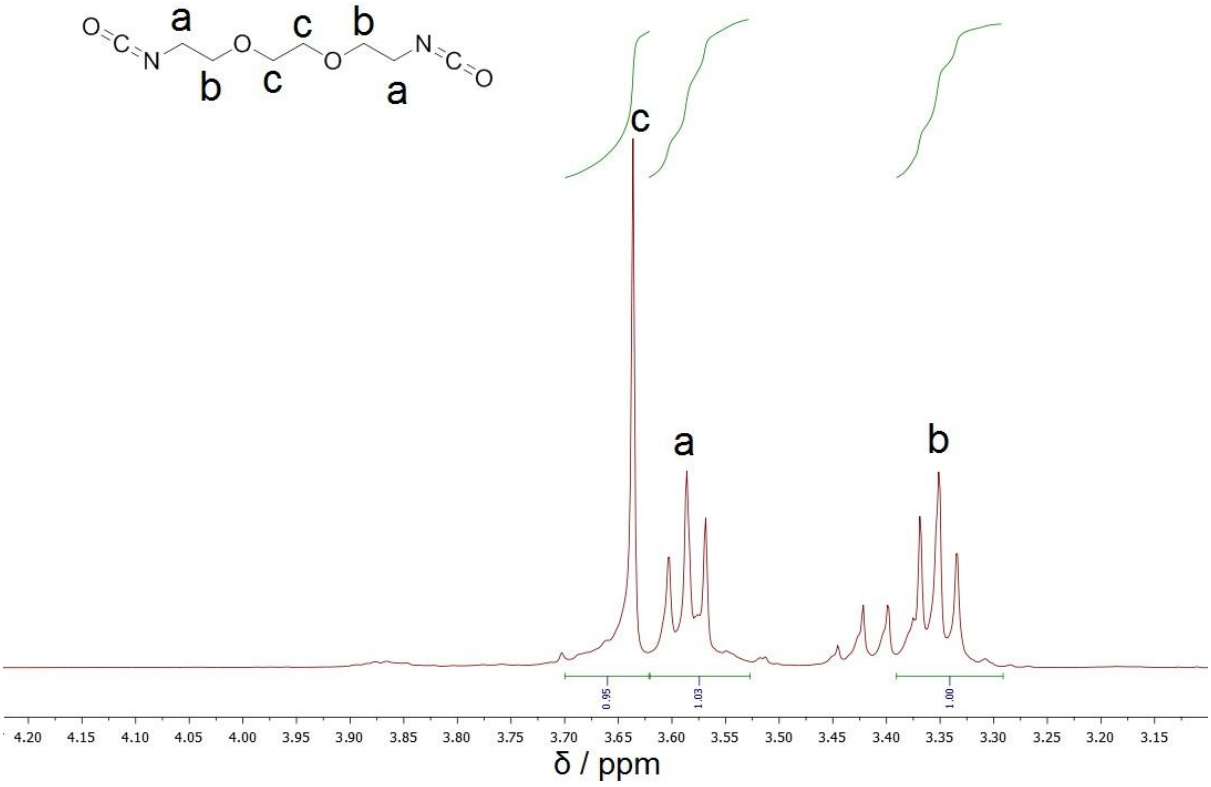

Figure 56. *^{1}H NMR spectrum of the diisocyanate 3 in $CDCl_3$ (300 MHz, 298K).*

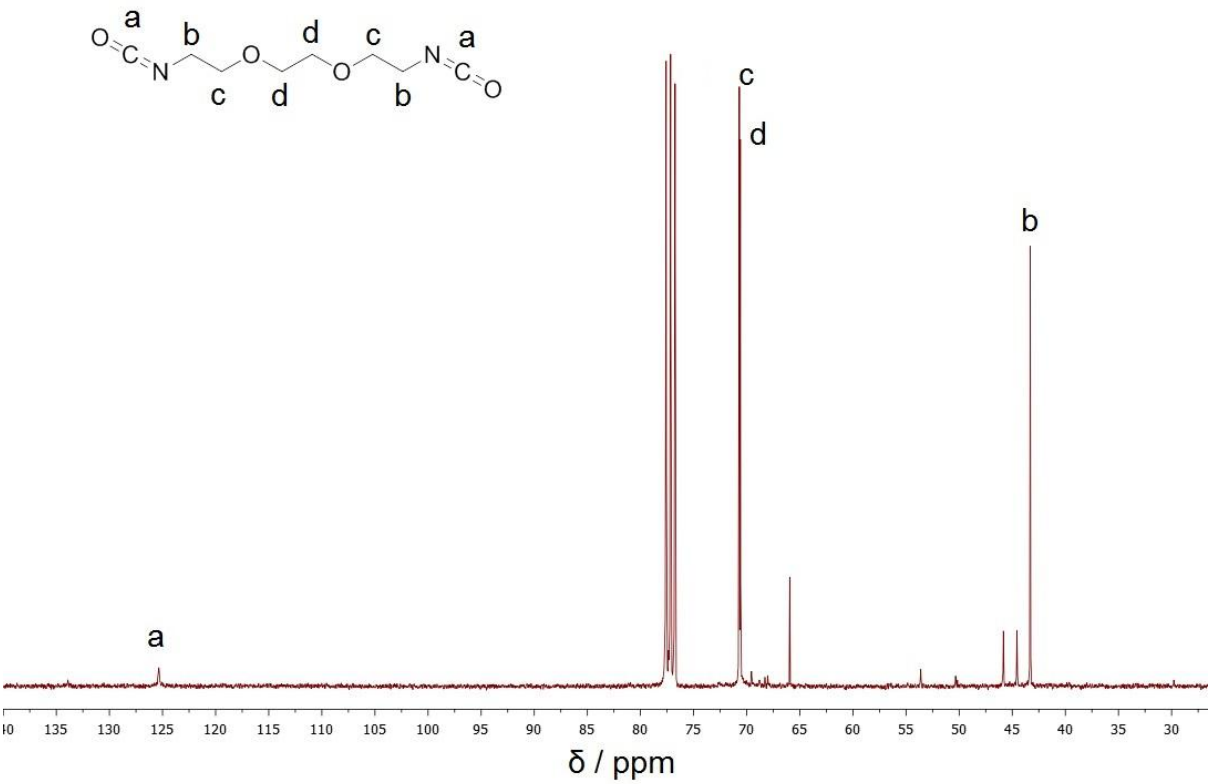

Figure 57. *^{13}C NMR of the diisocyanate 3 in $CDCl_3$ (300 MHz, 298K) .*

The 1-(2-azidoethyl)-3-(2-(2-(2-isocyanatoethoxy)ethoxy)ethyl)urea prepared by the reaction between diisocyanate 3 and the 2-azido-1-ethylamine is termed as the azidation agent 3, as can be seen in Scheme 16.

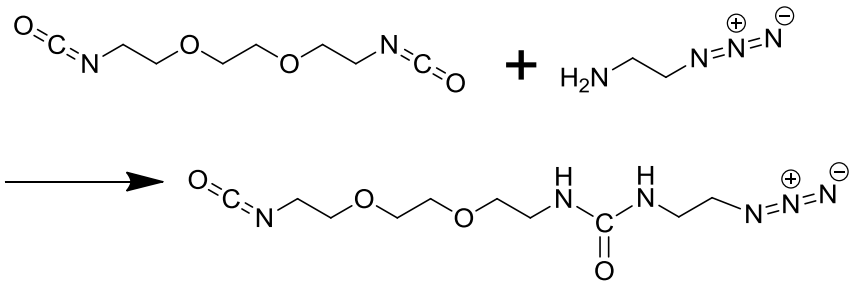

Scheme 16. *Synthesis of 1-(2-azidoethyl)-3-(2-(2-(2-isocyanatoethoxy) ethoxy)methyl) urea.*

As can be seen in Figure 58, the IR spectrum has verified the presence of both azide and isocyanate groups in the azidation agent 3.

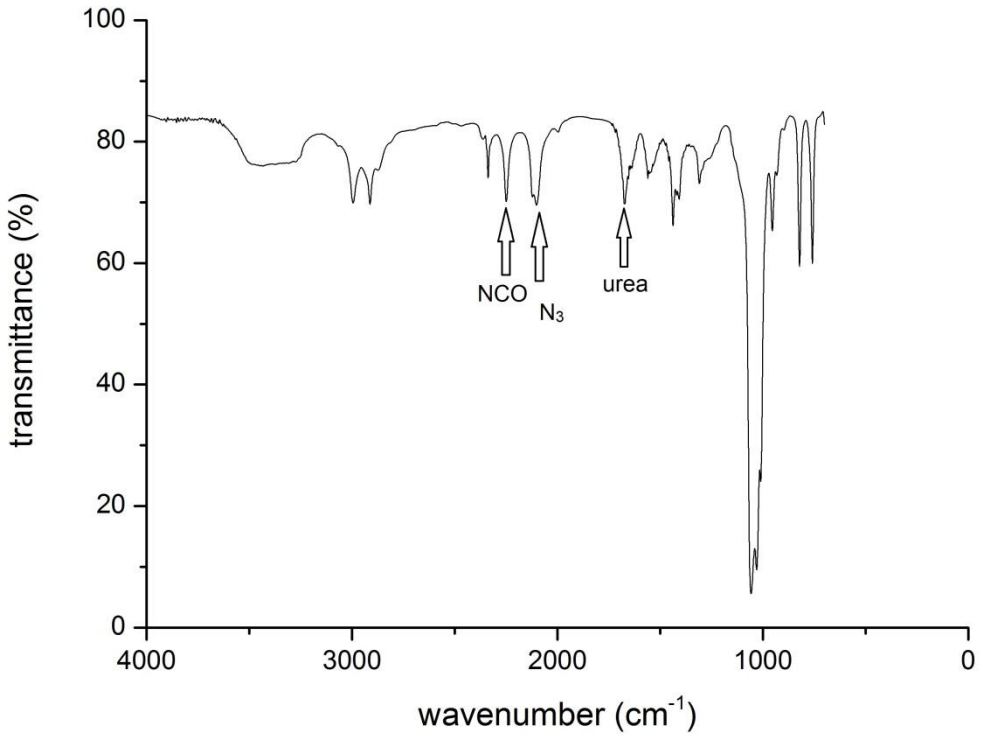

Figure 58. *IR of azidation agent 3. The presence of both isocyanate group, the azide group, and the urea group are proved.*

The presence of both groups has been further verified by ^{13}C NMR spectrum, as can be seen in Figure 59.

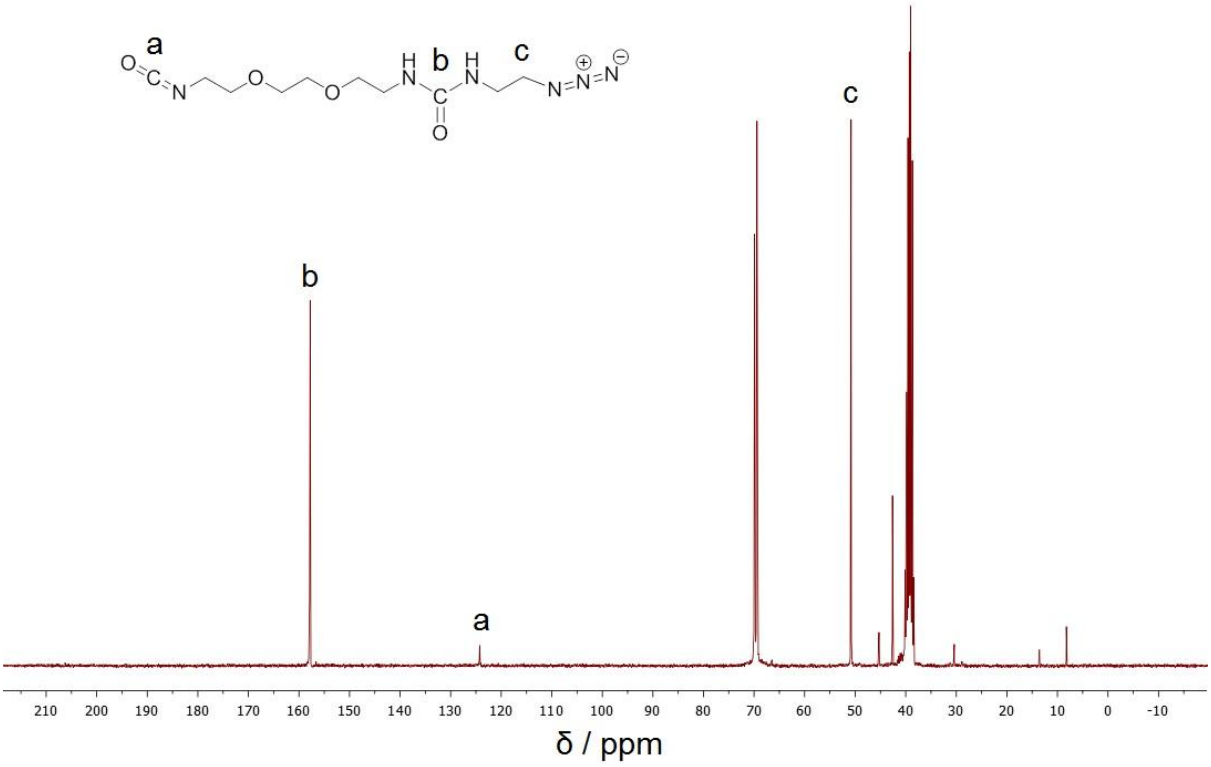

Figure 59. *^{13}C NMR spectrum of azidation agent 3 in DMSO-D_6 (300MHz, 298K).*

The structure of the azide HES prepared by azidation agent 3 is shown in Scheme 17.

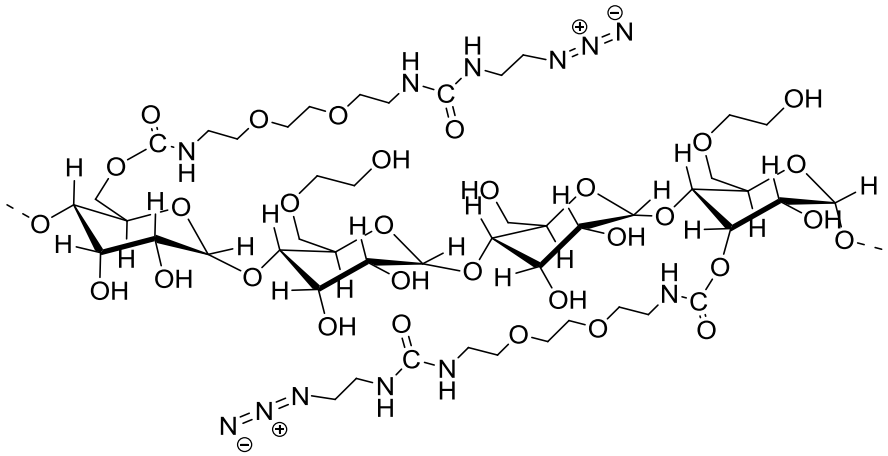

Scheme 17. *Structure of the newest azide HES 3.*

The obtained azide HES, named as azide HES 3, is soluble in water up to a concentration of 20 wt%. After dialyzing against water for 4 days, the IR measurement show both azide and urea groups in the azide HES formed, as can be seen in Figure 60.

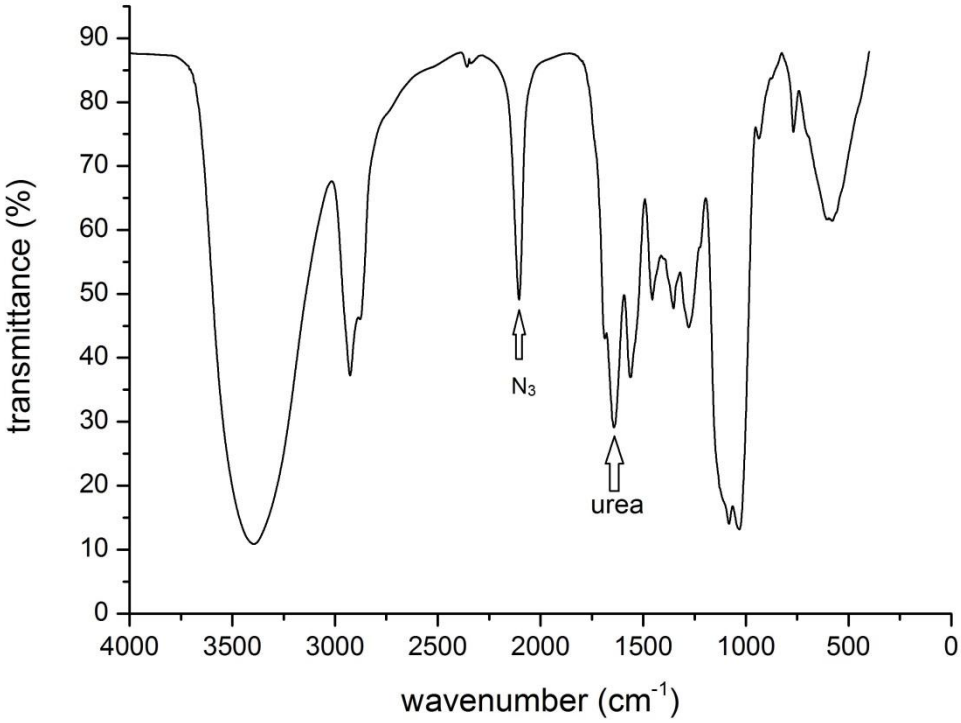

Figure 60. *IR spectrum of azide HES 3.*

The number of azide groups attached to the sugar was further quantified by integrable ^{13}C NMR spectroscopy and turned out to be 0.5 azide groups per glucose unit (degree of azidation is 0.5).

The advantages of the azide HES prepared by Method 3b in comparison to Method 1 are listed in Table 7.

Table 7. Comparison of Method 3b with Method 1.

	Method 1	Method 3b
Solubility in water	<2wt%	>15wt%
Structure of sugar back bond	Partially destroyed during azidation	intact
Quantification of degree of azidation	hard	Easy through integrable carbon NMR
Presence of hydrogen bond	none	Urea and urethane groups presented
Degree of functionalization	0.05	0.5
Yield	low	>95%

Nanocapsules by click chemistry

Polymerization & Characterization

HES-NCs have been prepared by a water-in-oil miniemulsion (Scheme 2), with the azide HES 3 obtained from Method 3b (degree of functionalization = 0.5), and using HDDP as crosslinker. The size of the HES-NCs in cyclohexane phase and after transferred in water is measured by DLS. The intensity weighted mean diameters in both cases are 170 nm, which is the proof of the formation of the nanocapsules, and the stability of the nano-capsules in both solvents. The morphology of the capsules can be seen in Figure 61 (TEM) and Figure 62 (SEM).

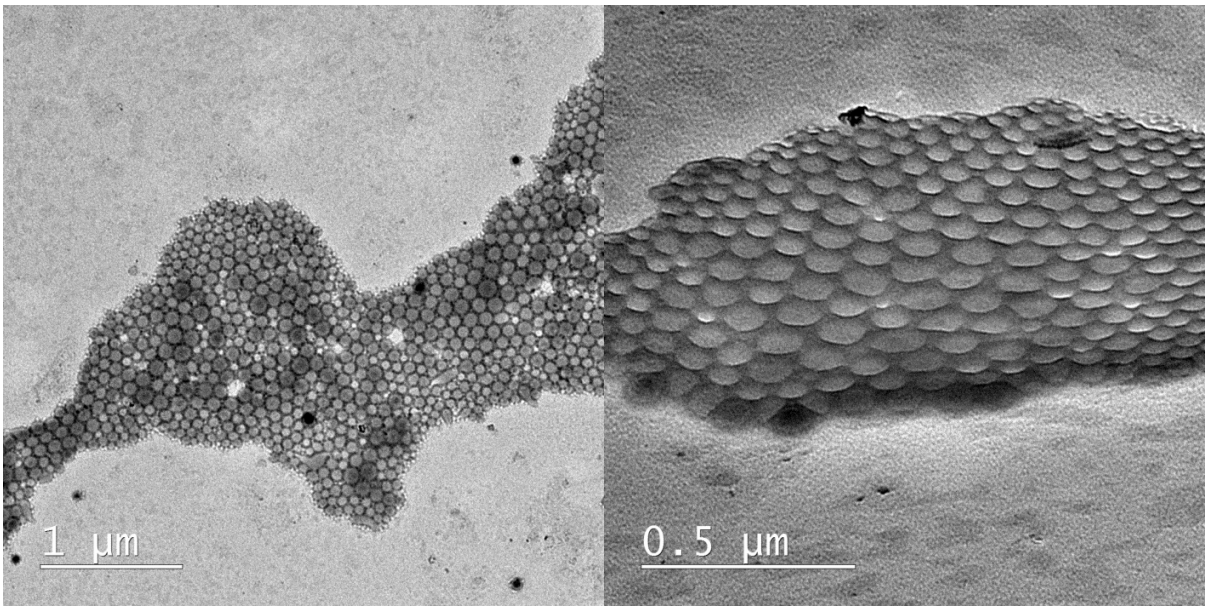

Figure 61. *TEM images of click nanocapsules with different magnifications and tilting angles.*

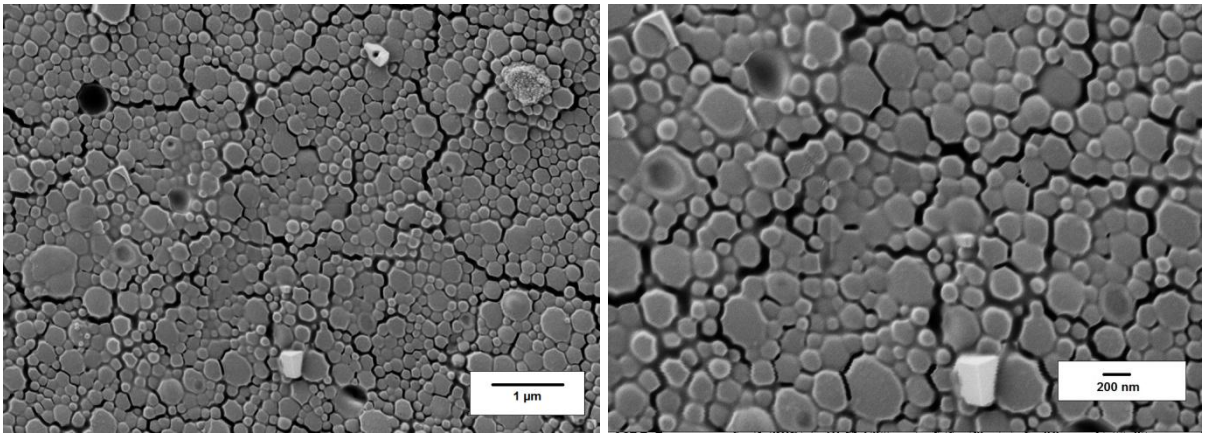

Figure 62. *SEM images of click nanocapsules with different magnifications.*

Encapsulation

Furthermore, in order to quantify the encapsulation efficiency, D-mannosamine was used as a modal drug, and the fluorogenic reaction between D-mannosamine and fluorescamine was used to quantify the release. Both empty and D-mannosamine loaded capsules were prepared, and transferred into water. A standard working function of fluorescamine and D-mannosamine was established, while the same concentration of empty capsules was added in all the stock solutions of D-mannosamine. The water dispersion of D-mannosamine-loaded capsules were tested under the same condition, to test the free D-mannosamine which was released from the nanocapsules (Figure 62). It turned out 32 % of the D-mannosamine was released into the water medium after redispersion, which stands for an encapsulation efficiency close to 70%. In the next two weeks, 6.2 % of payload was released into the aqueous media.

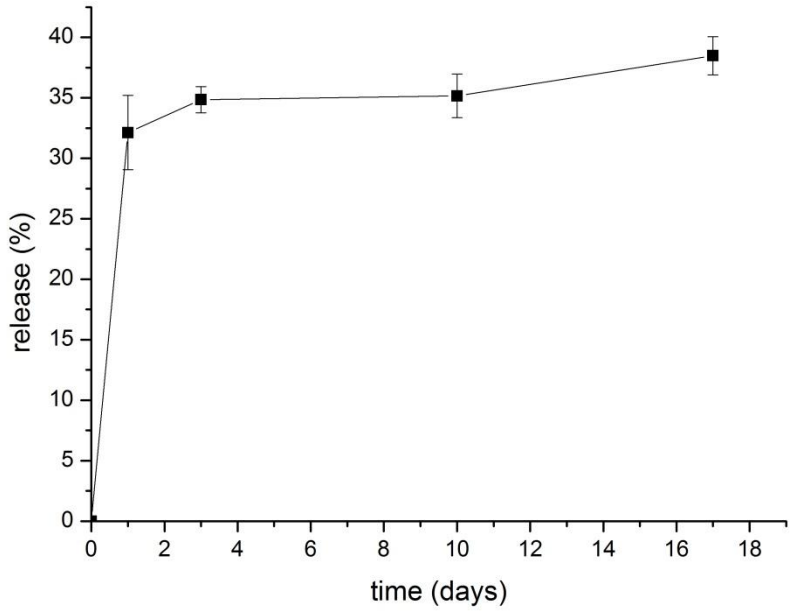

Figure 62. *Release of D-mannosamine after transfer the click capsules into water dispersion. The large initial release in the first day, from which the encapsulation efficiency is calculated, comes from the free D-mannosamine which is not encapsulated in the capsules.*

Conclusion

These results demonstrate that HES can be further functionalized with azide groups, while letting its sugar backbone and good water solubility intact. The azidation agent 1-(2-azidoethyl)-3-(2-(2-(2-isocyanatoethoxy)ethoxy)ethyl)urea developed in this work was used to functionalize the HES at room temperature in the absence of any catalyst. In addition, all the sugars, peptide, or any other molecule containing either primary amine or hydroxyl groups can be functionalized with azide group by applying this azidation agent. Due to the mild reaction condition of this method, it can be very useful to functionalize polymers which are too unstable to be functionalized otherwise, e.g. polyesters.

The azide-functionalized HES has been used to prepare nanocapsules via copper free click reaction, in a water-in-oil miniemulsion system by using HDDP as crosslinker. The capsule morphology has been proven by TEM, while the encapsulation efficiency and release profile of a payload, D-mannosamine in this case, has been studied. It has encapsulation efficiency close to 70%, and released 6.2% of the encapsulated payload in the next two weeks. Taking into consideration that D-mannosamine is a rather small molecule in comparison to most of the therapeutic agent, the click capsule is considered to be dense enough to use as the carrier for drugs.

5.2 Experimental Part

Materials

O-(2-Aminoethyl)-O'-(2-azidoethyl)pentaethylene glycol and 2,2'-(Ethylenedioxy)bis(ethylamine) was bought from Sigma Aldrich, and storage over molecular sieves for 4 days before use. 2,2'-(ethylenebis(oxy))bisacetic acid was ordered from Merck. All the other chemicals were bought from Sigma Aldrich without further purifications.

Method 1 (by tosylation, azidation)

1.36 g of starch was dissolved in 60 mL of DMA, followed by the addition of 3.14 g of TEA in 10 mL of DMA, the solution was then cooled to 0 °C and 15.0 g of tosylchloride was added into the solution dropwise. The reaction was allowed to proceed for 48 h, afterwards, the product was precipitated into cold water, filtrated, and redissolved in DMA. The procedure was repeated for three times, and 2.2 g of tosylated starch was dissolved in 15 mL DMF, 2.5 g of sodium azide was added, and the reaction was magnetically stirred at 80 °C for 24 h. The product was dialyzed k against MilliQ water for 3 days (MWCO 14 kDa). The product was freeze dried to obtain 1,17 g of product.

Method 2 (hydrophobic diisocyanate)

1.44 g (4 times excesses) of hexamethylene diisocyanate was dissolved in 5 mL of anhydrous DCM, while 520 mg of O-(2-Aminoethyl)-O'-(2-azidoethyl)pentaethylene glycol in 4 mL of anhydrous DCM was added at a speed of 2 ml/h by a syringe pump. The solvent and the excess of hexamethylene diisocyanate and the solvent was removed by vaccum, and the obtained azidation agent is redissolved in 2 mL anhydrous DMF, which was subsequently added dropwise into the solution of 1.36 g of HES in 10 mL anhydrous DMF. The reaction was allowed to proceed for 18 h, and the product was purified by dialysis. The solution and the precipitate form during dialysis is freeze dried together to get 1.5 g of product.

Method 3a

Synthesis of 1,2-bis(isocyanatomethoxy)ethane (diisocyanate 2)

820 mg of 2,2'-(ethylenebis(oxy))bisacetic acid was dissolved in 12 mL anhydrous THF. The solution was cooled to 0 °C, followed the dropwise addition of 1.01 g of TEA in 2 mL of anhydrous THF. In the end, 2.95 g of diphenylphosphoryl azide in 3 mL of anhydrous THF was added dropwise. The system was magnetically stirred at 0 °C for 2 h, at room temperature for 1 h, and refluxed at 66 °C for 1 h, the product was analyzed by ^{1}H NMR and ^{13}C NMR spectroscopy, and used without further purification in the next step.

Synthesis of the 1-(2-(2-(2-(2-azidoethoxy)ethoxy)ethoxy)ethyl)-3-((2-(isocyanatomethoxy)ethoxy)methyl)urea (azidation agent 2) and the azide HES 2

The THF solution of 1,2-bis(isocyanatomethoxy)ethane obtained from last step was cooled to -56 °C, by immersing the reaction container in the mixture of n-octane and dry ice. 420 mg of O-(2-Aminoethyl)-O'-(2-azidoethyl)pentaethylene glycol was dissolved in 2 mL of anhydrous THF, and added at a speed of 2 mL/h by a syringe pump into the diisocyanate 1 solution. After the addition, the precipitate at the bottom of the bottle was isolated, redissolved into anhydrous DMF, subsequently added dropwise into the solution of 500 mg of azide HES in 6 mL of anhydrous DMF. The reaction was allowed to proceed for 48 h, and the product was purified by dialysis against MilliQ water in a dialyzing tube with MWCO of 14kDa, while the solution after dialyzing was freeze dried to obtain 520 mg of Azide HES 2 (IR in Figure 53).

Method 3b

Synthesis of 2-azido-1-ethylamine

As a shorter substituent for O-(2-Aminoethyl)-O'-(2-azidoethyl)pentaethylene glycol, 2-Azido-1-ethylamine was prepared, by reaction of 2-Chloroethylamine hydrochloride (3g) together with sodium azide (5.12) g in MilliQ water at 80 °C for 18 h. Afterwards 1.05 g of sodium hydroxide was added, and the product is extracted by diethyl ether, dried over sodium sulfide, and solvent partially removed by rotary evaporation. The diethyl ether solution of 2-Azido-1-ethylamine with a concentration of 36.5% (quantified by ^{1}H NMR spectroscopy), containing 1.8 g (yield 80%) of 2-

azido-1-ethylamine was obtained. ^{1}H-NMR Spectroscopy ($CDCl_3$, 300 MHz) δ(ppm) = 3.35-3.26 (2H, t,J= 5.6 Hz, CH_2), 2.88-2.75 (2H, t,J= 5.6 Hz, CH_2). FT-IR (ATR)v = 3366 (br), 2104 (s).

Synthesis of 1,2-Bis(2-isocyanatoethoxy)ethane (diisocyanate 3)

4.5 g of 2,2'-(Ethylenedioxy)bis(ethylamine) was dissolved together with 5.2 g of TEA in 8 mL of anhydrous DCM, and added dropwise into the solution of 3 g of triphosgene in 30 mL of anhydrous DCM, while the latter is cooled to 4 °C. After finishing the addition, the system was kept at 4 °C for 20 min, then at room temperature for 1h, followed by refluxing at 50 °C for 2 h. The solvent is then removed in vaccuo, and the product extracted by anhydrous diethyl ether. The product was checked by NMR and used without further purification in the next step. ^{1}H-NMR Spectroscopy ($CDCl_3$, 300 MHz) δ(ppm) = 3.65 (s, 4 H);3.60 (t, 4 H); 3.36 (t, 4 H).^{13}C NMR ($CDCl_3$, 300 MHz), δ (ppm) 69.7,69.6, 42.5.

Synthesis of 1-(2-azidoethyl)-3-(2-(2-(2-isocyanatoethoxy)ethoxy)ethyl)urea (azidation agent 3)

1500 mg of 2-azido-1-ethylamine was dissolved in 2 mL of anhydrous diethyl ether, and added at a speed of 2 mL/h by a syringe pump into the diisocyanate 3 solution. After the addition, the solvent was removed at reduced pressure and the product was checked by IR, redissolved in anhydrous DMF without further purification, which was subsequently added dropwise into the solution of 500 mg of HES (with a theoretical degree of substitution of 3) in 6 mL of anhydrous DMF. The reaction was allowed to proceed for 48 h, and the product was purified by dialysis against MilliQ water in a dialyzing tube with MWCO of 14kDa, while the solution after dialyzing was freeze dried to obtain 520 mg of product (azide HES 3). FT-IR (ATR) v= 2000 (N_3), 1700 (urea). ^{13}C NMR (DMSO-D6, 300 MHz), δ (ppm) = 50.46 (CH_2-N_3), 60.96 (CH_2-OH), 158.34 (urea).

Synthesis of HES nanocontainers

50 mg of azide HES 3 was dissolved in 460 µL of MilliQ water as the aqueous phase, while 70 mg of P(E/B)-*b*-PEO was dissolved in the mixture of 5g cyclohexane and 2 g of toluene. The water phase was shaken gently at 40 °C for 3 h, to ensure the complete solvation of azide HES, after which it was mixed with oil phase, stirred magnetically at 200 rpm for 30 min, followed by ultrasonication at 70% amplitude for 3 min, with a pulse of 20 s on and 10 s off at 0 °C, using a Branson Sonifier W-450-Digital and a ½" tip. 80 mg of HDDP was dissolved together with 20 mg of P(E/B)-b-PEO in 800 µL of toluene and added into the system after sonication. The whole system was magnetically stirred at 500 rpm for 5 days, while the temperature was kept at 50 °C.

Summary and Outlook

In this work, hydroxyethyl starch (HES) based nanocapsules were prepared from different chemical reactions, surface functionalized by different methods in order to elongate its plasma halftime (improve its stealth property), and enable specific targeting effect. In addition, the interaction between the plasma protein with the unmodified HES-NCs, PEGlyated HES-NCs and mannose coupled HES-NCs was studied and compared by different methods in detail.

In chapter 3, nanocapsules based on polysaccharides were prepared via the reaction between HES and toluene diisocyanate (TDI). The surface of the nanocarriers was functionalized with poly(ethylene glycol) (PEG) via different methods in order to ensure a long circulation time in the blood plasma. The library of different PEGylated nanocapsules was investigated *in vitro* with respect to biocompatibility, protein interaction, cell uptake, and *in vivo* plasma half-life time. Highly PEGylated nanocapsules did show a reduced protein adsorption and a very low unspecific cell uptake in several blood cells. As a result, these nanocontainers show a pronounced plasma circulation time in blood which is higher than typically applied liposomal formulations. This versatile chemical platform in combination with the outstandingly long circulation times makes the PEGylated HES nanocontainers ideal for further studies for targeted cell uptake and subsequent drug release.

In chapter 4 it was proven that the PEGylated HES nanocarriers can be efficiently functionalized with mannose derivatives. Different chemistries have been investigated and a convenient two step protocol allowed a high PEG density on the nanocarriers and a high degree of “on top” functionalization with mannose. The influence of mannose on the PEGylated NCs on the pattern of the protein corona after plasma incubation was proven to be minimal by ITC, DLS, SDS-PAGE, and mass spectrometry. Furthermore, cellular uptake of the NCs by dendritic cells and a binding assay with c-type lectin proved that the targeting moieties were active and accessible to the biological receptors after incubation with human plasma. Taking into consideration that rather simple carbohydrates like the disaccharide in bleomycin,[226] have been proven to be able to selectively target cancer cells, the use of a combination of stealth nanocarriers (i.e. PEGylated materials) with such

saccharide-based targeting moieties could solve the important dilemma, where the stealth effect is lost after coupling of other targeting agents.

Furthermore, in chapter 5, in order to minimize the immobilization of the encapsulated therapeutical agent into the shell of the nanocapsule through the reaction between the amine, thiol, hydroxyl groups of the potential payload with toluene diisocyanate, hydroxyethyl starch nanocapsules were also prepared by copper free click reaction in the chapter 5. An azidation agent was developed, which can covalently attach azide groups to any polysaccharide at room temperature, with tunable degree of functionalization, and full range water solubility. Azide hydroxyethyl starch prepared by this azidation agent was used to prepare nanocapsules by copper free click reaction.

As nanocapsules with long plasma circulation time, specific cell targeting effect and formed by bio-orthogonal chemistry were prepared in this work, the efficiency of these nanocapsules as targeted delivery systems for different (potential) therapeutic agents could be tested both *in vitro* and *in vivo*. In addition, further efforts could be done, to substitute the poly(ethylene glycol) used in this work with polysaccharide, in order to prepare completely sugar based nano-carriers, which is fully biodegradable.

Based on the work in this thesis and many other studies which are published in recent years, when mono/oligo saccharides are used to surface functionalize nano-carriers, they are proven to have following advantages:

(i) specific targeting to different cell types;[37,39-41,128,131]

(ii) diagnostics and differentiation of healthy and malignant population of the same cell type;[19,128]

(iii) protecting the payload[131] and prolonged *in vivo* plasma half-life time (due to reduced protein adsorption);[88]

(iv) controlled release of a payload by specific protein interaction;[38]

(v) competing with and inhibiting the binding of other saccharide containing bacteria, virus, or pathogen with the corresponding cells.[36]

For nanocarriers that are surface modified by polysaccharides, similar properties are obtained, including:

(i) protecting the payload[134] and increasing the plasma half-life times;[24,77,138]

(ii) specific targeting;[133,137,138,183]

(iii) enzyme-induced released or activation of a therapeutic agent;[24,26,27,77,78]

(v) decreased toxicity of the payload;[132,135,137,183]

(vi) kinetics of metabolization are tunable by chemical functionalization to balance biocompatibility and stability.[24,77]

As carbohydrates are omnipresent as functional surface coatings in nature, their use in biomedical applications is obvious. They have been used to construct nanocarriers, which enable the encapsulation and protection[156,158] of different (mainly) water-soluble guests,[86,149-151,159-163] while keeping the biological properties such as specific targeting,[134,148,159-163,244] suppressed unspecific cell uptake,[86] and enzyme-triggered release.[150,157,159-162] In addition, the inherent high chemical functionality of different polysaccharides (mainly: hydroxyls, carboxylic acids, amines) allows straightforward crosslinking or on top functionalization of these molecules which is often a major factor of their application compared to synthetic macromolecules. However, it always must be considered, that the molecular weight distributions of these biopolymers are typically rather broad, making fractionation necessary in some cases. Nevertheless, due to the biodegradability of polysaccharides, their non-uniform molecular weight might not be too problematic for nanoparticular drug delivery devices, however, the toxicity after any chemical modification and also that of the degradation products after chemical modification need to be considered.

A major feature of all nanocarriers, either modified or constructed of carbohydrates is their low protein interaction: the high level of hydrophilicity induces for many of them a “stealth” behavior, and the unspecific cell uptake due to opsonization is low. Furthermore, targeting is achieved by carbohydrates in multiple cases. This behavior plus the inherent biodegradability renders carbohydrate-based nanocarriers as a high potential platform for developing the “magic bullet” that was coined by Paul

Ehrlich more than 100 years ago and makes research in this direction promising for many scientists. It is certain that several new developments in treating diseases or enabling sophisticated diagnostics will rely on carbohydrates in future.

Abbreviations

ASGP-R	Asialoglycoprotein receptors
BSA	Bovine serum albumin
cLSM	Confocal laser scanning microscopy
CuAAC	Copper-catalyzed azide-alkyne cycloaddition
DBCO	Dibenzocyclooctyl
DCC	Dicyclohexyl carbodiimide
DCM	Dichloromethane
DCs	Dendritic cells
DC-SIGN	Dendritic cell-specific intercellular adhesion molecule-3-grabbing non-integrin
Dec205	MOUSE ANTI HUMAN CD205
DLS	Dynamic light scattering
DMA	N,N-Dimethylformamide dimethyl acetal
DMF	Dimethylformamid
DMSO	Dimethyl sulfoxide
DNA	Deoxyribonucleic acid
DPPA	Diphenylphosphoryl azide
DSC	Differential scanning calorimetry
EDTA	Ethylenediaminetetraacetic acid
EPR	Enhanced permeability and retention
Et_3N	Triethylamine

FA	Fluorescamine
FACS	Fluorescence activated cell sorting
FTIR	Fourier transform infrared spectroscopy
GNP	Gold nanoparticle
GPC	Gel permeation chromatography
HA	Hyaluronic acid
HES	Hydroxyethyl starch
HES-NCs	Hydroxyethyl starch nanocapsules
HDDP	Hexanediol dipropiolate
HPLC	High-performance liquid chromatography
iDC	Immature dendritic cell
ITC	Isothermal Titration Calorimetry
KBr	Potassium bromide
kDa	Kilodaltons
KLE	poly((ethylene-*co*-butylene)-*b*-(ethylene oxide))
MC1R	Melanocortin 1 receptor
MCF-7	Michigan Cancer Foundation - 7
mDC	Mature dendritic cell
Mn	Number average molecular weight
MPS	Mononuclear phagocyte system
MWCO	Molecular weight cutoff
Mw	Weight average molecular weight
n. a.	not available

n. d.	not determined
NaCl	Sodium chloride
NHS	*N*-hydroxy succinimide
NMR	Nuclear magnetic resonance
nm	nanometer
NP	Nanoparticle
PBMC	Peripheral blood mononuclear cells
PBS	Phosphate-buffered saline
PDI	Polydispersity index
PEG	Poly(ethylene glycol)
ppm	Parts per million
PS	Polystyrene
SEM	Scanning electron microscopy
SD	Standard deviation
SDS	Sodium dodecyl sulfate
SDS-PAGE	Sodium dodecyl sulfate polyacrylamide gel electrophoresis
siRNA	Small interfering RNA
Sulfo-SMCC	Sulfosuccinimidyl 4-(N-maleimidomethyl)cyclohexane-1-carboxylate
SR101	Sulforhodamine 101
TCEP	Tris(2-carboxyethyl)phosphine
TDI	Toluene Diisocyanate
TEA	triethylamine
TEM	Transition electron microscopy

TGA	Thermogravimetric analysis
THF	Tetrahydrofuran

Erklärung

Hiermit versichern ich gemäß § 10 Abs. 3d der Promotionsordung vom 24.07.2007, dass ich die als Dissertation vorgelegte Arbeit selbst angefertigt und alle benutzen Hilfsmittel (Literatur, Apparaturen, Material) in der Arbeit angegeben habe.

Mainz, den 19. Oktober 2015

Biao Kang

Curriculum Vitae

Biao Kang

Date of Birth: 10 September 1986
Place of Birth: Shanxi, China

Education and experiences:

12. 2011- 09. 2015 Ph.D candidate, Polymer chemistry, in the group of Prof. Dr. Katharina Landfester, Max-Planck-Institut für Polymerforschung, Mainz, Germany.

10. 2009- 11. 2011 Master, Advanced Materials, Ulm University, Ulm, Germany.

09. 2005- 06. 2009 Double Bachelor, Chemical Engineering and Business Administration, Shandong University, Jinan, China

Publications during Ph.D.:

- Kang B, Till Opatz, Landfester K, Wurm F R. Sugars in biomedical applications: surface functionalization and construction of nanocarriers. Chem Soc Rev, DOI: 10.1039/C5CS00092K
- Kang B, Okwieka P, Schottler S, Winzen S, Langhanki J, Mohr K, et al. Carbohydrate-Based Nanocarriers Exhibiting Specific Cell Targeting with Minimum Influence from the Protein Corona. Angew Chem Int Ed Engl. 2015;54:7436-40.
- Kang B, Okwieka P, Schottler S, Seifert O, Kontermann RE, Pfizenmaier K, et al. Tailoring the stealth properties of biocompatible polysaccharide nanocontainers. Biomaterials. 2015;49:125-34.
- Weilbacher M, Prestel A, Kaps L, Bamberger D, Kang B, Tomcin S, et al. Nanoparticular targeting of tolerance inducing macrophages, DC and myeloid suppressor cells - new strategies for therapeutic approaches in immune-mediated diseases. Experimental Dermatology. 2014;23:E27-E.
- Kang B, Landfester K, Wurm F R. Study of the influence of hydrogen bond on the permeability of nanobarriers in a Hydroxyethyl starch nanocapsules prepared by click chemistry, to be submitted
- At least four other papers are in preparation, with me as one of the coauthers.

References

(1) Kang, B.; Opatz, T.; Landfester, K.; Wurm, F. R. *Chem. Soc. Rev.* **2015**, *44*, 8301.

(2) Strebhardt, K.; Ullrich, A. *Nature Reviews Cancer* **2008**, *8*, 473.

(3) Liu, Z.; Cai, W.; He, L.; Nakayama, N.; Chen, K.; Sun, X.; Chen, X.; Dai, H. *Nature Nanotechnology* **2007**, *2*, 47.

(4) Nasongkla, N.; Bey, E.; Ren, J.; Ai, H.; Khemtong, C.; Guthi, J. S.; Chin, S.-F.; Sherry, A. D.; Boothman, D. A.; Gao, J. *Nano Lett.* **2006**, *6*, 2427.

(5) Cheng, J.; Teply, B. A.; Sherifi, I.; Sung, J.; Luther, G.; Gu, F. X.; Levy-Nissenbaum, E.; Radovic-Moreno, A. F.; Langer, R.; Farokhzad, O. C. *Biomaterials* **2007**, *28*, 869.

(6) Wu, W.; Wieckowski, S.; Pastorin, G.; Benincasa, M.; Klumpp, C.; Briand, J. P.; Gennaro, R.; Prato, M.; Bianco, A. *Angewandte Chemie-International Edition* **2005**, *44*, 6358.

(7) Qian, X.; Peng, X.-H.; Ansari, D. O.; Yin-Goen, Q.; Chen, G. Z.; Shin, D. M.; Yang, L.; Young, A. N.; Wang, M. D.; Nie, S. *Nat. Biotechnol.* **2008**, *26*, 83.

(8) Gao, X. H.; Cui, Y. Y.; Levenson, R. M.; Chung, L. W. K.; Nie, S. M. *Nat. Biotechnol.* **2004**, *22*, 969.

(9) Liong, M.; Lu, J.; Kovochich, M.; Xia, T.; Ruehm, S. G.; Nel, A. E.; Tamanoi, F.; Zink, J. I. *Acs Nano* **2008**, *2*, 889.

(10) Tkachenko, A. G.; Xie, H.; Coleman, D.; Glomm, W.; Ryan, J.; Anderson, M. F.; Franzen, S.; Feldheim, D. L. *J. Am. Chem. Soc.* **2003**, *125*, 4700.

(11) Dai, Q.; Walkey, C.; Chan, W. C. W. *Angewandte Chemie-International Edition* **2014**, *53*, 5093.

(12) Laine, R. A. In *Glycosciences*; Wiley-VCH Verlag GmbH: 2008, p 1.

(13) Danguy, A.; Camby, I.; Kiss, R. *Biochim. Biophys. Acta* **2002**, *1572*, 285.

(14) Crowe, J. H.; Crowe, L. M.; Chapman, D. *Science* **1984**, *223*, 701.

(15) Kwong, P. D.; Wyatt, R.; Robinson, J.; Sweet, R. W.; Sodroski, J.; Hendrickson, W. A. *Nature* **1998**, *393*, 648.

(16) Xie, Y.-L.; Wang, M.-J.; Yao, S.-J. *Langmuir* **2009**, *25*, 8999.

(17) Sharon, N.; Lis, H. *Sci. Am.* **1993**, *268*, 82.

(18) Ye, S. Q.; Wang, C. Y.; Liu, X. X.; Tong, Z. *J Biomat Sci-Polym E* **2005**, *16*, 909.

(19) El-Boubbou, K.; Zhu, D. C.; Vasileiou, C.; Borhan, B.; Prosperi, D.; Li, W.; Huang, X. *J. Am. Chem. Soc.* **2010**, *132*, 4490.

(20) Knop, K.; Hoogenboom, R.; Fischer, D.; Schubert, U. S. *Angewandte Chemie-International Edition* **2010**, *49*, 6288.

(21) Besheer, A.; Vogel, J.; Glanz, D.; Kressler, J.; Groth, T.; Maeder, K. *Mol. Pharm.* **2009**, *6*, 407.

(22) Lemarchand, C.; Gref, R.; Couvreur, P. *Eur. J. Pharm. Biopharm.* **2004**, *58*, 327.

(23) Orlando, M. *Ph.D. Thesis, University of Giessen* **2003**.

(24) Noga, M.; Edinger, D.; Klaeger, R.; Wegner, S. V.; Spatz, J. P.; Wagner, E.; Winter, G.; Besheer, A. *Biomaterials* **2013**, *34*, 2530.

(25) Noga, M.; Edinger, D.; Roedl, W.; Wagner, E.; Winter, G.; Besheer, A. *J. Controlled Release* **2012**, *159*, 92.

(26) Ferguson, E. L.; Duncan, R. *Biomacromolecules* **2009**, *10*, 1358.

(27) Duncan, R.; Gilbert, H. R. P.; Carbajo, R. J.; Vicent, M. J. *Biomacromolecules* **2008**, *9*, 1146.

(28) Hardwicke, J.; Ferguson, E. L.; Moseley, R.; Stephens, P.; Thomas, D. W.; Duncan, R. *Journal of Controlled Release* **2008**, *130*, 275.

(29) Marchant, R. E.; Yuan, S.; Szakalasgratzl, G. *Journal of Biomaterials Science-Polymer Edition* **1994**, *6*, 549.

(30) Osterberg, E.; Bergstrom, K.; Holmberg, K.; Schuman, T. P.; Riggs, J. A.; Burns, N. L.; Vanalstine, J. M.; Harris, J. M. *Journal of Biomedical Materials Research* **1995**, *29*, 741.

(31) Brewer, C. F.; Miceli, M. C.; Baum, L. G. *Curr. Opin. Struct. Biol.* **2002**, *12*, 616.

(32) Gabius, H. J. *Biochem. Soc. Trans.* **2008**, *36*, 1491.

(33) Gabius, H. J.; Andre, S.; Kaltner, H.; Siebert, H. C. *Biochim. Biophys. Acta* **2002**, *1572*, 165.

(34) Yamazaki, N.; Kojima, S.; Bovin, N. V.; Andre, S.; Gabius, S.; Gabius, H. J. *Adv Drug Deliv Rev* **2000**, *43*, 225.

(35) Geijtenbeek, T. B. H.; Torensma, R.; van Vliet, S. J.; van Duijnhoven, G. C. F.; Adema, G. J.; van Kooyk, Y.; Figdor, C. G. *Cell* **2000**, *100*, 575.

(36) Martinez-Avila, O.; Hijazi, K.; Marradi, M.; Clavel, C.; Campion, C.; Kelly, C.; Penades, S. *Chemistry* **2009**, *15*, 9874.

(37) Chavez-Santoscoy, A. V.; Roychoudhury, R.; Pohl, N. L. B.; Wannemuehler, M. J.; Narasimhan, B.; Ramer-Tait, A. E. *Biomaterials* **2012**, *33*, 4762.

(38) Wu, S.; Huang, X.; Du, X. *Angew. Chem. Int. Ed. Engl.* **2013**, *52*, 5580.

(39) Yu, G.; Ma, Y.; Han, C.; Yao, Y.; Tang, G.; Mao, Z.; Gao, C.; Huang, F. *J. Am. Chem. Soc.* **2013**, *135*, 10310.

(40) Chen, W.; Zou, Y.; Meng, F.; Cheng, R.; Deng, C.; Feijen, J.; Zhong, Z. *Biomacromolecules* **2014**, *15*, 900.

(41) Lartigue, L.; Oumzil, K.; Guari, Y.; Larionova, J.; Guerin, C.; Montero, J. L.; Barragan-Montero, V.; Sangregorio, C.; Caneschi, A.; Innocenti, C.; Kalaivani, T.; Arosio, P.; Lascialfari, A. *Org. Lett.* **2009**, *11*, 2992.

(42) Zimmer, A. K.; Chetoni, P.; Saettone, M. F.; Zerbe, H.; Kreuter, J. *J. Controlled Release* **1995**, *33*, 31.

(43) Durrani, A. M.; Farr, S. J.; Kellaway, I. W. *Int. J. Pharm.* **1995**, *118*, 243.

(44) Lehr, C. M.; Bouwstra, J. A.; Schacht, E. H.; Junginger, H. E. *Int. J. Pharm.* **1992**, *78*, 43.

(45) Letourneur, D.; Parisel, C.; Prigent-Richard, S.; Cansell, M. *J Control Release* **2000**, *65*, 83.

(46) Cansell, M.; Parisel, C.; Jozefonvicz, J.; Letourneur, D. *J. Biomed. Mater. Res.* **1999**, *44*, 140.

(47) Demetriou, M.; Granovsky, M.; Quaggin, S.; Dennis, J. W. *Nature* **2001**, *409*, 733.

(48) Sacchettini, J. C.; Baum, L. G.; Brewer, C. F. *Biochemistry* **2001**, *40*, 3009.

(49) Lowe, J. B. *Cell* **2001**, *104*, 809.

(50) Rabinovich, G. A.; Baum, L. G.; Tinari, N.; Paganelli, R.; Natoli, C.; Liu, F. T.; Iacobelli, S. *Trends Immunol.* **2002**, *23*, 313.

(51) Hakomori, S. *Proc Natl Acad Sci U S A* **2002**, *99*, 10231.

(52) Danishefsky, S. J.; Allen, J. R. *Angew. Chem. Int. Ed. Engl.* **2000**, *39*, 836.

(53) Lis, H.; Sharon, N. *Chem. Rev.* **1998**, *98*, 637.

(54) Liu, F. T.; Rabinovich, G. A. *Nat. Rev. Cancer* **2005**, *5*, 29.

(55) Barondes, S. H.; Castronovo, V.; Cooper, D. N.; Cummings, R. D.; Drickamer, K.; Feizi, T.; Gitt, M. A.; Hirabayashi, J.; Hughes, C.; Kasai, K.; et al. *Cell* **1994**, *76*, 597.

(56) Lotan, R.; Ito, H.; Yasui, W.; Yokozaki, H.; Lotan, D.; Tahara, E. *Int. J. Cancer* **1994**, *56*, 474.

(57) Hsu, D. K.; Dowling, C. A.; Jeng, K. C. G.; Chen, J. T.; Yang, R. Y.; Liu, F. T. *Int. J. Cancer* **1999**, *81*, 519.

(58) Irimura, T.; Matsushita, Y.; Sutton, R. C.; Carralero, D.; Ohannesian, D. W.; Cleary, K. R.; Ota, D. M.; Nicolson, G. L.; Lotan, R. *Cancer Res.* **1991**, *51*, 387.

(59) Schoeppner, H. L.; Raz, A.; Ho, S. B.; Bresalier, R. S. *Cancer* **1995**, *75*, 2818.

(60) Sanjuan, X.; Fernandez, P. L.; Castells, A.; Castronovo, V.; van den Brule, F.; Liu, F. T.; Cardesa, A.; Campo, E. *Gastroenterology* **1997**, *113*, 1906.

(61) Xu, X. C.; el-Naggar, A. K.; Lotan, R. *Am J Pathol* **1995**, *147*, 815.

(62) Fernandez, P. L.; Merino, M. J.; Gomez, M.; Campo, E.; Medina, T.; Castronovo, V.; Sanjuan, X.; Cardesa, A.; Liu, F. T.; Sobel, M. E. *J. Pathol.* **1997**, *181*, 80.

(63) VandenBrule, F. A.; Buicu, C.; Berchuck, A.; Bast, R. C.; Deprez, M.; Liu, F. T.; Cooper, D. N. W.; Pieters, C.; Sobel, M. E.; Castronovo, V. *Hum Pathol* **1996**, *27*, 1185.

(64) Auzenne, E.; Ghosh, S. C.; Khodadadian, M.; Rivera, B.; Farquhar, D.; Price, R. E.; Ravoori, M.; Kundra, V.; Freedman, R. S.; Klostergaard, J. *Neoplasia* **2007**, *9*, 479.

(65) Peer, D.; Margalit, R. *Neoplasia* **2004**, *6*, 343.

(66) Zoller, M. *J Mol Med-Jmm* **1995**, *73*, 425.

(67) Smadja-Joffe, F.; Legras, S.; Girard, N.; Li, Y.; Delpech, B.; Bloget, F.; Morimoto, K.; Le Bousse-Kerdiles, C.; Clay, D.; Jasmin, C.; Levesque, J. P. *Leuk. Lymphoma* **1996**, *21*, 407.

(68) Jin, S.; Cheng, Y.; Reid, S.; Li, M.; Wang, B. *Med Res Rev* **2010**, *30*, 171.

(69) Salvati, A.; Pitek, A. S.; Monopoli, M. P.; Prapainop, K.; Bombelli, F. B.; Hristov, D. R.; Kelly, P. M.; Aberg, C.; Mahon, E.; Dawson, K. A. *Nat Nanotechnol* **2013**, *8*, 137.

(70) Pablo del Pino, B. P., Qian Zhang, Pauline Maffre, G. Ulrich Nienhaus and Wolfgang J. Parak *Materials Horizons* **2014**, *1*, 301.

(71) Knop, K.; Hoogenboom, R.; Fischer, D.; Schubert, U. S. *Angew. Chem. Int. Ed. Engl.* **2010**, *49*, 6288.

(72) Alconcel, S. N. S.; Baas, A. S.; Maynard, H. D. *Polym. Chem.* **2011**, *2*, 1442.

(73) Bendele, A.; Seely, J.; Richey, C.; Sennello, G.; Shopp, G. *Toxicol. Sci.* **1998**, *42*, 152.

(74) Conover, C. D.; Gilbert, C. W.; Shum, K. L.; Shorr, R. G. *Artif. Organs* **1997**, *21*, 907.

(75) Treib, J.; Baron, J. F.; Grauer, M. T.; Strauss, R. G. *Intensive Care Med* **1999**, *25*, 258.

(76) Pelegri-O'Day, E. M.; Lin, E. W.; Maynard, H. D. *J. Am. Chem. Soc.* **2014**, *136*, 14323.

(77) Noga, M.; Edinger, D.; Rodl, W.; Wagner, E.; Winter, G.; Besheer, A. *J Control Release* **2012**, *159*, 92.

(78) Hardwicke, J.; Ferguson, E. L.; Moseley, R.; Stephens, P.; Thomas, D. W.; Duncan, R. *J Control Release* **2008**, *130*, 275.

(79) Besheer, A.; Vogel, J.; Glanz, D.; Kressler, J.; Groth, T.; Mader, K. *Mol. Pharm.* **2009**, *6*, 407.

(80) Lemarchand, C.; Gref, R.; Couvreur, P. *Eur J Pharm Biopharm* **2004**, *58*, 327.

(81) Besheer, A.; Hause, G.; Kressler, J.; Maeder, K. *Biomacromolecules* **2007**, *8*, 359.

(82) Marchant, R. E.; Yuan, S.; Szakalas-Gratzl, G. *J Biomater Sci Polym Ed* **1994**, *6*, 549.

(83) Osterberg, E.; Bergstrom, K.; Holmberg, K.; Schuman, T. P.; Riggs, J. A.; Burns, N. L.; Van Alstine, J. M.; Harris, J. M. *J. Biomed. Mater. Res.* **1995**, *29*, 741.

(84) Woodle, M. C.; Lasic, D. D. *Biochim. Biophys. Acta* **1992**, *1113*, 171.

(85) Allen, T. M. *Adv Drug Deliv Rev* **1994**, *13*, 285.

(86) Baier, G.; Baumann, D.; Siebert, J. M.; Musyanovych, A.; Mailaender, V.; Landfester, K. *Biomacromolecules* **2012**, *13*, 2704.

(87) Jancik, J. M.; Schauer, R.; Andres, K. H.; Vonduring, M. *Cell Tissue Res* **1978**, *186*, 209.

(88) Ohyanagi, T.; Nagahori, N.; Shimawaki, K.; Hinou, H.; Yamashita, T.; Sasaki, A.; Jin, T.; Iwanaga, T.; Kinjo, M.; Nishimura, S. *J. Am. Chem. Soc.* **2011**, *133*, 12507.

(89) Pierce, J. G.; Parsons, T. F. *Annu. Rev. Biochem* **1981**, *50*, 465.

(90) Kruse, J.; Mailhammer, R.; Wernecke, H.; Faissner, A.; Sommer, I.; Goridis, C.; Schachner, M. *Nature* **1984**, *311*, 153.

(91) Yeh, Y.; Feeney, R. E. *Chem. Rev.* **1996**, *96*, 601.

(92) Paulson, J. C. *Trends Biochem. Sci.* **1989**, *14*, 272.

(93) Ebbinghaus, S.; Meister, K.; Born, B.; DeVries, A. L.; Gruebele, M.; Havenith, M. *J. Am. Chem. Soc.* **2010**, *132*, 12210.

(94) Morell, A. G.; Gregoria.G; Scheinbe.Ih; Hickman, J.; Ashwell, G. *J. Biol. Chem.* **1971**, *246*, 1461.

(95) Hase, K.; Kawano, K.; Nochi, T.; Pontes, G. S.; Fukuda, S.; Ebisawa, M.; Kadokura, K.; Tobe, T.; Fujimura, Y.; Kawano, S.; Yabashi, A.; Waguri, S.; Nakato, G.; Kimura, S.; Murakami, T.; Iimura, M.; Hamura, K.; Fukuoka, S.-I.; Lowe, A. W.; Itoh, K.; Kiyono, H.; Ohno, H. *Nature* **2009**, *462*, 226.

(96) Lichtenthaler, S. F.; Dominguez, D.; Westmeyer, G. G.; Reiss, K.; Haass, C.; Saftig, P.; De Strooper, B.; Seed, B. *J. Biol. Chem.* **2003**, *278*, 48713.

(97) Nesbitt, W. S.; Kulkarni, S.; Giuliano, S.; Goncalves, I.; Dopheide, S. M.; Yap, C. L.; Harper, I. S.; Salem, H. H.; Jackson, S. P. *J. Biol. Chem.* **2002**, *277*, 2965.

(98) Veronese, F. M.; Pasut, G. *Drug Discov Today* **2005**, *10*, 1451.

(99) Mero, A.; Pasqualin, M.; Campisi, M.; Renier, D.; Pasut, G. *Carbohydr. Polym.* **2013**, *92*, 2163.

(100) Liebner, R.; Mathaes, R.; Meyer, M.; Hey, T.; Winter, G.; Besheer, A. *Eur. J. Pharm. Biopharm.* **2014**, *87*, 378.

(101) Ferguson, E. L.; Alshame, A. M. J.; Thomas, D. W. *Int. J. Pharm.* **2010**, *402*, 95.

(102) Davis, J. A.; Freeze, H. H. *Biochim. Biophys. Acta* **2001**, *1528*, 116.

(103) Weis, W. I.; Drickamer, K.; Hendrickson, W. A. *Nature* **1992**, *360*, 127.

(104) Ahire, J. H.; Chambrier, I.; Mueller, A.; Bao, Y.; Chao, Y. *ACS Appl Mater Interfaces* **2013**, *5*, 7384.

(105) Kouyoumdjian, H.; Zhu, D. C.; El-Dakdouki, M. H.; Lorenz, K.; Chen, J.; Li, W.; Huang, X. *ACS Chem Neurosci* **2013**, *4*, 575.

(106) Frigell, J.; Garcia, I.; Gomez-Vallejo, V.; Llop, J.; Penades, S. *J. Am. Chem. Soc.* **2014**, *136*, 449.

(107) Cedervall, T.; Lynch, I.; Lindman, S.; Berggard, T.; Thulin, E.; Nilsson, H.; Dawson, K. A.; Linse, S. *Proc Natl Acad Sci U S A* **2007**, *104*, 2050.

(108) Aggarwal, P.; Hall, J. B.; McLeland, C. B.; Dobrovolskaia, M. A.; McNeil, S. E. *Adv Drug Deliv Rev* **2009**, *61*, 428.

(109) Walczyk, D.; Bombelli, F. B.; Monopoli, M. P.; Lynch, I.; Dawson, K. A. *J. Am. Chem. Soc.* **2010**, *132*, 5761.

(110) Rocker, C.; Potzl, M.; Zhang, F.; Parak, W. J.; Nienhaus, G. U. *Nat Nanotechnol* **2009**, *4*, 577.

(111) Deng, Z. J.; Liang, M.; Monteiro, M.; Toth, I.; Minchin, R. F. *Nat Nanotechnol* **2011**, *6*, 39.

(112) Walkey, C. D.; Chan, W. C. *Chem. Soc. Rev.* **2012**, *41*, 2780.

(113) Monopoli, M. P.; Walczyk, D.; Campbell, A.; Elia, G.; Lynch, I.; Bombelli, F. B.; Dawson, K. A. *J. Am. Chem. Soc.* **2011**, *133*, 2525.

(114) Albanese, A.; Walkey, C. D.; Olsen, J. B.; Guo, H.; Emili, A.; Chan, W. C. *ACS Nano* **2014**, *8*, 5515.

(115) Kang, B.; Okwieka, P.; Schottler, S.; Winzen, S.; Langhanki, J.; Mohr, K.; Opatz, T.; Mailander, V.; Landfester, K.; Wurm, F. R. *Angew. Chem. Int. Ed. Engl.* **2015**, *54*, 7436.

(116) Watkins, W. M. *Science* **1966**, *152*, 172.

(117) Adokoh, C. K.; Quan, S.; Hitt, M.; Darkwa, J.; Kumar, P.; Narain, R. *Biomacromolecules* **2014**, *15*, 3802.

(118) Angata, T.; Varki, A. *Chem. Rev.* **2002**, *102*, 439.

(119) Schauer, R. *Trends Biochem. Sci* **1985**, *10*, 357.

(120) Kelm, S.; Gerlach, J.; Brossmer, R.; Danzer, C. P.; Nitschke, L. *J Exp Med* **2002**, *195*, 1207.

(121) Jin, L.; McLean, P. A.; Neel, B. G.; Wortis, H. H. *J. Exp. Med.* **2002**, *195*, 1199.

(122) Farr, T. D.; Lai, C. H.; Grunstein, D.; Orts-Gil, G.; Wang, C. C.; Boehm-Sturm, P.; Seeberger, P. H.; Harms, C. *Nano Lett.* **2014**, *14*, 2130.

(123)Selim, K. M. K.; Ha, Y.-S.; Kim, S.-J.; Chang, Y.; Kim, T.-J.; Lee, G. H.; Kang, I.-K. *Biomaterials* **2007**, *28*, 710.

(124) Giraud, M. F.; Naismith, J. H. *Curr. Opin. Struct. Biol.* **2000**, *10*, 687.

(125) Levi, J. A.; Raghavan, D.; Harvey, V.; Thompson, D.; Sandeman, T.; Gill, G.; Stuart-Harris, R.; Snyder, R.; Byrne, M.; Kerestes, Z.; et al. *J Clin Oncol* **1993**, *11*, 1300.

(126) deWit, R.; Stoter, G.; Kaye, S. B.; Sleijfer, D. T.; Jones, W. G.; Huinink, W. W. T.; Rea, L. A.; Collette, L.; Sylvester, R. *J Clin Oncol* **1997**, *15*, 1837.

(127) Goodwin, D. A.; Meares, C. F.; DeRiemer, L. H.; Diamanti, C. I.; Goode, R. L.; Baumert, J. E., Jr.; Sartoris, D. J.; Lantieri, R. L.; Fawcett, H. D. *J Nucl Med* **1981**, *22*, 787.

(128) Yu, Z.; Schmaltz, R. M.; Bozeman, T. C.; Paul, R.; Rishel, M. J.; Tsosie, K. S.; Hecht, S. M. *J. Am. Chem. Soc.* **2013**, *135*, 2883.

(129) Willmann, J. K.; Paulmurugan, R.; Chen, K.; Gheysens, O.; Rodriguez-Porcel, M.; Lutz, A. M.; Chen, I. Y.; Chen, X.; Gambhir, S. S. *Radiology* **2008**, *246*, 508.

(130) Bhattacharya, C.; Yu, Z.; Rishel, M. J.; Hecht, S. M. *Biochemistry* **2014**, *53*, 3264.

(131) Sizovs, A.; Xue, L.; Tolstyka, Z. P.; Ingle, N. P.; Wu, Y.; Cortez, M.; Reineke, T. M. *J. Am. Chem. Soc.* **2013**, *135*, 15417.

(132) Valodkar, M.; Rathore, P. S.; Jadeja, R. N.; Thounaojam, M.; Devkar, R. V.; Thakore, S. *J. Hazard. Mater.* **2012**, *201-202*, 244.

(133) Asthana, S.; Gupta, P. K.; Konwar, R.; Chourasia, M. K. *J. Nanopart. Res.* **2013**, *15*.

(134) Li, J.; Huang, P. S.; Chang, L. L.; Long, X. W.; Dong, A. J.; Liu, J. J.; Chu, L. P.; Hu, F. Q.; Liu, J. F.; Deng, L. D. *Macromol Res* **2013**, *21*, 1331.

(135) Boca, S. C.; Potara, M.; Gabudean, A. M.; Juhem, A.; Baldeck, P. L.; Astilean, S. *Cancer Lett.* **2011**, *311*, 131.

(136) Sun, I. C.; Na, J. H.; Jeong, S. Y.; Kim, D. E.; Kwon, I. C.; Choi, K.; Ahn, C. H.; Kim, K. *Pharm. Res.* **2014**, *31*, 1418.

(137) Needham, C. J.; Williams, A. K.; Chew, S. A.; Kasper, F. K.; Mikos, A. G. *Biomacromolecules* **2012**, *13*, 1429.

(138) Liu, L.; He, H.; Zhang, M.; Zhang, S.; Zhang, W.; Liu, J. *Biomaterials* **2014**, *35*, 8002.

(139) Wang, Z.; Chen, Z.; Liu, Z.; Shi, P.; Dong, K.; Ju, E.; Ren, J.; Qu, X. *Biomaterials* **2014**, *35*, 9678.

(140)Stark, D. M.; Timmerman, K. P.; Barry, G. F.; Preiss, J.; Kishore, G. M. *Science* **1992**, *258*, 287.

(141) Hey, T.; Knoller, H.; Vorstheim, P. In *Therapeutic Proteins*; Wiley-VCH Verlag GmbH & Co. KGaA: 2012, p 117.

(142) Kumar, M. N.; Muzzarelli, R. A.; Muzzarelli, C.; Sashiwa, H.; Domb, A. J. *Chem. Rev.* **2004**, *104*, 6017.

(143) Al-Assaf, S.; Sakata, M.; McKenna, C.; Aoki, H.; Phillips, G. O. *Struct. Chem.* **2009**, *20*, 325.

(144) Dias, A. M.; Hussain, A.; Marcos, A. S.; Roque, A. C. *Biotechnol. Adv.* **2011**, *29*, 142.

(145) Devi, P. R.; Kumar, C. S.; Selvamani, P.; Subramanian, N.; Ruckmani, K. *Mater. Lett.* **2015**, *139*, 241.

(146) Gamal-Eldeen, A. M.; Moustafa, D.; El-Daly, S. M.; Katti, K. V. *Eur. J. Cancer* **2014**, *50*, e46.

(147)Fraser, J. R.; Laurent, T. C.; Laurent, U. B. *J Intern Med* **1997**, *242*, 27.

(148) Percec, V.; Leowanawat, P.; Sun, H. J.; Kulikov, O.; Nusbaum, C. D.; Tran, T. M.; Bertin, A.; Wilson, D. A.; Peterca, M.; Zhang, S.; Kamat, N. P.; Vargo, K.; Moock, D.; Johnston, E. D.; Hammer, D. A.; Pochan, D. J.; Chen, Y.; Chabre, Y. M.; Shiao, T. C.; Bergeron-Brlek, M.; Andre, S.; Roy, R.; Gabius, H. J.; Heiney, P. A. *J. Am. Chem. Soc.* **2013**, *135*, 9055.

(149) Anette, P.-N.; Fichter, M.; Dedters, M.; Pretsch, L.; Gregory, S. H.; Meyer, C.; Doganci, A.; Diken, M.; Landfester, K.; Baier, G.; Gehring, S. *Biomacromolecules* **2014**, *15*, 2378.

(150)Baier, G.; Cavallaro, A.; Vasilev, K.; Mailaender, V.; Musyanovych, A.; Landfester, K. *Biomacromolecules* **2013**, *14*, 1103.

(151) Taheri, S.; Baier, G.; Majewski, P.; Barton, M.; Forch, R.; Landfester, K.; Vasilev, K. *J Mater Chem B* **2014**, *2*, 1838.

(152)Kang, B.; Okwieka, P.; Schottler, S.; Seifert, O.; Kontermann, R. E.; Pfizenmaier, K.; Musyanovych, A.; Meyer, R.; Diken, M.; Sahin, U.; Mailander, V.; Wurm, F. R.; Landfester, K. *Biomaterials* **2015**, *49*, 125.

(153) Roux, R.; Sallet, L.; Alcouffe, P.; Chambert, S.; Sintes-Zydowicz, N.; Fleury, E.; Bernard, J. *Acs Macro Lett* **2012**, *1*, 1074.

(154) Alexandrino, E. M.; Buchold, P.; Wagner, M.; Fuchs, A.; Kreyes, A.; Weiss, C. K.; Landfester, K.; Wurm, F. R. *Chem Commun (Camb)* **2014**, *50*, 10495.

(155) Malzahn, K.; Marsico, F.; Koynov, K.; Landfester, K.; Weiss, C. K.; Wurm, F. R. *Acs Macro Letters* **2014**, *3*, 40.

(156) Giri, J.; Li, W. J.; Tuan, R. S.; Cicerone, M. T. *Adv. Mater.* **2011**, *23*, 4861.

(157) Kwag, D. S.; Oh, K. T.; Lee, E. S. *J Control Release* **2014**, *187*, 83.

(158) Amar-Lewis, E.; Azagury, A.; Chintakunta, R.; Goldbart, R.; Traitel, T.; Prestwood, J.; Landesman-Milo, D.; Peer, D.; Kost, J. *J Control Release* **2014**, *185*, 109.

(159) Choi, K. Y.; Chung, H.; Min, K. H.; Yoon, H. Y.; Kim, K.; Park, J. H.; Kwon, I. C.; Jeong, S. Y. *Biomaterials* **2010**, *31*, 106.

(160)Choi, K. Y.; Yoon, H. Y.; Kim, J.-H.; Bae, S. M.; Park, R.-W.; Kang, Y. M.; Kim, I.-S.; Kwon, I. C.; Choi, K.; Jeong, S. Y.; Kim, K.; Park, J. H. *Acs Nano* **2011**, *5*, 8591.

(161) Choi, K. Y.; Min, K. H.; Na, J. H.; Choi, K.; Kim, K.; Park, J. H.; Kwon, I. C.; Jeong, S. Y. *J. Mater. Chem.* **2009**, *19*, 4102.

(162) Choi, K. Y.; Min, K. H.; Yoon, H. Y.; Kim, K.; Park, J. H.; Kwon, I. C.; Choi, K.; Jeong, S. Y. *Biomaterials* **2011**, *32*, 1880.

(163) Ray, L.; Kumar, P.; Gupta, K. C. *Biomaterials* **2013**, *34*, 3064.

(164) Ernsting, M. J.; Tang, W.-L.; MacCallum, N.; Li, S.-D. *Bioconjugate Chem.* **2011**, *22*, 2474.

(165) Dev, A.; Mohan, J. C.; Sreeja, V.; Tamura, H.; Patzke, G. R.; Hussain, F.; Weyeneth, S.; Nair, S. V.; Jayakumar, R. *Carbohyd Polym* **2010**, *79*, 1073.

(166) Jorfi, M.; Foster, E. J. *J. Appl. Polym. Sci.* **2015**, *132*, n/a.

(167) Jayakumar, R.; Menon, D.; Manzoor, K.; Nair, S. V.; Tamura, H. *Carbohydr. Polym.* **2010**, *82*, 227.

(168) Kang, B.; Okwieka, P.; Schoettler, S.; Seifert, O.; Kontermann, R. E.; Pfizenmaier, K.; Musyanovych, A.; Meyer, R.; Diken, M.; Sahin, U.; Mailaender, V.; Wurm, F. R.; Landfester, K. *Biomaterials* **2015**, *49*, 125.

(169)Maxwell, D. J.; Taylor, J. R.; Nie, S. M. *J. Am. Chem. Soc.* **2002**, *124*, 9606.

(170) Vallhov, H.; Gabrielsson, S.; Stromme, M.; Scheynius, A.; Garcia-Bennett, A. E. *Nano Lett.* **2007**, *7*, 3576.

(171) Koppolu, B.; Zaharoff, D. A. *Biomaterials* **2013**, *34*, 2359.

(172)Qazilbash, M. M.; Brehm, M.; Chae, B.-G.; Ho, P. C.; Andreev, G. O.; Kim, B.-J.; Yun, S. J.; Balatsky, A. V.; Maple, M. B.; Keilmann, F.; Kim, H.-T.; Basov, D. N. *Science* **2007**, *318*, 1750.

(173) Giljohann, D. A.; Seferos, D. S.; Daniel, W. L.; Massich, M. D.; Patel, P. C.; Mirkin, C. A. *Angewandte Chemie-International Edition* **2010**, *49*, 3280.

(174) Horcajada, P.; Chalati, T.; Serre, C.; Gillet, B.; Sebrie, C.; Baati, T.; Eubank, J. F.; Heurtaux, D.; Clayette, P.; Kreuz, C.; Chang, J.-S.; Hwang, Y. K.; Marsaud, V.; Bories, P.-N.; Cynober, L.; Gil, S.; Ferey, G.; Couvreur, P.; Gref, R. *Nature Materials* **2010**, *9*, 172.

(175) Min, K. H.; Park, K.; Kim, Y.-S.; Bae, S. M.; Lee, S.; Jo, H. G.; Park, R.-W.; Kim, I.-S.; Jeong, S. Y.; Kim, K.; Kwon, I. C. *J. Controlled Release* **2008**, *127*, 208.

(176) Vila, A.; Gill, H.; McCallion, O.; Alonso, M. J. *J. Controlled Release* **2004**, *98*, 231.

(177) Laouini, A.; Andrieu, V.; Vecellio, L.; Fessi, H.; Charcosset, C. *Int. J. Pharm.* **2014**, *471*, 385.

(178) Du, D.; Chang, N.; Sun, S.; Li, M.; Yu, H.; Liu, M.; Liu, X.; Wang, G.; Li, H.; Liu, X.; Geng, S.; Wang, Q.; Peng, H. *J. Controlled Release* **2014**, *182*, 99.

(179) Yamada, Y.; Tabata, M.; Yasuzaki, Y.; Nomura, M.; Shibata, A.; Ibayashi, Y.; Taniguchi, Y.; Sasaki, S.; Harashima, H. *Biomaterials* **2014**, *35*, 6430.

(180) Ju, R.-J.; Li, X.-T.; Shi, J.-F.; Li, X.-Y.; Sun, M.-G.; Zeng, F.; Zhou, J.; Liu, L.; Zhang, C.-X.; Zhao, W.-Y.; Lu, W.-L. *Biomaterials* **2014**, *35*, 7610.

(181) Ara, M. N.; Matsuda, T.; Hyodo, M.; Sakurai, Y.; Hatakeyama, H.; Ohga, N.; Hida, K.; Harashima, H. *Biomaterials* **2014**, *35*, 7110.

(182) Guo, Z.; He, B.; Jin, H.; Zhang, H.; Dai, W.; Zhang, L.; Zhang, H.; Wang, X.; Wang, J.; Zhang, X.; Zhang, Q. *Biomaterials* **2014**, *35*, 6106.

(183)Zhang, X.; Zhang, Q.; Peng, Q.; Zhou, J.; Liao, L.; Sun, X.; Zhang, L.; Gong, T. *Biomaterials* **2014**, *35*, 6130.

(184) Qin, C.; He, B.; Dai, W.; Lin, Z.; Zhang, H.; Wang, X.; Wang, J.; Zhang, X.; Wang, G.; Yin, L.; Zhang, Q. *Biomaterials* **2014**, *35*, 5908.

(185) Kuo, Y.-C.; Wang, C.-T. *Biomaterials* **2014**, *35*, 5954.

(186) Miyabe, H.; Hyodo, M.; Nakamura, T.; Sato, Y.; Hayakawa, Y.; Harashima, H. *J. Controlled Release* **2014**, *184*, 20.

(187) Liu, Z.; Xiong, M.; Gong, J.; Zhang, Y.; Bai, N.; Luo, Y.; Li, L.; Wei, Y.; Liu, Y.; Tan, X.; Xiang, R. *Nature Communications* **2014**, *5*.

(188) Qhattal, H. S. S.; Hye, T.; Alali, A.; Liu, X. *Acs Nano* **2014**, *8*, 5423.

(189) She, Z.; Zhang, T.; Wang, X.; Li, X.; Song, Y.; Cheng, X.; Huang, Z.; Deng, Y. *Biomaterials* **2014**, *35*, 5216.

(190) Cheng, Z.; Al Zaki, A.; Hui, J. Z.; Muzykantov, V. R.; Tsourkas, A. *Science* **2012**, *338*, 903.

(191) Davis, M. E.; Chen, Z.; Shin, D. M. *Nature Reviews Drug Discovery* **2008**, *7*, 771.

(192) Yan, Y.; Such, G. K.; Johnston, A. P. R.; Best, J. P.; Caruso, F. *Acs Nano* **2012**, *6*, 3663.

(193) Brannon-Peppas, L.; Blanchette, J. O. *Adv. Drug Del. Rev.* **2004**, *56*, 1649.

(194) Landfester, K. *Angewandte Chemie-International Edition* **2009**, *48*, 4488.

(195) Landfester, K.; Bechthold, N.; Tiarks, F.; Antonietti, M. *Macromolecules* **1999**, *32*, 5222.

(196) Baier, G.; Musyanovych, A.; Dass, M.; Theisinger, S.; Landfester, K. *Biomacromolecules* **2010**, *11*, 960.

(197) Lv, L.-P.; Zhao, Y.; Vilbrandt, N.; Gallei, M.; Vimalanandan, A.; Rohwerder, M.; Landfester, K.; Crespy, D. *J. Am. Chem. Soc.* **2013**, *135*, 14198.

(198) Siebert, J. M.; Baier, G.; Musyanovych, A.; Landfester, K. *Chem. Commun.* **2012**, *48*, 5470.

(199)Zarychanski, R.; Abou-Setta, A. M.; Turgeon, A. F.; Houston, B. L.; McIntyre, L.; Marshall, J. C.; Fergusson, D. A. *Jama-Journal of the American Medical Association* **2013**, *309*, 678.

(200) Yoshida, M.; Kishikawa, T. *Starke* **1984**, *36*, 167.

(201) Stolnik, S.; Illum, L.; Davis, S. S. *Adv. Drug Del. Rev.* **1995**, *16*, 195.

(202) Baier, G.; Cavallaro, A.; Vasilev, K.; Mailander, V.; Musyanovych, A.; Landfester, K. *Biomacromolecules* **2013**, *14*, 1103.

(203) Bohlen, P.; Stein, S.; Dairman, W.; Udenfrie.S *Arch. Biochem. Biophys.* **1973**, *155*, 213.

(204) Cedervall, T.; Lynch, I.; Lindman, S.; Berggard, T.; Thulin, E.; Nilsson, H.; Dawson, K. A.; Linse, S. *Proc. Natl. Acad. Sci. U. S. A.* **2007**, *104*, 2050.

(205) Aggarwal, P.; Hall, J. B.; McLeland, C. B.; Dobrovolskaia, M. A.; McNeil, S. E. *Adv. Drug Del. Rev.* **2009**, *61*, 428.

(206) Walczyk, D.; Bombelli, F. B.; Monopoli, M. P.; Lynch, I.; Dawson, K. A. *J. Am. Chem. Soc.* **2010**, *132*, 5761.

(207) Roecker, C.; Poetzl, M.; Zhang, F.; Parak, W. J.; Nienhaus, G. U. *Nature Nanotechnology* **2009**, *4*, 577.

(208) Deng, Z. J.; Liang, M.; Monteiro, M.; Toth, I.; Minchin, R. F. *Nature Nanotechnology* **2011**, *6*, 39.

(209) Walkey, C. D.; Chan, W. C. W. *Chem. Soc. Rev.* **2012**, *41*, 2780.

(210) Monopoli, M. P.; Walczyk, D.; Campbell, A.; Elia, G.; Lynch, I.; Bombelli, F. B.; Dawson, K. A. *J. Am. Chem. Soc.* **2011**, *133*, 2525.

(211) Albanese, A.; Walkey, C. D.; Olsen, J. B.; Guo, H.; Emili, A.; Chan, W. C. W. *Acs Nano* **2014**, *8*, 5515.

(212) Schlaad, H.; Kukula, H.; Rudloff, J.; Below, I. *Macromolecules* **2001**, *34*, 4302.

(213) Kang, B.; Okwieka, P.; Schoettler, S.; Winzen, S.; Langhanki, J.; Mohr, K.; Opatz, T.; Mailaender, V.; Landfester, K.; Wurm, F. R. *Angewandte Chemie-International Edition* **2015**, *54*, 7436.

(214) Meng, H.; Xue, M.; Xia, T.; Ji, Z.; Tarn, D. Y.; Zink, J. I.; Nel, A. E. *ACS Nano* **2011**, *5*, 4131.

(215) Salvati, A.; Pitek, A. S.; Monopoli, M. P.; Prapainop, K.; Bombelli, F. B.; Hristov, D. R.; Kelly, P. M.; Aberg, C.; Mahon, E.; Dawson, K. A. *Nature Nanotechnology* **2013**, *8*, 137.

(216) K. Mohr, M. S., G. Baier, S. Schöttler, P. Okwieka, S. Tenzer, K. Landfester, V. Mailänder, M. Schmidt, R.G. Meyer *J. Nanomed Nanotechnol.* **2014**, *5(2)*, 1000193.

(217) Walkey, C. D.; Olsen, J. B.; Guo, H.; Emili, A.; Chan, W. C. W. *J. Am. Chem. Soc.* **2012**, *134*, 2139.

(218)Lundqvist, M.; Stigler, J.; Elia, G.; Lynch, I.; Cedervall, T.; Dawson, K. A. *Proc. Natl. Acad. Sci. U. S. A.* **2008**, *105*, 14265.

(219) Deng, Z. J.; Mortimer, G.; Schiller, T.; Musumeci, A.; Martin, D.; Minchin, R. F. *Nanotechnology* **2009**, *20*.

(220)Tenzer, S.; Docter, D.; Rosfa, S.; Wlodarski, A.; Kuharev, J.; Rekik, A.; Knauer, S. K.; Bantz, C.; Nawroth, T.; Bier, C.; Sirirattanapan, J.; Mann, W.; Treuel, L.; Zellner, R.; Maskos, M.; Schild, H.; Stauber, R. H. *Acs Nano* **2011**, *5*, 7155.

(221) Casals, E.; Pfaller, T.; Duschl, A.; Oostingh, G. J.; Puntes, V. *Acs Nano* **2010**, *4*, 3623.

(222) Sudimack, J.; Lee, R. J. *Adv. Drug Del. Rev.* **2000**, *41*, 147.

(223) Wu, S.; Huang, X.; Du, X. *Angewandte Chemie-International Edition* **2013**, *52*, 5580.

(224)Kikkeri, R.; Lepenies, B.; Adibekian, A.; Laurino, P.; Seeberger, P. H. *J. Am. Chem. Soc.* **2009**, *131*, 2110.

(225) Freichels, H.; Wagner, M.; Okwieka, P.; Meyer, R. G.; Mailaender, V.; Landfester, K.; Musyanovych, A. *Journal of Materials Chemistry B* **2013**, *1*, 4338.

(226) Yu, Z.; Schmaltz, R. M.; Bozeman, T. C.; Paul, R.; Rishel, M. J.; Tsosie, K. S.; Hecht, S. M. *J. Am. Chem. Soc.* **2013**, *135*, 2883.

(227) B. Kang, P. O., S.Schöttler, O. Seifert, R. E. Kontermann, K. Pfizenmaier, A. Musyanovych, R. Meyer, M. Diken, U. Sahin, V. Mailänder, F. R. Wurm, K. Landfester *submitted*.

(228) K, H. R. H. *The Dow Chem Co* **(1998)**.

(229) Becer, C. R.; Hoogenboom, R.; Schubert, U. S. *Angewandte Chemie-International Edition* **2009**, *48*, 4900.

(230) Ning, X.; Guo, J.; Wolfert, M. A.; Boons, G.-J. *Angewandte Chemie-International Edition* **2008**, *47*, 2253.

(231) Liang, P.-H.; Wang, S.-K.; Wong, C.-H. *J. Am. Chem. Soc.* **2007**, *129*, 11177.

(232) Smith, E. A.; Thomas, W. D.; Kiessling, L. L.; Corn, R. M. *J. Am. Chem. Soc.* **2003**, *125*, 6140.

(233) Shibuya, N.; Goldstein, I. J.; Vandamme, E. J. M.; Peumans, W. J. *J. Biol. Chem.* **1988**, *263*, 728.

(234) Baier, G.; Costa, C.; Zeller, A.; Baumann, D.; Sayer, C.; Araujo, P. H. H.; Mailaender, V.; Musyanovych, A.; Landfester, K. *Macromol. Biosci.* **2011**, *11*, 628.

(235) Rausch, K.; Reuter, A.; Fischer, K.; Schmidt, M. *Biomacromolecules* **2010**, *11*, 2836.

(236) Hemmelmann, M.; Mohr, K.; Fischer, K.; Zentel, R.; Schmidt, M. *Mol. Pharm.* **2013**, *10*, 3769.

(237) Fulmer, G. R.; Miller, A. J. M.; Sherden, N. H.; Gottlieb, H. E.; Nudelman, A.; Stoltz, B. M.; Bercaw, J. E.; Goldberg, K. I. *Organometallics* **2010**, *29*, 2176.

(238) Baier, G.; Siebert, J. M.; Landfester, K.; Musyanovych, A. *Macromolecules* **2012**, *45*, 3419.

(239) Sardzik, R.; Noble, G. T.; Weissenborn, M. J.; Martin, A.; Webb, S. J.; Flitsch, S. L. *Beilstein J. Org. Chem.* **2010**, *6*, 699.

(240)Silva, J. C.; Gorenstein, M. V.; Li, G. Z.; Vissers, J. P.; Geromanos, S. J. *Mol. Cell. Proteomics* **2006**, *5*, 144.

(241) Kolb, H. C.; Finn, M. G.; Sharpless, K. B. *Angew. Chem. Int. Ed. Engl.* **2001**, *40*, 2004.

(242) Moses, J. E.; Moorhouse, A. D. *Chem. Soc. Rev.* **2007**, *36*, 1249.

(243) Siebert, J. M.; Baier, G.; Musyanovych, A.; Landfester, K. *Chem Commun (Camb)* **2012**, *48*, 5470.

(244) Fichter, M.; Baier, G.; Dedters, M.; Pretsch, L.; Pietrzak-Nguyen, A.; Landfester, K.; Gehring, S. *Nanomedicine* **2013**, *9*, 1223.